



City Research Online

City, University of London Institutional Repository

Citation: Kumar, P. (2023). Investigations on the structure-function relationship in keratoconus. (Unpublished Doctoral thesis, City, University of London/L V Prasad Eye Institute)

This is the accepted version of the paper.

This version of the publication may differ from the final published version.

Permanent repository link: <https://openaccess.city.ac.uk/id/eprint/33222/>

Link to published version:

Copyright: City Research Online aims to make research outputs of City, University of London available to a wider audience. Copyright and Moral Rights remain with the author(s) and/or copyright holders. URLs from City Research Online may be freely distributed and linked to.

Reuse: Copies of full items can be used for personal research or study, educational, or not-for-profit purposes without prior permission or charge. Provided that the authors, title and full bibliographic details are credited, a hyperlink and/or URL is given for the original metadata page and the content is not changed in any way.

City Research Online:

<http://openaccess.city.ac.uk/>

publications@city.ac.uk



Investigations on the structure-function relationship in keratoconus

Preetam Kumar

Thesis submitted in fulfilment of the requirements for the degree of Doctor of Philosophy in
Optometry and Vision Sciences

Supervisors

City, University of London

Prof. Christopher C Hull

Dr Peter Campbell

L V Prasad Eye Institute

Dr Shrikant R Bharadwaj

Centre for Applied Vision Research

School of Health and Psychological Sciences

City, University of London, UK

Brien Holden Institute of Optometry and Vision Sciences

L V Prasad Eye Institute, India

August, 2023

Contents

List of tables	5
List of figures	7
Acknowledgements	10
COVID-19 impact statement	11
Funding information	12
Abstract.....	13
List of Abbreviations	14
1. Chapter 1: Historical perspectives, demographics and characteristics of keratoconus	16
1.1. General introduction	16
1.2. Global perspective of aetiology, prevalence, and role of ethnicity in keratoconus	16
1.3. Clinical presentation of keratoconus	18
1.4. Characteristics of structural and functional changes in keratoconus.....	22
1.5. Management of keratoconus.....	23
1.6. Outline of the thesis	24
2. Chapter 2: Literature review on structural and functional changes in keratoconus	26
2.1. Structural changes in keratoconus	26
2.1.1. Evolution of diagnostic tools to detect keratoconus	26
2.1.2. Metrics used for detection of keratoconus	30
2.1.3. Assessment of progression in keratoconus.....	36
2.1.4. Grading severity scales in keratoconus.....	40
2.2. Functional changes in keratoconus	44
2.2.1. Optical performance of eyes with keratoconus	44
2.2.2. Visual performance of eyes with keratoconus	47
2.2.3. Threshold Vs suprathreshold performance in keratoconus	51
2.2.4. Response of visual system to optical blur in keratoconus	52
2.3. Management strategies in keratoconus	54
2.3.1. Optical management strategies	54
2.3.2. Surgical management strategies	60
2.4. Relationship between structure and function in keratoconus.....	62
2.5. Lacuna in the literature	63
2.6. Aims.....	64
3. Chapter 3: Structure-Function relationship in keratoconus: Spatial and depth vision	65
3.1. Introduction	65
3.2. Methods	68
3.2.1. Patient selection, inclusion, and exclusion criteria	68

3.2.2. Assessment of corneal structure.....	71
3.2.3. Assessment of visual functions.....	71
3.3. Assessment of the structure-function relationship.....	75
3.4. Statistical analysis.....	77
3.5. Results.....	77
3.5.1. Demographic, refractive and topographic and visual parameters.....	77
3.5.2. Overall trend in the structure-function relationship.....	78
3.6. Discussions.....	87
3.6.1. Major findings from the study.....	87
3.6.2. Implications of these results for the clinical management of keratoconus.....	88
3.6.3. Modelling the structure-function relationship data.....	90
3.6.4. Explaining the structure-function relationship from the optical quality of the eye.....	92
3.7. Summary.....	95
4. Chapter 4: Comparative analysis of different optical management strategies in keratoconus.....	96
4.1. Introduction.....	96
4.2. Methods.....	98
4.2.1. Patient selection, inclusion, and exclusion criteria.....	98
4.2.2. Study protocol- contact lens fitting.....	99
4.2.3. Study protocol- ocular aberration and psychophysical testing.....	100
4.3. Data analysis and hypothesis.....	101
4.4. Results.....	103
4.4.1. Demographic and refractive features.....	103
4.4.2. Individual trends in visual performance with CLs.....	105
4.4.3. LogMAR acuity and contrast sensitivity function.....	105
4.4.4. Sub-analysis of the contrast sensitivity function.....	108
4.4.5. Stereoacuity.....	109
4.4.6. Multiple regression analysis.....	110
4.4.7. Higher order wavefront aberrations.....	112
4.5. Discussions.....	113
4.5.1. Overall clinical implication of the result.....	113
4.5.2. Magnitude of improvement in visual performance with CLs.....	116
4.5.3. Inter-subject variability in the results.....	117
4.5.4. Study limitations.....	119
4.6. Summary.....	120
5. Chapter 5: Assessment of suprathreshold contrast perception in keratoconus.....	121
5.1. Introduction.....	121

5.2.	Methods	125
5.2.1.	Patient selection, inclusion, and exclusion criteria.....	125
5.2.2.	Assessment of corneal structure	126
5.2.3.	Psychophysical measurements.....	126
5.3.	Data analysis	130
5.4.	Results	131
5.4.1.	Demographic and refractive features	131
5.4.2.	Experiment 1- visual acuity and contrast sensitivity	131
5.4.3.	Experiment 1- Suprathreshold contrast matching.....	132
5.4.4.	Experiment 2- Suprathreshold contrast matching in bilaterally asymmetric keratoconus 135	
5.4.5.	Experiment 3- Changes in suprathreshold contrast matching with short-term changes in the eye’s optical quality	137
5.5.	Discussions.....	139
5.5.1.	Summary of results.....	139
5.5.2.	Implication of results for contrast perception in keratoconus	140
5.5.3.	Comparison of results with previous literature.....	142
5.5.4.	Interpretation of results in the context of the prevalent models of contrast constancy 145	
5.6.	Summary.....	147
6.	Chapter 6: Global summary and discussions	148
6.1.	Summary of results	148
6.2.	Learnings from the thesis to implement in the clinical management of keratoconus.....	150
6.2.1.	Extrapolation of psychophysical testing to the clinical tests in the spatial and depth domain 150	
6.2.2.	Interpretation of temporal changes of keratoconic eyes in the clinic	153
6.2.3.	Understanding the role of contact lenses in management of keratoconus.....	155
6.3.	Future directions	157
6.4.	Conclusions.....	160
	Appendix 1	161
	A1: Structure-function relationship with other indices of corneal structure.....	161
	Appendix 2	165
	A2: Protocol approval by the Ethics committee	165
	Appendix 3	170
	A3: <i>Published work from the thesis</i>	170
	References.....	171

List of tables

Table 1.1: A comprehensive summary of the major reports on keratoconus along with merging the findings from the Collaborative Longitudinal Evaluation of Keratoconus (CLEK) study. The question marks in the table represents unavailable data from the literature (Taken from (Zadnik et al., 1998)) 22

Table 2.1: This table lists the different models adapted by Ucakhan et al. (2011), that includes multiple indices to detect keratoconus(Taken from Ucakhan et al. (2011)). 33

Table 3.1: Demographic, refractive and topographic details of study participants. The values indicate median (interquartile range) for each parameter described in the study. The M, J0 and J45 terms represent the spherо-cylindrical refractive error in power vectors, wherein M = spherical equivalent of refraction and J0 and J45 represent the regular and oblique astigmatic components of refraction (Thibos et al., 1997). 78

Table 3.2: Coefficients of the best-fit logistic regression equation for the different spatial vision parameters considered in this study (Eq. 4). x_0 = midpoint of the fit, y_0 = lower asymptote of the fit, a = height of the sigmoid between the asymptotes, b = rate of loss of visual function, and c = sharpness of the edge roll-offs. An additional parameter, y_1 , describes the value at the upper asymptote of the function. This parameter is derived by simply adding the lower asymptote (y_0) to the height of the function (a). 81

Table 3.3: Median (interquartile range) of stereoacuity (arc sec) for the subjects with mild, moderate, or severe keratoconus in the better eye and with lower-than median or higher-than median interocular difference (IOD) in disease severity. 86

Table 4.1: Median (interquartile range) base curve (BC), back-vertex power (BVP), diameter and vault values for the four different CLs that were finalized across the keratoconic subjects that participated in this study. All scleral lenses used in this study had a central base curve of 8.0 mm and a diameter of 16.0 mm. 104

Table 4.2: Overall demographics along with the median (interquartile range) D-index, keratometry, HORMS, uncorrected subjective refraction and over-refraction with different CL options in both eyes of subjects that participated in the study. The subjective refraction and over-refraction values are represented as M, J0 and J45 power vector components. 104

Table 4.3: Results of the multiple regression analysis for the outcome variables monocular and binocular high contrast logMAR acuity and area under the curve of CSF, as well as for stereoacuity. B = the unstandardized beta, CI = confidence intervals for B, β = the standardized beta, t = the t-test statistic. The bold numbers in the table indicates the independent variables that had significant contribution to the predicted outcome variables. 112

Table 4.4: Median (interquartile range) HORMS obtained over 3 mm pupil diameter for controls and in the keratoconus cohort under unaided viewing conditions and with different CL designs. Data are shown for the overall population and separately for the mild to moderate and advanced keratoconus cohorts. For the overall population, the average and interocular difference (IOD) in HORMS between the two eyes are also shown. 113

Table 5.1: Demographic and clinical details of study participants. Cases are presented individually while control data is represented as mean \pm 1SD of the outcome variable. All cases participated in Experiment 1, cases P4, P7, P9, P11 and P12 participated in Experiment 2 and cases P3, P6 and P8 participated in Experiment 3. For participants in Experiment 2, data from each eye and from both eyes are noted in the table. The M, J0 and J45 terms represent the spherо-cylindrical refractive error in power vectors, wherein M = spherical equivalent of refraction and J0 and J45 represent the regular and oblique astigmatic components of refraction (Thibos et al., 1997). M: F = Male: Female; HCVA= spectacle corrected high contrast visual acuity; Cpd = cycles per degree; AUCSF = Area under curve of contrast sensitivity function. 132

Table 5.2: Outcomes of the 3-factor RM-ANOVA and post-hoc Bonferroni test performed to evaluate the statistical significance of the fold-change in contrast match with test spatial frequency and suprathreshold contrast in controls and cases. 134

Table 5.3: Mean ($\pm 1SD$) expected and observed fold-change in contrast matching and the P-value of the corresponding paired T-tests for the 10% and 50% suprathreshold contrast in controls and cases. 135

List of figures

Figure 1.1: Panel A shows a schematic diagram of a scissors reflex (Taken from Lawless et al., 1989). Panel B shows a clinical picture of a scissors reflex in a keratoconic eye, captured by the author from the clinical facilities of L V Prasad Eye Institute.	19
Figure 1.2: Clinical signs of keratoconus at different stages of the disease, captured with the slit lamp biomicroscope, from the clinical facilities of L V Prasad Eye Institute.	20
Figure 2.1: The different images from the one-position Bausch & Lomb keratometer represent contrasting difficulties faced during Keratometry procedure in a keratoconic eye (Taken from Lawless et al., 1989).	26
Figure 2.2: Panel A and B represents a photokeratoscope and videokeratoscope image of the cornea (Taken from Wilson and Klyce, 1991)).	28
Figure 2.3: Receiver operating curves for the different thickness indices for detection of keratoconus. (Taken from Ambrosio et al., 2011).....	32
Figure 2.4: Receiver operating curves comparing the performance of the multi-metric D-index against different curvature, thickness and elevation-based indices for detection of subclinical keratoconus (Taken from Muftuoglu et al., 2015).	35
Figure 2.5: Cumulative frequency curve showing the years taken to reach the progression group as defined by the authors. (Taken from Choi and Kim, 2012).	37
Figure 2.6: Receiver operating curves suggesting a superior performance of multi-metric D-index and keratoconus progression index (KPI) compared to other unimetric indices from Scheimpflug imaging (Taken from Shajari et al., 2019).....	39
Figure 2.7: Different elements of “ABCD” grading system and a representative image of a keratoconus eye, where this grading system has quantified the severity stage of keratoconus (Taken from Duncan et al., 2016).	43
Figure 2.8: The correlation of different image quality metrics with high contrast visual acuity (Adapted from Marsack et al., 2004).....	45
Figure 2.9: The low and high contrast logMAR acuity plotted against the two retinal image quality metrics (Adapted from Schoneveld et al., 2009).....	46
Figure 2.10: The computationally analysed through focus curve depicted the peak IQ (horizontal red arrow) and the depth of focus (Vertical solid and broken arrows) for 20 control eyes (a), right eyes of 12 bilateral keratoconus eyes under unaided condition (b) and the same keratoconus eyes with RGP CLs (c) (Adapted from Nilagiri et al.,2020).	47
Figure 2.11: High contrast visual acuity of each eye individually as well as binocularly for a cohort of bilateral keratoconus subjects, with their best corrected spectacles (A) and RGP contact lenses (B) along with the performance of the age-similar controls with their best corrected spectacles (C) (Adapted from Nilagiri et al., 2018).....	48
Figure 2.12: Box and whisker plots showing the stereoacuity results for a cohort of unilateral and bilateral keratoconus with mild to moderate disease severity, with their best corrected spectacles and with the RGP contact lenses (Adapted from Nilagiri et al., 2018).	49
Figure 2.13: The perception of contrast at threshold (outer most curve of the graph) and different suprathreshold levels (inner curves) for a particular subject (M.A.G) (Taken from Georgeson and Sullivan, 1975).....	51
Figure 2.14: Shows the presence of neural insensitivity due to the visual system getting exposed to chronic optical blur (Adapted from Sabesan and Yoon, 2009).	53

Figure 2.15: Shows the presence of neural adaptation, where the visual acuity in habitually keratoconic eyes were better in comparison to normal eyes where keratoconus aberrations were induced (Taken from Sabesan and Yoon, 2010). 54

Figure 2.16: Images of different form of contact lenses available to the clinicians to optically manage a case of keratoconus 55

Figure 2.17: The histogram shows optical performance (A) and visual performance (B) with habitual RGP lenses as well as two different forms of aberration corrected contact lenses (Adapted from Jinabhai et al., 2014). 59

Figure 2.18: Histogram shows the performances of aberration corrected scleral lens prosthetic device compared to the conventional scleral lenses (Taken from Sabesan et al., 2013)..... 59

Figure 3.1: Schematic of the four trends of structure-function relationship envisaged for spatial vision and depth vision in keratoconus 68

Figure 3.2: The flow chart provides an overview of the methodology used in this study 70

Figure 3.3: Figure shows the computer screen registering the response of an individual during the thresholding technique for assessing high contrast visual acuity 72

Figure 3.4: Figure shows the experimental set up for assessment of the contrast sensitivity function 73

Figure 3.5: Figure shows the experimental set up for stereoacuity assessment. 75

Figure 3.6: Scatter diagram of normalized spectacle-corrected high contrast visual acuity (panel A) and normalized area under the CSF (AUCSF; panel B) plotted as a function of the D-index for all study subjects 79

Figure 3.7: Same data as Figure 3.6 plotted along with the best-fit regression equations describing the pattern of structure-function relationship for high-contrast visual acuity and area under CSF (AUCSF) 81

Figure 3.8: The best fit logistic equation shown in Figure 3.7D and L for high-contrast visual acuity and area under CSF, respectively, shown along with their first derivative to describe the rate of change of the visual function with per unit change in D-index 82

Figure 3.9: Panel A shows representative contrast sensitivity functions (CSFs) from a control subject and a case with keratoconus. Panels B and C shows scatter diagram of the normalized cut-off spatial frequency and sensitivity at 3cpd plotted as a function of the D-index for the present cohort. Panel D shows the two best-fit logistic regression equations along with their first derivative to determine the rate of change of performance per unit change in D-index. All other details are the same as Figure 3.8. .. 83

Figure 3.10: Panels A and B shows scatter diagrams plotting the normalized stereoacuity as a function of the D-index of the better eye and interocular difference (IOD) in D-index. Panel C presents the bubble plot showing the distribution of stereoacuity as a function of both the D-index of the better eye and the IOD in D-index. Panel D shows a heatmap representing the statistical significance of the difference in stereoacuties between any two groups identified in Panel C. 86

Figure 3.11: Rotationally averaged modulation transfer functions (MTFs) for diffraction-limited optics and for representative subjects with mild, moderate, and severe keratoconus (KC). The MTF's derived from the ocular higher-order wavefront aberrations for 3mm pupil diameter at 555nm and the neural transfer function (NTF) for a 25-yrs old subject at 400Td of retinal illuminance, as described by Hastings et al. (2020). Panel A highlights the intersection point between the MTF and NTF for different severities of keratoconus (filled circles). Panel B depicts the matching spatial frequency and the associated interocular difference in contrast for three asymmetry pairs of keratoconus. 94

Figure 4.1: Data of binocular logMAR acuity (panel A), area under the CSF (panel B) and stereoacuity (panel C) for all 27 subjects on whom data was successfully collected in this study..... 106

Figure 4.2: Scatter diagram of monocular (right eye: circles; left eye: triangles) and binocular (squares) logMAR acuity obtained with spectacles (panel A), Kerasoft CL (panel B), Rose K2 CL (panel C),

conventional RGP CL (panel D) and Scleral CL (panel E) plotted as a function of the subject's D-index value	107
Figure 4.3: Scatter diagram of the area under CSF (AUC-CSF) obtained under monocular and binocular viewing conditions with spectacles (panel A) and different CL designs (panels B–E) plotted as a function of the subject's D-index value.	107
Figure 4.4: Scatter diagram of the cut-off spatial frequency of the CSF curve obtained under monocular and binocular viewing conditions with the spectacles (panel A) and different CL designs (panels B – E) plotted as a function of the subject's D-index value	109
Figure 4.5: Scatter diagram of peak spatial frequency of the CSF curve's sensitivity obtained under monocular and binocular viewing conditions with spectacles (panel A) and different CL designs (panels B–E) plotted as a function of the subject's D-index value	109
Figure 4.6: Scatter diagram of stereoacuity obtained with spectacles (panel A) and different CL designs (panels B–E) plotted as a function of the subject's average D-index value.....	110
Figure 4.7: Summary chart describing the visual performance (HCVA, contrast sensitivity and stereoacuity), optical quality (higher-order wavefront aberrations) and nonvisual parameters that define lens wear with different optical corrections in subjects with mild to moderate (left panel) and advanced keratoconus (right panel), all relative to controls	116
Figure 5.1: Panel A representative contrast threshold function for a control subject and three cases with mild, moderate, and severe keratoconus that participated in this study. Representative pairs of the test (T) and reference (R) grating patterns used in the contrast matching paradigm of this study are shown in this figure. Panel B shows Fold-change in suprathreshold matching contrast expected from the contrast threshold functions for the different spatial frequencies tested in this study.	124
Figure 5.2: Panels A – D: Fold-change in contrast of test grating required to match the perceived contrast of the reference grating for one representative control subject (panel A) and three representative cases with different severities of keratoconus	133
Figure 5.3: Scatter diagram of the fold-change in suprathreshold contrast match plotted as a function of the D-index for all controls (open symbols within the red band) and cases (filled symbols) that participated in the study. Panels A and B show data for 10% contrast while Panels C and D show data for 50% contrast.	136
Figure 5.4: Panels A and B show contrast threshold functions of the worse eye, better eye and binocular viewing of two representative cases with keratoconus with large interocular asymmetry in their disease severity. Panels C and D show scatter diagram of the fold-change in suprathreshold contrast match observed for the worse eye viewing (filled symbols) or binocular viewing (open symbols) plotted against the corresponding fold-change obtained for the better eye viewing in five participants with bilateral asymmetry in keratoconus.	137
Figure 5.5: Panels A – C show the monocular contrast threshold functions of the three cases with keratoconus that participated in Experiment 3. Contrast threshold curves are plotted for contact lens wear and with their best-corrected spectacle correction immediately after switching from contact lens wear, one week of spectacle wear and two weeks of spectacle wear for each participant.	139
Figure 5.6: Comparative analysis of the present study results with those of previous studies investigating the contrast constancy phenomenon.	145

Acknowledgements

I would like to begin by acknowledging all participants of this study, for spending their valuable time for the experiments. My sincere gratitude to all my supervisors- Professor Chris Hull and Dr Peter Campbell from City, University of London and Dr Shrikant Bharadwaj from the L V Prasad Eye Institute, India for the constant support, guidance, motivation and for being ever-present throughout the journey.

I am grateful to the senior leadership, directors, and scientists of LVPEI for providing their support, and feedback for my work during this time and creating an enabling environment for pursuing PhD and allowing me to have access to of various software and websites on the campus to execute the study.

A special thanks to Dr Shrikant Bharadwaj for going through the daily grind and making my transition from the clinics to the research as memorable experience for me as possible. Professor Chris Hull and Dr Peter Campbell for making sure to have kind words of encouragement, no matter how little the achievements were throughout the entire process.

I extend my heartfelt gratitude to Ms Banu and Mr Sudhakar, our dedicated librarians, for their unwavering assistance and prompt assistance with the requested journal articles. I also extend my thanks to the dedicated group of clinicians in L V Prasad Eye Institute, whom I shared the clinic with, for helping me out though the data collection process and for their words of encouragement throughout my journey. My lab mates, Dr Bhagyalakshmi Marella, Mr Sabyasachi Goswami, Ms Preetirupa Devi and Ms Ketkee Jain, for helping me with the data analysis and providing with their valuable feedback on the projects. And finally, my PhD mates- Reena Durai, Rohit Dhakal, Bhagya Lakshmi Marella, and Rebecca Sumalini, whose support and motivation were incredible throughout the entire journey of my PhD.

A big heartfelt thanks to my mother, Ms Abha Kumar, my father, Mr Amal Kumar and my sister, Ms Poulami Kumar for their amazing support, encouragement, and everything else throughout the whole journey. Last, but not the least, I want to acknowledge my wife, Sreya, for being amazing and supporting me through the thick and thin during this entire time.

COVID-19 impact statement

This statement is provided for the aid and benefit of future readers to summarize the impact of the COVID-19 pandemic on the scope, methodology and research activity associated with this thesis. The academic standards for a research degree awarded by City, University of London and for which this thesis is submitted remain the same regardless of this context.

Title of research project: *Investigations on the structure-function relationship in keratoconus*

1. Summary of how the research project, scope or methodology has been revised because of COVID-19 restrictions.

The COVID-19 restrictions delayed the overall functioning of the thesis work, specifically the data collection for all the three experiments, where the subjects were required to visit the clinic on multiple occasions. This study relied on in-person observations during experiments. I had to postpone the data collection process by a year due to the lockdown restrictions.

2. Summary of how research activity and / or data collection was impacted because of COVID-19 restrictions and how any initially planned would have fitted within the thesis narrative.

The COVID-19 restrictions have significantly impacted research activities and data collection. Suspension of in-person data collection until the lift of lockdown, less in-person interaction with the supervisors. Post lockdown, I continued with the activities as planned.

3. Summary of actions, or decisions taken to mitigate for the impact of data collection or research activity that was prevented by COVID-19.

Regarding the first aim of the study, the initial plan was to conduct a longitudinal study that required subjects to visit the clinics on multiple occasions. Post COVID-19 restrictions, I had to take a blended approach of a pseudo-longitudinal study, due to the reluctance of subjects to visit the clinics on regular basis.

Extension of three months was granted from City, University of London. This helped me to catch up with the lost time for the data collection.

4. Summary of how any planned work might have changed the thesis narrative, including new research questions that have arisen from adjusting the scope of the research project

The overall scope of the project was not changed

Funding information

- Partnership grant from the Dept. of Biotechnology, Govt. of India, to Hyderabad Eye Research Foundation, LVPEI, India (BT/PR32404/MED/30/2136/2019)
- Grant from the Cognitive Science Research Initiative, Department of Science and Technology, Govt. of India to Shrikant R. Bharadwaj [Grant#: SR/CSRI/189/2013 (G)]
- Grant to attend ARVO 2022, Denver was jointly supported by City, University of London, and Hyderabad Eye Research Foundation, LVPEI, India

Abstract

Background and aims: Keratoconus is an ocular condition that causes a change in corneal shape and consequently degrades the retinal image quality and visual function. Despite extensive studies on the impact of the disease on corneal structure and visual function in isolation, the precise relationship between structure and function in keratoconus has not yet been determined. A structure-function relationship in a progressive condition such as keratoconus can provide valuable insight and evidence that can inform its treatment. The overarching aim of this thesis was to understand the structure-function relationship in keratoconus. Specifically, an attempt was made to determine the structure-function relationship for threshold and suprathreshold levels of visual performance, with the aid of spectacles and contact lenses.

Methods: For the three main studies reported in this thesis, threshold level spatial visual performance was assessed using high contrast visual acuity (COMPlog[®] software) and the contrast sensitivity function (quick CSF). Random dot stereograms and Howard-Dolman apparatus were used to assess stereoacuity. Corneal curvature, elevation, and thickness-based indices such as maximum keratometry, index of surface variance, vertical asymmetry, height decentration, keratoconus index and D-index were assessed using Scheimpflug imaging. The D-index was used as an indicator of disease severity. In the first study, these parameters were determined for varying severity of keratoconus in a total of 155 participants (310 eyes) and the structure-function relationship investigated for four different mathematical models using regression analysis. In the second study, the effect of best corrected spectacles and different contact lenses, namely, conventional and Rose K2 rigid gas permeable contact lenses, a custom-designed soft toric contact lens (Kerasoft), and scleral contact lenses, on threshold level visual performance was determined using the tests already listed. In the final study, suprathreshold visual performance was determined in twelve subjects with keratoconus and twelve age-similar controls with a contrast matching paradigm implemented in Matlab.

Results: Threshold level visual functions progressively deteriorated with increasing severity of keratoconus. The loss in all three functional measures was best explained by the five-parameter sigmoid-shaped logistic regression model ($r^2 \geq 0.66$; $p < 0.001$). The high contrast visual acuity showed a distinct ceiling phase and a steeper loss rate with increasing D-index (1.8units/D-index) relative to the CSF (0.28units/D-index). Stereoacuity was poorly correlated with D-index ($p \leq 0.2$, for both inter-ocular difference and the D-index of the best eye). Assessment with contact lenses revealed that all the outcome variables improved with all forms of lenses relative to spectacles ($p < 0.05$). This improvement was smaller with Kerasoft lenses but higher and comparable with the other three lens designs, across the disease severity. Interestingly, none of the visual function measures or the optical quality reached the level of controls for any correction modality. The assessment of suprathreshold performance showed that the perceptual contrast match for eyes with mild to moderate keratoconus across spatial frequencies were found at a comparable level to that of the controls, complying with the well-established phenomenon of contrast constancy in the literature.

Conclusions: Results suggest that the vision loss in keratoconus cannot be generalized and is critically dependent on the overall disease severity, interocular symmetry and the type of function being evaluated. The presence of constancy in contrast perception irrespective of the disease severity, inter-ocular asymmetry and short-term change in optical quality may indicate an active gain control mechanism across spatial frequency channels for the visual system at a suprathreshold level in keratoconus.

List of Abbreviations

AO: *Adaptive optics*

ART: *Ambrosio relational thickness*

AUCSF: *Area under the contrast sensitivity function*

BAD: *Belin Ambrosio enhanced ectasia display*

CKI: *Central keratoconus index*

CL: *Contact lens*

CPD: *Cycles per degree*

CLEK: *Collaborative longitudinal evaluation of keratoconus*

CSF: *Contrast sensitivity function*

CSI: *Centre surround index*

CTSP: *Corneal thickness spatial profile*

CXL: *Collagen cross-linking*

DSI: *Differential sector index*

HCVA: *High contrast visual acuity*

HOA: *Higher order aberration*

HORMS: *Higher order root-mean-square*

ICRS: *Intra-corneal ring segment*

IHA: *Index of height asymmetry*

IHD: *Index of height decentration*

IOL: *Intra-ocular lens*

I-S: *Inferior-Superior*

ISV: *Index of surface variance*

IVA: *Index of vertical asymmetry*

KC: *Keratoconus*

KI: *Keratoconus index*

KPI: *Keratoconus progression index*

KSS: *Keratoconus severity score*

LASIK: *laser-assisted in situ keratomileusis*

LOA: *Lower order aberration*

MAR: *Minimum angle of resolution*

μm : *Microns*

MOA: *Method of adjustment*

MTF: *Modulation transfer function*

NTF: *Neural transfer function*

OSI: *Opposite sector index*

OTF: *Optical transfer function*

PPI: *Pachymetry progression index*

PRK: *Photorefractive keratectomy*

PSF: *Point spread function*

PTF: *Phase transfer function*

PTI: *Percentage thickness increase*

PTK: *Phototherapeutic keratectomy*

R_{min} : *Minimum radius of curvature*

RMS: *Root mean square*

RGP: *Rigid gas permeable*

SAI: *Surface asymmetry index*

SIM K: *Simulated keratometry*

SRAX: *Skewing of radial axis*

UVA: *Ultra-violet A*

1. Chapter 1: Historical perspectives, demographics and characteristics of keratoconus

1.1. General introduction

Keratoconus is a progressive, non-inflammatory disease of the eye, characterized by thinning, anterior protrusion, increased asphericity and scarring of the cornea (Krachmer et al., 1984, Rabinowitz and Rasheed, 1999). These changes have a significant impact on an individual's visual performance (Ridley, 1956, Tuft et al., 1994). The first mention of a conical cornea was made 170 years ago (Nottingham, 1854). Since then, significant efforts have been made to systematically elucidate various facets of the disease. A substantial amount of work has been published over the past three decades aimed at understanding disease presentation, epidemiology (Armstrong et al., 2021, Chan et al., 2021, Santodomingo-Rubido et al., 2022), genetic susceptibility (Gonzalez and McDonnell, 1992, Mathan et al., 2020, Shneor et al., 2020), alterations in the structure and biomechanical strength of the cornea (Andreassen et al., 1980, Vellara and Patel, 2015), visual performance (Ridley, 1956, Tuft et al., 1994) as well as changes in ocular surface parameters in keratoconus (D'Souza et al., 2021, Erdinest et al., 2023). However, a review of recent literature highlights the ongoing need for research into this condition. In aiming to address this need, this PhD will primarily focus on understanding the impact of keratoconus on visual function and how this correlates with structural changes in the eye. This chapter will outline the features of keratoconus, the prevalence of the condition and some of the common concerns that are pertinent to this thesis.

1.2. Global perspective of aetiology, prevalence, and role of ethnicity in keratoconus

The prevalence and incidence of keratoconus, although not fully understood, are known to vary with geographic location, race and ethnicity (Santodomingo-Rubido et al., 2022). Technological advances in screening tools and imaging (such as Scheimpflug imaging) have led to an increase in detection rates at an earlier stage (Toprak et al., 2021) whereas diagnosis

was previously based on the clinical features at a later stage of the condition (see section 1.3). The prevalence and incidence of the disease have been shown to vary considerably based on the geographic location and the ethnicity of the population. Prevalence is known to be higher in Asian countries and more specifically, in the Middle-Eastern region of the Asian and African continent compared to the continents of Europe and North America, ranging from 1500 to 5000 per 1,00,000 population (1.5% - 5%) for the former (Jonas et al., 2009, Hashemi et al., 2013, Shehadeh et al., 2015, Torres Netto et al., 2018) compared to under 1000 per 1,000,000 population (1%) for the latter (Ihalainen, 1986, Godefrooij et al., 2017, Bak-Nielsen et al., 2019). Incidence also shows a similar pattern with around 20 per 1,000,000 persons/year for the former group compared to up to 4 per 1,000,000 persons/year for the latter (Santodomingo-Rubido et al., 2022).

Interestingly, studies conducted on different ethnic group within the same geographical region have shown significant differences in prevalence. For instance, prevalence reports from countries like Japan and South Korea have shown significantly less prevalence of keratoconus (0.009% (Tanabe et al., 1985) and 0.04% (Hwang et al., 2018) respectively). Similarly, there have been studies conducted in the United Kingdom (UK), that have compared the prevalence of keratoconus between Asian population residing in the UK (specifically of Indian and Pakistani ethnicity) and the Caucasian population. Results have shown a greater prevalence in the former group (Pearson et al., 2000, Georgiou et al., 2004). This might indicate that there is a stronger influence of ethnicity on the disease rather than the geographical location.

To understand the reason for such variability in the prevalence of keratoconus, we need to investigate the factors that can potentially cause the disease. For instance, genetic studies have showed significant variability in genes associated with keratoconus across ethnicity. Specific loci and polymorphism have been detected that may increase susceptibility to keratoconus in these groups. For example, studies have confirmed that keratoconus is a polygenic disease

where more than one affected gene is involved (Bykhovskaya et al., 2016). Moreover, polymorphism has been noted in genes such as VSX1 and SOD1, which play important roles in maintaining corneal structural integrity (Mas Tur et al., 2017). Therefore, differing expression of these genes across ethnic groups can mean that certain groups can be relatively more predisposed to keratoconus than the others. Environmental factors and the associated behavioural factors have also been shown to have a significant association with keratoconus. For example, an increased temperature and dust in the environment in certain parts of Asia and Africa can potentially lead to chronic ocular irritation and increase the likelihood of eye rubbing, which has already been a proven factor to increase the risk of developing keratoconus (Hashemi et al., 2020).

The incidence and prevalence of keratoconus depends greatly on the efficiency of detecting the disease. An increased capability to detect keratoconus would result in a greater number of cases getting diagnosed. There has been significant technological development as well as understanding of the disease in the past two decades (discussed in detail in the chapter 2). As a result, data from the earlier studies may not reveal the true prevalence and incidence of the disease. For instance, the report by Jonas et al. (2009) is the only report available from the subcontinent of India. The number of diagnosed keratoconus cases would be higher if we were to conduct similar studies at present with more advanced technologies available to detect keratoconus. Therefore, conducting these population-based studies and updating the information in a periodic manner is important.

1.3. Clinical presentation of keratoconus

Keratoconus is a degenerative corneal disorder that results in a change in shape, primarily in corneal curvature, thickness and elevation (Ambrosio et al., 2006, Belin and Khachikian, 2007). It is, by definition, a bilateral and asymmetrical disease, and the full aetiology is not fully understood (Vazirani and Basu, 2013). Predominantly presenting in isolation or in

association with systemic diseases (e.g., Down’s syndrome, Leber’s congenital amaurosis etc.), the condition is thought to have its onset typically at puberty (Elder, 1994, Mathan et al., 2020). Clinically it presents with a common subset of signs that have been comprehensively documented (Krachmer et al., 1984, Zadnik et al., 1998). Originally, clinical observation, in the form of case reports, documented the general features of the condition. However, with the advent of slit lamp biomicroscopy, the impact of the disease on the different layers of the cornea could be investigated (Nottingham, 1854, Graves, 1925, Greene, 1945).

In the early stages of the disease, the patient remains asymptomatic, and diagnosis is often made opportunistically during a routine eye examination. One of the early reports by Amsler (1946) coined the term “forme-fruste” for pre-clinical form of keratoconus. An unusual reflection on the cornea, termed an “oil-droplet reflex” that is especially visible against retro-illumination in a dilated pupil, or an irregularity in the retinoscopic reflex, known as a “scissor’s reflex” (Figure 1.1), along with a poor reliability of the refraction could be enough evidence to suspect a case of Keratoconus (Lawless et al., 1989).

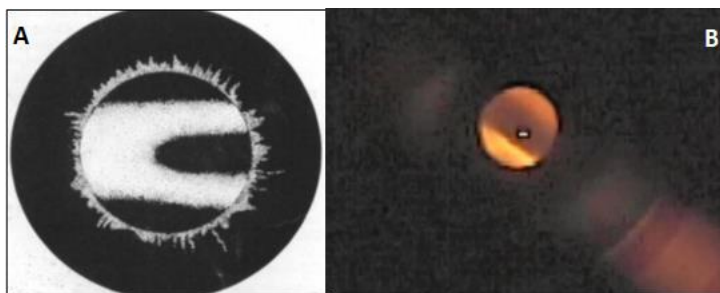


Figure 1.1: Panel A shows a schematic diagram of a scissor's reflex (Lawless et al., 1989). The central circle represents the pupillary aperture and the central dark band within the white retinoscopic reflex creates a scissor's reflex (Taken from (Lawless et al., 1989)). Panel B shows a clinical picture of a scissor's reflex in a keratoconic eye, where the dark band is seen within the bright yellow retinoscopic reflex. This picture has been captured by the author from the clinical facilities of L V Prasad Eye Institute.

Clinical slit lamp biomicroscopic signs include:

- Increased visibility of corneal nerves

- Olive-green lining of iron deposition around the base of the cone (“Fleischer’s ring”)- usually used as a marker to indicate the extent / diameter of the cone (Figure 1.2B)
- Vertical striations at the depth of posterior stroma (Vogt’s striae) caused by stretching of the cornea at the stromal collagen level and which typically disappear upon applying digital pressure (Figure 1.2E)
- Sub-epithelial corneal scar probably caused by breaks at Bowman’s layer

These may present variably based on the severity of keratoconus (Krachmer et al., 1984). Some of the external signs such as the ‘V’ shaped conical appearance of the lower eye lid due to extensive protrusion (Munson’s sign) (Figure 1.2C) or the unique sharp light focus at the margin of the limbus, when illuminated from the other limbal plane (Rizzuti’s sign) (Figure 1.2D) are classic demonstrations of the disease (Rizzuti, 1970, Krachmer et al., 1984).



Figure 1.2: Clinical signs of keratoconus at different stages of the disease, captured with the slit lamp biomicroscope. Panel A shows stromal thinning on optic section (arrowhead pointing towards the central ectatic zone). Panel B shows an incomplete Fleischer’s ring, where the arrowhead points towards the superior and the inferior arcs of the ring. Panel C shows Munson’s sign, where the dotted line demarcates the ‘V’ shaped stretching of the lower lid in the down - gaze. Panel D demonstrates Rizzuti’s sign, where the arrowhead points towards the sharp light focus on the margin of the limbus, when the illumination is projected from the other side of the limbus. Panel E shows Vogt’s striae where the vertical arrow heads point towards the multiple vertical striations seen around the apex of the cone. These pictures have been captured by the author from the clinical facilities of L V Prasad Eye Institute.

The clinical signs may present in isolation or in combination depending on the severity of the disease. These clinical signs are not always consistently reported in the literature. The extensive database compiled by Zadnik et al. (1998) from the Collaborative Longitudinal Evaluation of Keratoconus (CLEK) study group has collected the different clinical signs reported by major studies of keratoconus from 1986 -1996 (Table 1.1). The gender predisposition of keratoconus has not been conclusively reported in the literature. In the studies included in table 1, only Swann and Waldron (1986) found keratoconus more commonly in females than males, which was in contrast to other studies listed in the table. The exact reason for this finding was not explained in the paper. In an extensive review article by Santodomingo-Rubido et al. (2022), among the entire list of articles that were reviewed, sixty percent of studies reported a male predisposition whereas 40% reported the opposite. There was no specific trend noted in this distribution regarding the geographic location or ethnicity. This study therefore concluded no specific bias in occurrence of keratoconus in this regard.

Study	Source of patients	Number of eyes/patients	% Unilateral cases	% Female	% With Vogt's striae	% With Fleischer's ring	% With corneal scarring	% Undergoing corneal transplantation
Kennedy et al (1986)	Mayo clinic	102/64	20	45	6	2	??	14
Macsal et al (1990)	Cornea specialty practice	398/199	0	44	??	??	??	9
Eggink et al (1988)	Academic and non-academic clinical centers	??/874	8	45	??	??	??	20
Lass et al (1990)	Three cornea specialty practices	834/417	3.5	45	??	??	??	33
Swann & Waldron (1986)	Private optometry practice	87/57	9	56	46	25	2	??
Ihalainen et al (1986)	University hospital	??/212	9	37	??	??	??	31

Crews et al (1994)	Cornea and contact lens specialty practice	118/66	??	42	51	33	29	24
Tuft et al (1994)	Specialty contact lens clinic	5,242/2,723	4.3	34	??	??	??	22
Dao et al (1994)	Cornea and contact lens specialty practice	99/64	??	22	60	??	??	??
Zadnik et al (1995), CLEK survey	38 clinical centers	2,379/1,579	13	41	52 (in at least one eye)	64	43	12

Table 1.1: A comprehensive summary of the major reports on keratoconus along with merging the findings from the Collaborative Longitudinal Evaluation of Keratoconus (CLEK) study. The question marks in the table represents unavailable data from the literature (Taken from (Zadnik et al., 1998))

1.4. Characteristics of structural and functional changes in keratoconus

Stromal corneal thinning, coinciding with prominent corneal ectasia, is one of the hallmark signs of keratoconus that distinguishes keratoconus from the other ectatic corneal disorders (Krachmer et al., 1984). Ectasia is defined by changes in three fundamental parameters: cornea-curvature, thickness, and elevation. Advancement in diagnostic tools has allowed the quantification of these aspects (see details in Chapter 2). A multifactorial approach to define the corneal structure has significant relevance to three fundamental aspects of the disease condition. Firstly, to diagnose keratoconus at a very early stage, even before the other clinical signs are apparent, (usually referred to “forme-fruste”). Secondly, this approach allows a precise documentation of the categorization and severity of keratoconus (Krumeich et al., 1998, Belin et al., 2022). Thirdly, it allows quantification of the disease progression during its natural course (Romano et al., 2018, Shajari et al., 2019). This, in conjunction with the second point, are key elements in helping the practitioners to formulate a treatment course for these individuals.

The cornea is one of the main refracting components in the eye and corneal structure plays a key role in the optical performance and hence visual function (see chapter 2, Section 2.2). Keratoconus is associated with a reduction in visual performance (Carney and Lembach, 1991, Davis et al., 2006). In early studies, visual performance and refraction were used as markers to indicate the severity of the disease (Ridley, 1956). High Contrast Visual Acuity (HCVA) was predominantly used as the marker to define visual performance (Ridley, 1956, Davis et al., 2006). However, reports have suggested that keratoconic eyes can still maintain HCVA, to a level comparable to that of the controls. However, these eyes can show a deficit in the contrast sensitivity function (CSF) performance. Therefore, the CSF is perhaps more useful at explaining the loss in spatial vision (Carney and Lembach, 1991, Shneor et al., 2021). Binocular visual functions have also been shown to be prominently affected by keratoconus, due to its asymmetric nature (Vazirani and Basu, 2013). Sherafat et al. (2001) reported an adverse impact of asymmetric keratoconus on both the sensory and motor visual function. A recent report by Nilagiri et al. (2018) has shown an average 12-to-15-fold deterioration of stereoacuity in unilateral as well as bilateral keratoconus.

1.5. Management of keratoconus

Management of keratoconus patients typically follows two parallel streams; visual rehabilitation with the help of best corrected spectacles and contact lenses and monitoring the progression of the disease condition over time. The working principle of a contact lens is to create an artificial refracting surface, which is relatively regular compared to the native keratoconic cornea. This in turn significantly reduces the ocular aberrations and therefore has a positive influence on visual function (Betts et al., 2002, Edrington et al., 1999). With improvements in technology, new designs of contact lenses are being developed that are better both in terms of visual performance as well as on-eye comfort (Mandathara et al., 2017, Santodomingo-Rubido et al., 2022). As the disease progresses, the benefit of optical corrections

may reduce and surgical interventions may be required (Mandathara et al., 2017). The surgical intervention can be of two types, ablative or additive. Ablative surgery is where the corneal curvature is modified by the influence of an excimer laser (e.g., LASIK, PRK or PTK). Reports of ablative procedures are very few and contradictory in nature as the procedures are believed to result in post-procedure ectasia and further deterioration of optical and visual performance (Elsahn et al., 2009). Additive procedures are more common, where adjustments are carried out to the existing refracting surface such as intra corneal ring segment implantation (ICRS) or phakic IOL implantation (Leccisotti and Fields, 2003, Colin et al., 2000). However, in a direct attempt to improve the biomechanical strength of the cornea (Spoerl et al., 2004), the procedure called collagen cross linking has gained prominence as the surgical treatment of choice (Wollensak et al., 2003, Mazzotta et al., 2012). In advanced forms of keratoconus, these options do not help and corneal transplantation (partial or complete) may be the best treatment option (Mandathara et al., 2017).

1.6. Outline of the thesis

The present chapter has provided general information about the features and prevalence of keratoconus. The second chapter will summarize the literature relevant for the thesis and will outline the lacuna that are presently there in the literature. This chapter will define the specific aims of the thesis. The third chapter investigates the impact of keratoconus on various threshold level visual functions both in the spatial and depth domain. This chapter also derives structure-function relationships to explain how functional loss is related to changes in corneal structure. The fourth chapter explores the extent to which, the threshold level performance of the eye can be improved with the help of different contact lenses. The performance of four different contact lenses is compared in order to provide evidence for selecting the best option for a given keratoconus patient. The fifth chapter assesses suprathreshold visual performance in keratoconus. This chapter also explores the influence of optical correction on the

suprathreshold contrast. Finally, the sixth chapter provides a summary of the results and suggests possible future directions for research work into keratoconus based on the results.

2. Chapter 2: Literature review on structural and functional changes in keratoconus

2.1. Structural changes in keratoconus

2.1.1. Evolution of diagnostic tools to detect keratoconus

Measurement of corneal curvature has predominantly been considered the most fundamental measurement to explain ectatic corneal disorders such as keratoconus. Traditionally, keratometers were used to measure corneal curvature. Irregularity of the projected mires during keratometry was suggested as one of the earliest signs of keratoconus along with a scissor's retinoscopic reflex. However, it is often difficult to quantify the corneal curvature in keratoconus using keratometry due to the inability to focus the mires properly (Figure 2.1) (Lawless et al., 1989). In addition, keratometry assumes regular astigmatism and measures curvature values along the two principal meridians by averaging two points on the anterior surface of the cornea across an approximately 3mm annulus. As a result of these assumptions, keratometry only gives limited information about the overall corneal shape.

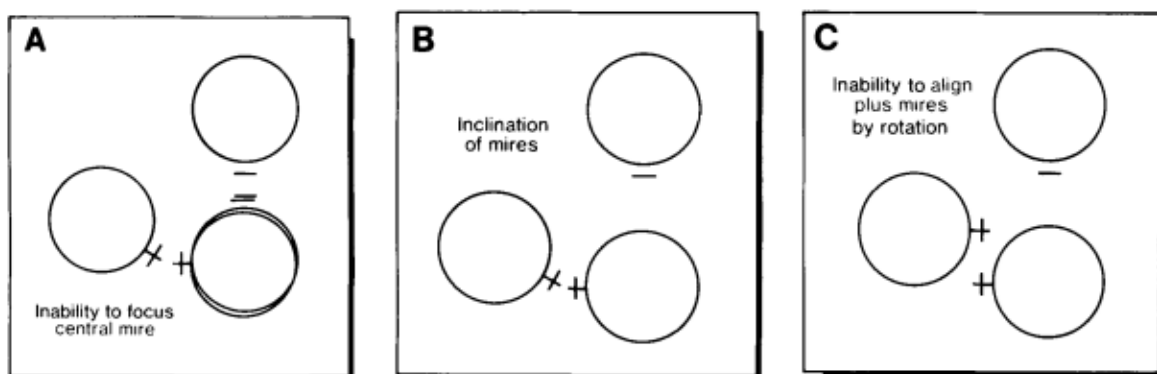


Figure 2.1: The different images from the one-position Bausch & Lomb keratometer represent contrasting difficulties faced during Keratometry procedure in a keratoconic eye. In addition to these, an advanced form of keratoconus may also show a distortion that makes it difficult to recognize the mires (Taken from Lawless et al. (1989)).

A need to understand the shape of the entire cornea led to advances in the field of corneal topography. One of the earliest reports by Amsler (1946) confirmed that the distortions in the

reflections from a Placido ring can actually detect the signs of keratoconus that may otherwise go unnoticed by the slit lamp examination. The distortion of the ring mires made possible the qualitative assessment of the corneal shape. The principle behind quantifying these distortions originated as early as 1619 when Father Christopher Scheiner compared the reflection of a candle-light source from the corneal surface with the known curvature of marbles of varying sizes. Henry Goode proposed the first keratoscope in 1847, which assessed the reflection of a luminous square from the eye's surface (Levine, 1965). His methods were the first to allow the comparison of the reflection from the central and the peripheral part of the cornea simultaneously. The most widely accepted and used clinical form of a keratoscope was however introduced by Antonio Placido in 1880. It consisted of a flat disc with an array of concentric black and white rings. This ring was illuminated from either the top or the temporal side and the reflection of the rings on the corneal surface was observed through an aperture placed at the centre of the disc. As the outer rings created larger angles on the corneal surface, a greater area of the cornea could be assessed (Levine, 1965). Photokeratoscopes allowed the distortion of the reflected ring mires to be recorded and subsequently analysed. These devices were an adaptation of Placido's disc, by adding a camera at the central aperture. The use of a flat Placido disc was a major limitation for the assessment as it restricted the overall area of the corneal surface that could be assessed. Using an elliptical surface was a significant development that allowed the corneal surface to be assessed out to the limbus. The Wesley-Jessen Photo-electric keratoscope (PEK) was an instrument developed with such specifications, and it allowed quantification of the corneal shape, which was quantified using the least-square fitting of an elliptical curve. This instrument was widely used in early contact lens practice (Townesley, 1967, Wesley, 1969). Work by Donaldson (1972) and Rowsey et al. (1981) further modified the photokeratoscope enabling quantification of corneal curvature along multiple meridians along with better visualization of the Placido rings out towards the limbus. Wilson and Klyce

(1991) made further progress and introduced colour coded graphical displays to consolidate the large amounts of data generated and to help explain the corneal contour.

One of the fundamental issues with the photokeratoscope was the insufficiently accurate measurement of the cornea at the centre due to the scarcity of the number of Placido rings located in that region. In addition, the photokeratoscope findings were based on the analysis of a photograph of the reflected Placido ring mire. This was time consuming and eventually limited its widespread adoption. Videokeratoscopes were introduced to address these issues. The captured digital image was processed to find the ring edges prior to using reconstruction algorithms to determine local corneal curvature. In addition, a significantly higher number of points on the ocular surface could be measured and introduction of a stable central fixation reference resulted in a reproducible computerized assessment of the anterior corneal shape (Figure 2.2) (Wilson and Klyce, 1991).

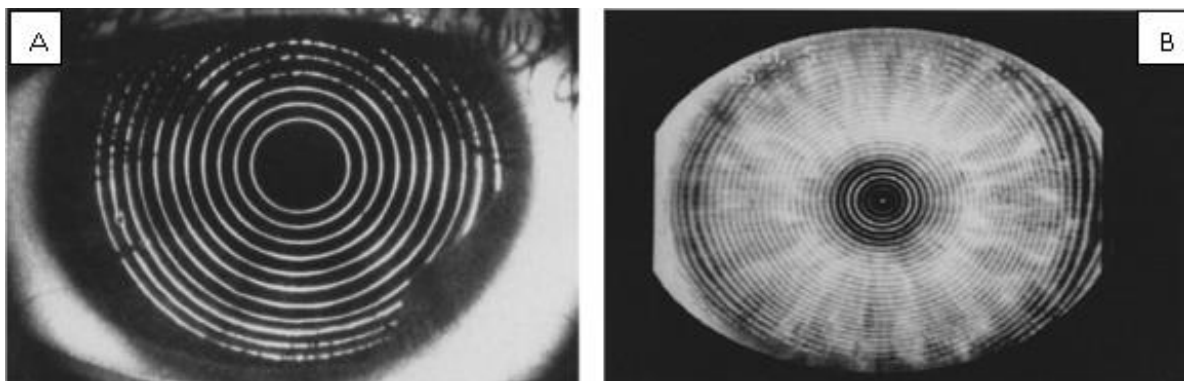


Figure 2.2: Panel A represents a photokeratoscope image. The central dark area indicates a lack of Placido rings available there. Panel B represents a videokeratoscope image where the Placido mires reach up to the apex of the cornea and therefore, provides an upgraded quantification of the cornea (Taken from Wilson and Klyce (1991)).

A need to investigate the tomographic changes on the posterior surface of the cornea was identified mainly for two reasons: first, the change in corneal structure involves both the anterior as well as the posterior corneal surface; and second, there is ambiguity in understanding where do the first changes occur in keratoconus. Morphological studies suggest

that the first changes in a keratoconic cornea occur in the anterior limiting lamina and the anterior stroma. However, tomographical reports show that the earliest changes in keratoconus are often detected at the posterior surface before the anterior surface is affected (Bergmanson et al., 2021). Slit scanning technology was able to address this limitation of Placido-based videokeratoscopes (Cairns and McGhee, 2005). Slit-scanning videokeratoscopy involved recording digital images of the reflections of a slit from the anterior and posterior corneal surfaces as a slit was scanned across the cornea. Analysis, based on stereo-photogrammetry, allowed the elevation of the anterior and posterior corneal surfaces to be derived. For the first time, a three-dimensional representation of the cornea, as well as information about the anterior segment, could be realised (Quisling et al., 2006). A combination of Placido-based ring mires along with slit-scanning technology resulted in an accurate measurement of the anterior corneal surface as well as providing useful information about the posterior corneal surface (Quisling et al., 2006). Despite the notable advantages over its predecessors, slit-scanning topographers depend on the reflection of light from the corneal surface; any loss of transparency, for example, corneal haze or scarring, could be a major hindrance to acquiring reliable information from the posterior surface. The latest development in the field of corneal tomography is the assessment of corneal shape using Scheimpflug imaging (Ambrosio et al., 2006). This technique derives 25,000 data points that are used to reconstruct the shape of the cornea and anterior segment and uses information derived from sections to reconstruct the corneal shape. Importantly, the elevation measurements on the cornea do not depend on the axis, orientation and clarity of the corneal interface (Ambrosio et al., 2006). Understanding the characteristics of the posterior corneal surface has been particularly of interest from the refractive surgery perspective, as the forme-fruste keratoconus is a significant risk factor for developing post operative corneal ectasia following laser in-situ keratomileusis (Randleman et al., 2008). A three-dimensional reconstruction of the corneal shape with the Scheimpflug imaging has been

regularly compared with a more direct measurement of the corneal surface with the optical coherence tomography (OCT) techniques. The assessment of corneal structures obtained with Scheimpflug imaging has been shown to be comparable with the high resolution swept-source OCT imaging devices (Nam et al., 2010, Saad et al., 2023).

2.1.2. Metrics used for detection of keratoconus

The use of metrics to detect keratoconus has developed in parallel to the changes in keratoscopes. Very early in the development of photo and videokeratoscopes, it was evident that a measure of central corneal curvature provided by keratometers, which assumed regular astigmatism, could not explain the structural complexity of the change in ectactic corneal disorders such as keratoconus. During the rapid development of Placido-based topographers in the 1990s, all the possible indices for detecting keratoconus were derived from measures of the front surface of the cornea, either the spatial and global distribution of curvature across cornea, or, the difference in curvature values across different meridians (Maeda et al., 1994). Indices included simulated keratometry (Sim K), surface asymmetry index (SAI), inferior-to-superior asymmetry (I-S), skewing of radial axis (SRAX), differential sector index (DSI), opposite sector index (OSI), centre surround index (CSI), irregular astigmatism index and analysed corneal area (Maeda et al., 1994). They form the basis of indices that have become widely used such as the keratoconus prediction index (KPI) (Maeda et al., 1994) and the KISA% index proposed by Rabinowitz (1995) and Rabinowitz and Rasheed (1999).

The addition of slit-scanning and Scheimpflug imaging technology introduced three additional important parameters to the previous list of indices for detecting keratoconus: the posterior corneal curvature (Tomidokoro et al., 2000); corneal thickness parameters such as thinnest pachymetry and central corneal thickness (Kawana et al., 2005, Saad and Gatinel, 2010); and, anterior and posterior surface elevation (Rao et al., 2002, Saad and Gatinel, 2010). Saad and Gatinel (2010) explained the global nature of the corneal thickness parameter and suggested

that the change in corneal thickness from centre to the periphery of the cornea can be a better predictor to assess early changes in keratoconus as compared to using only thinnest pachymetry or central thickness values. Kawana et al. (2005) noted that slit-scanning technology systematically underestimates the pachymetry values compared to ultra-sound pachymetry. A mean difference in central corneal thickness of 35 microns between the two different techniques was noted to be statistically significant (Kawana et al., 2005). Two possible reasons were postulated for this: first, the reconstruction algorithm that is usually calibrated for the control population gets disrupted in cases of an ectatic corneal disorder; and, second, the pathway of the reflected light ray gets interrupted in the possible presence of any optical interfaces in the cornea. Scheimpflug imaging did compensate for these methodological limitations; O'Donnell and Maldonado-Codina (2005) showed a comparable assessment of central corneal thickness with Scheimpflug imaging and ultrasound pachymetry. In line with the observation of Saad and Gatinel (2010), Ambrosio et al. (2006), with the help of Scheimpflug imaging, introduced indices such as corneal thickness spatial profile (CTSP), percentage thickness increase (PTI) and pachymetry progression index (PPI), which provided the spatial distribution of thickness profile of the cornea from the centre to the periphery. Later, Ambrosio et al. (2011) introduced a cumulative index called the Ambrosio relational thickness (ART) that includes both the element of thinnest pachymetry and the maximum PPI values. This index was shown to have the highest sensitivity and specificity compared to single point assessments such as the thinnest pachymetry or the central corneal thickness alone (Figure 2.3).

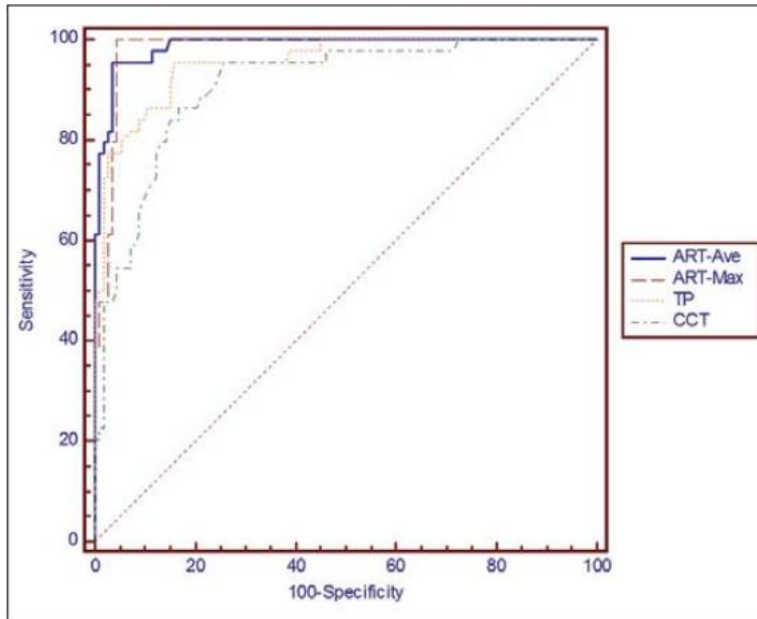


Figure 2.3: Receiver operating curves for the different thickness indices. The highest area under the curve occurs for the Ambrosio relational thickness-maximum (ARTmax) compared to single point measurements such as thinnest pachymetry and central corneal thickness (Taken from Ambrosio et al. (2011)).

Similar to the corneal thickness, evaluation of corneal elevation was made possible with the slit-scanning and Scheimpflug imaging technology, which added another dimension to the detection of keratoconus, as the quantification of elevation maps could provide a better explanation of the morphology of the cone. Rao et al. (2002), with the help of slit scanning videokeratoscopy, showed an increase in posterior corneal elevation in a cohort of keratoconus suspects who otherwise had a corneal thickness comparable to that of the controls. de Sanctis et al. (2008) used the Scheimpflug technique to reiterate this finding and showed the posterior elevation maps to have a high sensitivity and specificity for both established keratoconus (97.3% and 96.9% respectively) as well as forme-fruste keratoconus (92% and 75.4% respectively). Pinero et al. (2012) and Ucakhan et al. (2011), in their respective reports, introduced surface irregularity indices, such as the surface asymmetry index (SAI), index of surface variance (ISV), index of vertical asymmetry (IVA), keratoconus index (KI), central keratoconus index (CKI), smallest radius of curvature (R_{\min}), index of height asymmetry (IHA) and index of height decentration (IHD), which could be derived from proprietary software used

in Scheimpflug imaging devices. Ucakhan et al. (2011) tried to assess the diagnostic ability of the different curvature, thickness and elevation-based indices, when they are used in combination as compared to when used in isolation. The results clearly suggested that the effectivity becomes higher when they are used in combination, as was evident from a higher sensitivity, specificity and area under the receiver operating curve for both the established as well as sub-clinical keratoconus cohort (Ucakhan et al., 2011).

Table 4. Sensitivity and specificity of the logistic regression analysis of the 7 models studied in keratoconus and subclinical keratoconus versus normal eyes.

Parameter	Normals Vs Keratoconus		Normals Vs Subclinical Keratoconus	
	Sensitivity	Specificity	Sensitivity	Specificity
Model 1	88.6	95.2	68.2	90.5
Model 2	79.5	88.9	54.5	85.7
Model 3	86.4	88.9	56.8	85.7
Model 4	93.2	87.3	70.5	85.7
Model 5	97.7	95.2	70.5	88.9
Model 6	93.2	95.2	77.3	92.1
Model 7	88.6	95.2	75.0	92.1

Model 1 = flat keratometry + steep keratometry + mean keratometry + ventral corneal thickness + minimum corneal thickness + maximum anterior power at central 4.0 mm + maximum posterior power at central 4.0 mm; Model 2 = maximum anterior elevation at central 5.0 mm + maximum anterior depression at central 5.0 mm + anterior elevation depression difference + anterior elevation depression difference/best-fit sphere; Model 3 = maximum posterior elevation at central 5.0 mm + maximum posterior depression at central 5.0 mm + posterior elevation depression difference + posterior elevation depression difference/best-fit sphere; Model 4 = maximum progression index + minimum progression index + mean progression index; Model 5 = Model 1 + Model 2; Model 6 = Model 1 + Model 3; Model 7 = Model 1 + Model 4

Table 2.1: This table lists the different models adapted by Ucakhan et al. (2011), that includes multiple indices to detect keratoconus (Taken from Ucakhan et al. (2011)).

During the period when the multifactorial approach was gaining significant recognition, Ambrósio Jr et al. (2013) used the Belin-Ambrosio enhanced ectasia display (BAD) to introduce the multimetric D-index. The D-index, which is proprietary to the Scheimpflug imaging techniques from the Oculus Pentacam device (Oculus Optikgeräte GmbH, Wetzlar, Germany), is a composite index that usually comprises of five different elements based on thickness and elevation measures of the cornea: deviation of front surface elevation difference (D_f), deviation of back surface elevation difference (D_b), deviation of pachymetric progression (D_p), deviation of thinnest point (D_t) and deviation of ART_{Max} (D_a) (Ambrósio Jr et al., 2013, Duncan et al., 2016). The BAD display uses an “enhanced reference surface” compared to the

routinely used “best-fit sphere” reference surface (Ambrósio Jr et al., 2013, Belin and Duncan, 2016). The enhanced reference surface is calculated by excluding a three to four mm zone, which is centred around the thinnest point of the cornea. The thinnest point of the cornea usually coincides with the steepest curvature points in keratoconus and therefore, the enhanced reference surface becomes significantly flatter than the regular one. This approach improves the ability to detect early elevation on the corneal surface. Muftuoglu et al. (2015) compared the diagnostic performance of the D-index against all the previously mentioned curvature, pachymetry and elevation based metrics. Their report showed an absolute sensitivity and specificity (100%) for a cut-off value of 2.1 units of D-index to diagnose keratoconus from a normal cornea, which was superior to any other index used. In spite of a drop in the sensitivity and the specificity values, this index remained superior while detecting subclinical keratoconus compared to controls (Figure 2.4) (Muftuoglu et al., 2015). In a recent retrospective cohort study, Koc et al. (2020) reported the diagnostic performance of different topographic and tomographic indices to detect subclinical keratoconus. The results were closely aligned to those of Muftuoglu et al. (2015). and reaffirmed the superior ability of the multimetric D-index to diagnose keratoconus (Muftuoglu et al., 2015).

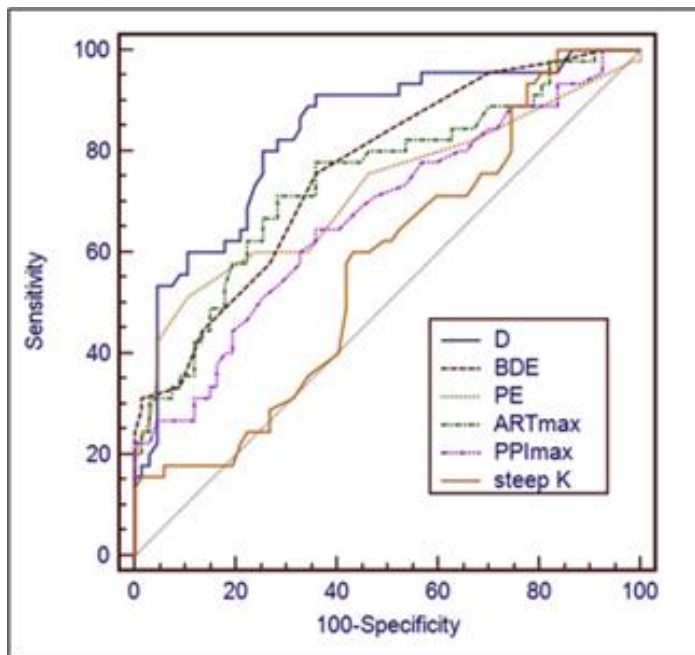


Figure 2.4: Receiver operating curves comparing the performance of the multi-metric D-index against different curvature, thickness and elevation-based indices for detection of subclinical keratoconus from the controls. This shows the highest area under the curve for the D-index (Taken from Muftuoglu et al. (2015)).

Optical coherence tomography has been used to explore different other dimensions of corneal shape. In a retrospective comparative study, Temstet et al. (2015) used a Fourier domain OCT to demonstrate that the corneal epithelial mapping can improve the ability to detect forme-fruste keratoconus. The results showed a typical pattern of the epithelial thickness map in keratoconic corneas, where forme-fruste keratoconus had epithelial thinning at the thinnest corneal zone relative to the age-matched controls, this was greater than established keratoconus subjects. They also suggested that the location of the thinnest point of epithelium may not be an independent marker to identify keratoconus. However, when combined with the other conventional parameters of corneal curvature, thickness, and elevation, the location of the thinnest point of the epithelium may significantly improve the detection ability of forme-fruste keratoconus. Interestingly, some studies have hypothesized a compensatory mechanism behind this occurrence, wherein, the epithelium becomes thinner in the area corresponding to the cone of keratoconus in order to maintain a more regular anterior surface of the cornea and minimize the irregularity caused by the protrusion (Reinstein et al., 2009).

Presently, a significant amount of research is exploring the biomechanical properties of the cornea and the potential role it plays in development of keratoconus. Although the role of corneal biomechanics is well established in the literature, these results have been largely inferred from indirect and static morphological observations of the cornea. De Stefano et al. (2020) addressed this knowledge gap by assessing the displacement of the cornea for a known amount of applied pressure, using a swept-source optical coherence elastography system. Their method also helped to delineate the depth-related biomechanical properties of the cornea. In normal eyes, the anterior stroma is expected to have greater stiffness compared to the posterior stroma. However, this equation changes in keratoconus, wherein, the anterior stroma shows a significant drop in its stiffness. This result generates new perspectives for keratoconus; the relative weakening of the anterior stroma, possibly combining with alteration of microscopic structures such as the arrangements of the collagen fibrils, could be hypothesized as a potential cause of the protrusion.

2.1.3. Assessment of progression in keratoconus

An intrinsic characteristic of keratoconus is the progressive change in corneal structure. A change in corneal curvature does not comprehensively capture the structural change in the cornea. Therefore, having a comprehensive understanding of the different corneal parameters (e.g., curvature, thickness, and elevation) remains critical in terms of determining the course of action the practitioner should take. Practically, all the indices that were discussed in the previous section, have been tested as potential markers of progression of the disease. Although, there are some indices that have been shown to have good correlation with keratoconus progression, there is still a lack of consistency in the definition of progression (Gomes et al., 2015).

Traditionally, the term progression is related to a chronic increase in corneal curvature. Choi and Kim (2012) longitudinally assessed the different curvature, thickness and elevation-based indices from slit-scanning technology combined with a Placido-based faceplate (Orbscan IIz) in a cohort of mild to moderate keratoconics. An increase in the central corneal curvature of at least 1.50 D was considered for the keratoconus to be termed progressive. Their results found that 26.5% eyes showed progression after one year, which increased to 76% after five years of follow up (Figure 2.5). The maximum keratometry, anterior as well as posterior elevation maps, and thinnest pachymetry values were the significant predictors of disease progression. While assessing the rate of change in the topometric indices, the progressive keratoconus cohort also revealed a mean change of ≥ 0.15 D/year in the maximum keratometry value (Choi and Kim, 2012).

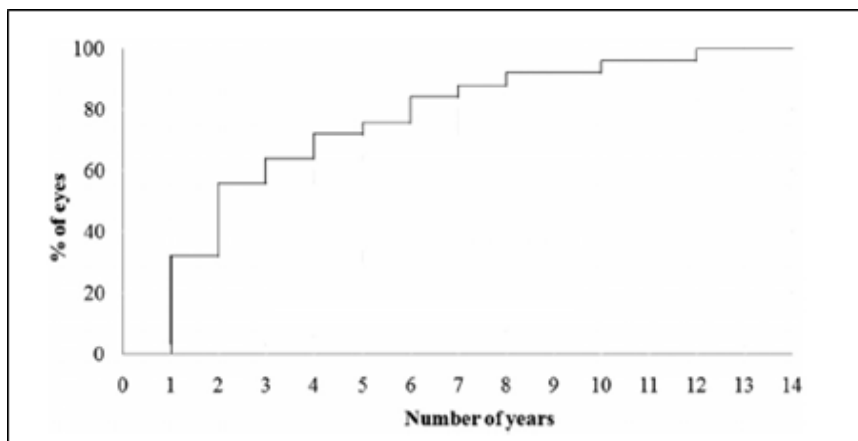


Figure 2.5: Cumulative frequency curve showing the years taken to reach the progression group as defined by the authors. (Taken from Choi and Kim (2012)).

Kanellopoulos and Asimellis (2013) studied the topometric features derived from Scheimpflug imaging (see section 2.1.2) and their ability to assess progression of keratoconus. In general, the correlation was found to be moderate to low with all the indices. However, the global curvature-based index of surface variance (ISV) and the global elevation-based index of height deviation (IHD) were shown to have the best correlation with disease severity (Pearson's

correlation, $r = -0.75$ and $r = -0.63$ respectively) and therefore the authors concluded they were reliable markers to explain disease progression (Kanellopoulos and Asimellis, 2013).

In general, the parameters used to detect keratoconus are very similar to those used to determine progression of the disease. The shift from a single metric approach (e.g., steep keratometry or thinnest pachymetry or elevation) to multi metric approach (e.g., combination of curvature and thickness or curvature and elevation) for the detection of keratoconus was analogous to that discussed in the section 2.1.2. In their review article, Martinez-Abad and Pinero (2017) addressed this shift by explaining the heterogeneous nature of the disease and the fact that a single factor would therefore not be sufficient to define progression of keratoconus. A general consensus was achieved that topographic and refractive measures should be complimented by comprehensive pachymetry as well as corneal aberration reports that can be derived from Scheimpflug imaging technology (Martinez-Abad and Pinero, 2017). Analogous to the work by Muftuoglu et al. (2015) discussed in section 2.1.2, Shajari et al. (2019) tested the performance of multi-metric D index and compared its effectivity in detecting progression with respect to other single metric and global topometric indices. Their results clearly established that the D-index and the keratoconus progression index have a higher sensitivity and specificity to assess keratoconus progression compared to unimetric indices (Figure 2.6).

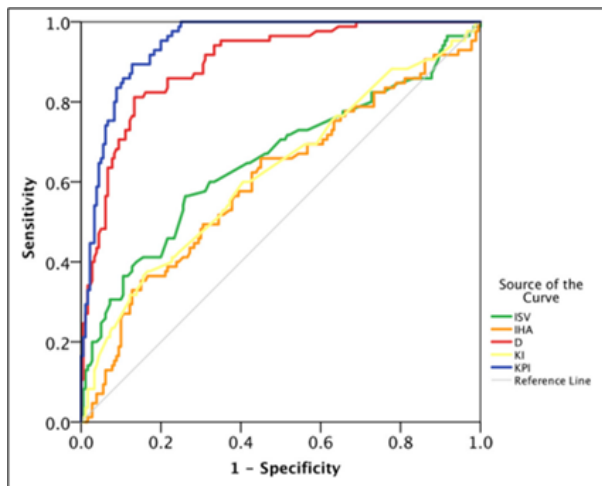


Figure 2.6: Receiver operating curves suggesting a superior performance of multi-metric D-index and keratoconus progression index (KPI) compared to other unimetric indices from Scheimpflug imaging (Taken from Shajari et al. (2019)).

Repeatability of the indices are necessary as a viable option to detect keratoconus as well as monitoring its progression. A lack of repeatability would result in developing erroneous management strategies for keratoconus., Primarily, intra-session repeatability is essential for the metric to be considered reliable. This suggests minimum variations among the multiple tests conducted from the same instrument across different trials. Secondly, agreement of measurements within instrument, specifically considering the different instruments available in the clinic for detecting keratoconus. Meyer et al. (2017) assessed both of these measures of repeatability with a combination slit-scanning and Placido disc-based instrument, and single and dual-Scheimpflug based instruments. Results suggested that the overall intrasession repeatability was high with all the instruments with Scheimpflug imaging techniques having the highest repeatability. However, the outcome from the different instruments varied independent to each other suggesting a lack of agreement between them. Shetty et al. (2014) reported a similar result where the standard deviation for the intra-session measurements within the instruments was low and within acceptable range. However, a wide 95% limits of agreement among the different devices suggested that they cannot be used interchangeably to detect and monitor the disease progression.

2.1.4. Grading severity scales in keratoconus

As discussed in the section 2.1.3., keratoconus is a progressive condition and patients can present at different stages of the disease. To determine the stage of disease is useful for two reasons: first, from a clinical standpoint, understanding the degree of keratoconus is essential as that can play a role in tracking the disease severity and eventually have an implication for treatment options. Second, from a research standpoint, it will be inappropriate to extrapolate the result of a keratoconus cohort at a specific stage of severity to the general disease population because the condition is progressive.

Over the years, attempts have been made to grade the severity of keratoconus. The indices discussed in sections 2.1.2 and 2.1.3 have been explored as methods to grade the change in keratoconus severity and therefore create a grading scale. Individual indices such as the keratoconus prediction index (Maeda et al., 1994), KISA % index (Rabinowitz and Rasheed, 1999) and cone location and magnitude index (Mahmoud et al., 2008) have been discussed at great length to classify keratoconus. However, for a grading scale to achieve wide applicability, particularly in a clinical scenario, different facets of the condition need to be considered rather than focussing on indices that represent specific features.

Amsler-Krumeich classification is one of the most commonly used grading systems to date (Krumeich et al., 1998, Kanellopoulos and Asimellis, 2013, Kamiya et al., 2014, Kamiya et al., 2018, Ortiz-Toquero et al., 2020, Marella et al., 2021). The classification includes four different components of the disease: mean central corneal curvature; central corneal pachymetry; degree of induced myopia with/without astigmatism; and, presence or absence of a corneal apical scar. Alio and Shabayek (2006) argued that inclusion of the degree of myopia without considering the axial length could cause a significant overlap between the groups. In addition, they measured the higher order aberrations from the anterior corneal surface and showed a significant correlation of coma-like aberrations with the different grading scales. Therefore,

they proposed a modified version of the Amsler-Krumeich classification with the exclusion of the refractive error and astigmatism component and including coma-like aberrations (Alio and Shabayek, 2006). A recent study by Ortiz-Toquero et al. (2020) found similar results to the work of Alio and Shabayek (2006). Their group conducted a cross-validation study where the aim was to find out if corneal front surface higher order aberrations are able to discriminate between the different keratoconus stages. Their results clearly suggested that the third-order aberrations and specifically coma-like aberrations had high sensitivity and specificity values for differentiating between normal controls and mild keratoconus (sensitivity 99%; specificity 100%), mild and moderate keratoconus (sensitivity 90%; specificity 100%) and between moderate to severe keratoconus (sensitivity 97%; specificity 81%). These values were significantly improved compared to the other aberrations such as trefoil, tetrafoil, secondary aberrations and spherical aberration (Ortiz-Toquero et al., 2020).

Another prominent grading scale proposed in the literature comes from the Collaborative Longitudinal Evaluation of Keratoconus (CLEK) study group. This scale initially included only the average keratometry value (Zadnik et al., 1996). However, McMahon et al. (2006) later restructured the grading scale to create the keratoconus severity score (KSS), which included other aspects such as higher order RMS, presence of biomicroscopic signs, as well as a corneal scar. The components from both the Amsler-Krumeich and the KSS grading systems are very similar to each other apart from the additional consideration of corneal thickness in the Amsler-Krumeich classification. This might explain the wider usage of the Amsler-Krumeich grading system.

One of the common traits discussed in the sections 2.1.2 and 2.1.3 is the consideration of the posterior corneal surface. Kanellopoulos and Asimellis (2013) showed that global topometric indices such as the index of surface variance (ISV) and the index of height deviation (IHD) were able to successfully determine the different stages of keratoconus and therefore, proposed

the inclusion of these parameters into the Amsler-Krumeich grading scale. However, this new scale has not been used further in the literature, possibly due to significant intra-observer variability as well as the complex nature of the algorithm determining these metrics (Kanellopoulos and Asimellis, 2013).

An important aspect to note in this context is that the single metric and multimetric indices that have been mentioned in the sections 2.1.2 and 2.1.3 are used in the literature to grade disease severity. Many of these indices are not instrument specific and therefore, can be derived from different instruments and can be used as a metric to determine the severity. Typically, a cut-off value is assigned to these metrics to allow differentiation between a normal cornea, a keratoconus suspect and an established keratoconus. For example, unimetric indices such as simulated keratometry (Smolek and Klyce, 1997), corneal asphericity (Pinero et al., 2010), inferior to superior difference (I-S index) (Shetty et al., 2017), surface asymmetry index (SAI) (Wilson et al., 1991), or multimetric indices such as KISA% index (Rabinowitz and Rasheed, 1999), keratoconus probability index (KPI) and its components (Shetty et al., 2017) could be derived from any videokeratographic system based on either Placido-disc, slit-scanning or Scheimpflug imaging. However, there are also indices such as the index of surface variance (ISV) (Kanellopoulos and Asimellis, 2013) or D-index (Duncan et al., 2016) that are proprietary to the Scheimpflug imaging techniques from the Oculus Pentacam device (Oculus Optikgeräte GmbH, Wetzlar, Germany) alone.

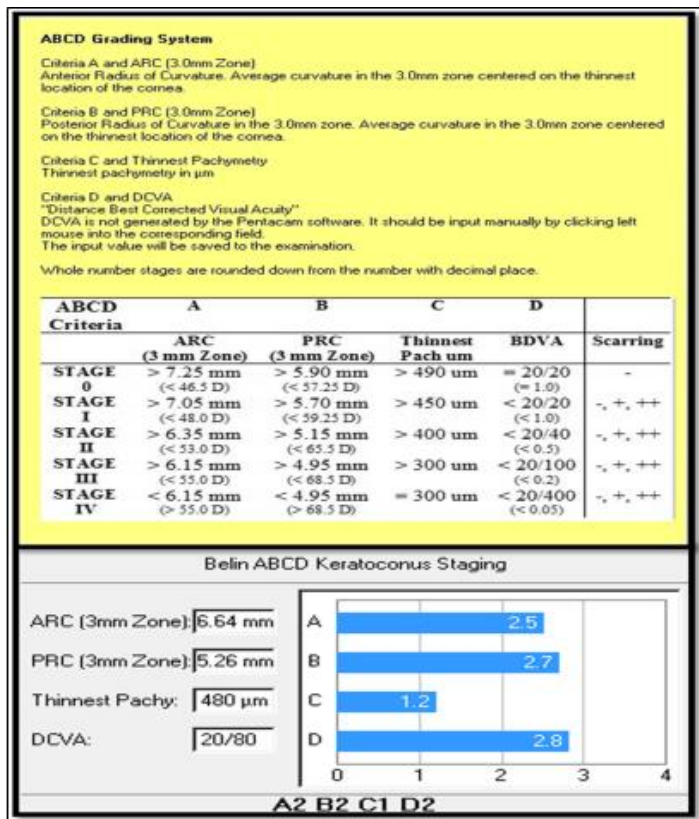


Figure 2.7: The upper image (in yellow) shows the different elements of “ABCD” grading system. The lower image shows a representative image of a keratoconus eye from the output image from the Oculus Pentacam Scheimpflug imaging device, where the “ABCD” map has quantified the stage of keratoconus. (Taken from Duncan et al. (2016)).

There are two major limitations of the Amsler-Krumeich classification. First, the structural assumptions are based solely on the anterior surface of the cornea. Second, the consideration of central corneal thickness may not be a correct representation of the actual thinning of the cornea, specifically when the apex of the cone is decentred (Kamiya et al., 2014). To address these issues, Duncan et al. (2016) proposed the “ABCD grading system”, using the Belin-Ambrosio enhanced ectasia display algorithm (see section 2.1.2). The three mm optical zone, centred on the thinnest point of the cornea that was eliminated to create the “enhanced reference surface” (discussed in section 2.1.2) was now used as a reference to measure the different elements of this ABCD grading scale (Figure 2.7). This contained four parameters: “A” represented the curvature of the anterior surface, for a three mm zone centered on the thinnest point of the particular cornea; “B” represented the curvature value for the posterior cornea; “C”

represents the thinnest pachymetry value itself; and “D” represented the best corrected visual acuity with spectacle correction. The element of acuity was included to add a functional element to the grading scale. The recent review by Belin et al. (2022) suggested that, in spite of the obvious advantages of the ABCD grading scale, the Amsler-Krumeich classification remains the most widely used in clinical as well as research fields.

2.2. Functional changes in keratoconus

2.2.1. Optical performance of eyes with keratoconus

The irregularities in the corneal shape in conditions such as keratoconus result in significant ocular aberrations. These ocular aberrations are usually classified using Zernike polynomial terms and can be categorized into two groups, lower order aberrations (LOAs) and higher order aberrations (HOAs). The aberrations up to the second order polynomial terms are called the LOAs and are correctable with regular spectacles or conventional soft contact lenses. Aberrations calculated from the third order terms and above are called the higher order aberrations, and they cannot be corrected with conventional soft contact lenses. In an otherwise normal eye, the LOAs largely account for any deficit in vision. However, for conditions such as keratoconus, where the HOAs are abnormally raised compared to the normal population, HOAs have a significant impact on vision.

In the spatial domain, the impact on retinal image quality can be described by the point spread function (PSF), which is defined as the image of a point object after it has passed through an optical imaging system. The PSF remains radially symmetric in the presence of spherical ametropia (defocus) and has an axis of symmetry in the presence of regular astigmatism, both lower order aberrations. However, it can become increasingly asymmetric when HOAs increase. Pupil size fundamentally affects the magnitude of aberrations and has been shown to be directly proportional to the size of the point spread function (Marcos, 2003). As a result, the impact of aberrations on visual performance will be dependent on pupil size. In the frequency

domain, the same information can be expressed in the form of the optical transfer function (OTF). The OTF has two parts, the phase transfer function (PTF) and the modulation transfer function (MTF). The modulation transfer function describes the amount of contrast retained in the image for different spatial frequencies (Thibos et al., 2004). Artal and Guirao (1998) showed that under normal circumstances, the higher order aberrations of the two major refractive components of the eye, cornea and crystalline lens, act against each other in young eyes to optimize the resultant retinal image quality.

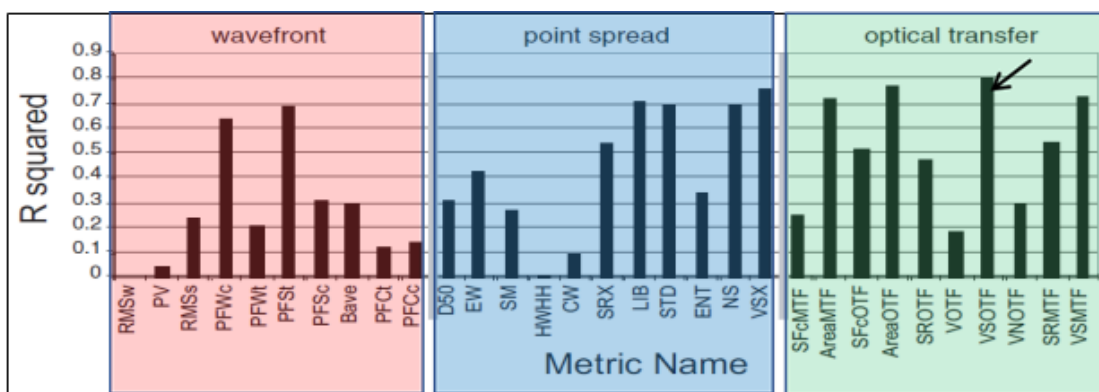


Figure 2.8: The correlation of different image quality metrics with high contrast visual acuity. The three panels indicate pupil-based metrics (Red), PSF-based metrics (Blue) and OTF-based metrics (Green). The VSOTF metric showed the best correlation among all the other metrics (indicated with black arrow head) (Adapted from Marsack et al. (2004)).

Overall, 33 different metrics have been mentioned in the literature that have been used to assess retinal image quality. These metrics are either based on the quality of the wavefront aberration pattern captured at the pupillary plane, based on point spread function or based on the optical transfer function. Marsack et al. (2004) reviewed the predictability of all these metrics for visual performance in normal eyes. Their reports showed that the Visual Strehl ratio had the highest association with both the point spread function and the optical transfer function compared to other metrics of visual performance (Figure 2.8).

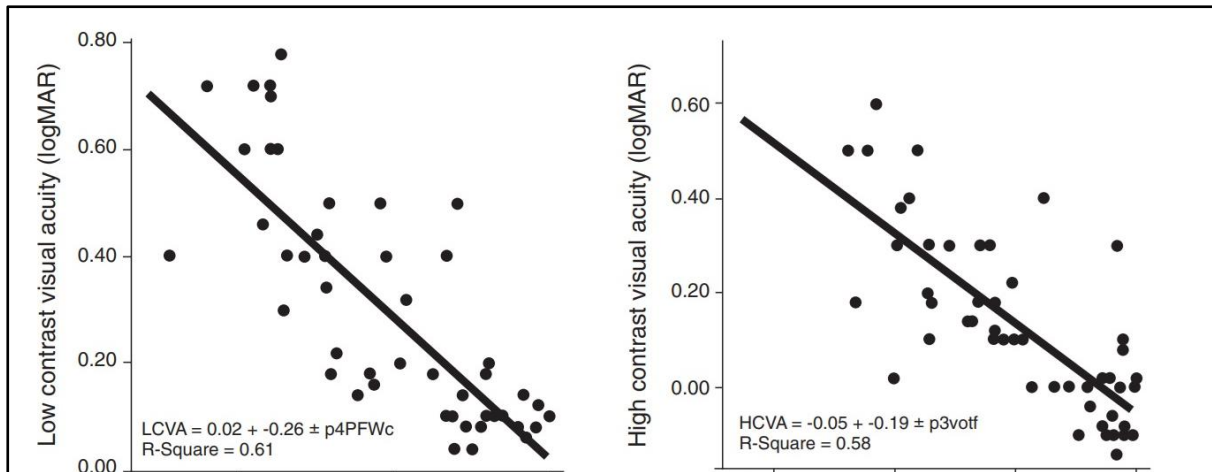


Figure 2.9: The low and high contrast logMAR acuity plotted against the two retinal image quality metrics. Both these metrics showed better correlation with visual functions compared to the others (Adapted from Schoneveld et al. (2009)).

In general, the increase in HOAs in a keratoconic eye results in a radially asymmetric wavefront pattern and a large point spread function. In the frequency domain, these changes are characterized by a loss in contrast as a function of spatial frequency, or in other words, an attenuation of the OTF (Thibos et al., 2004). In these eyes, few metrics have been shown to correlate well with different measures of visual function. Schoneveld et al. (2009) compared the ability of different metrics to predict a range of acuity and contrast sensitivity tasks in keratoconic eyes. Their results showed that pupil fraction for curvature, a pupil plane metric, and volume optical transfer function, an OTF based metric, had a very good correlation with measures of visual function ($r > 0.75$) (Figure 2.9). Ravikumar et al. (2013) reported that a change in high contrast visual acuity was best correlated ($r > 0.8$) with two PSF-based metrics, neural sharpness and visual Strehl ratio (Ravikumar et al., 2013). Using the same neural sharpness metric, Nilagiri et al. (2020) provided a detailed explanation of the retinal image quality in keratoconus and compared it to age-similar controls. A through focus analysis of the image quality showed that unlike controls, where a distinct peak image was accompanied by a systematic drop in quality on either side of defocus, the keratoconic eyes showed a significantly flatter profile, where the peak image was deteriorated significantly. Here, a drop in image

quality was related to a reduction in neurally weighted visual Strehl ratio (Guirao and Williams, 2003, Thibos et al., 2004). In addition, the image quality remained similar across a large range of defocus, indicating a deficiency of the optical system to differentiate between different levels of defocus, making the system less sensitive (Figure 2.10) (Nilagiri et al., 2020).

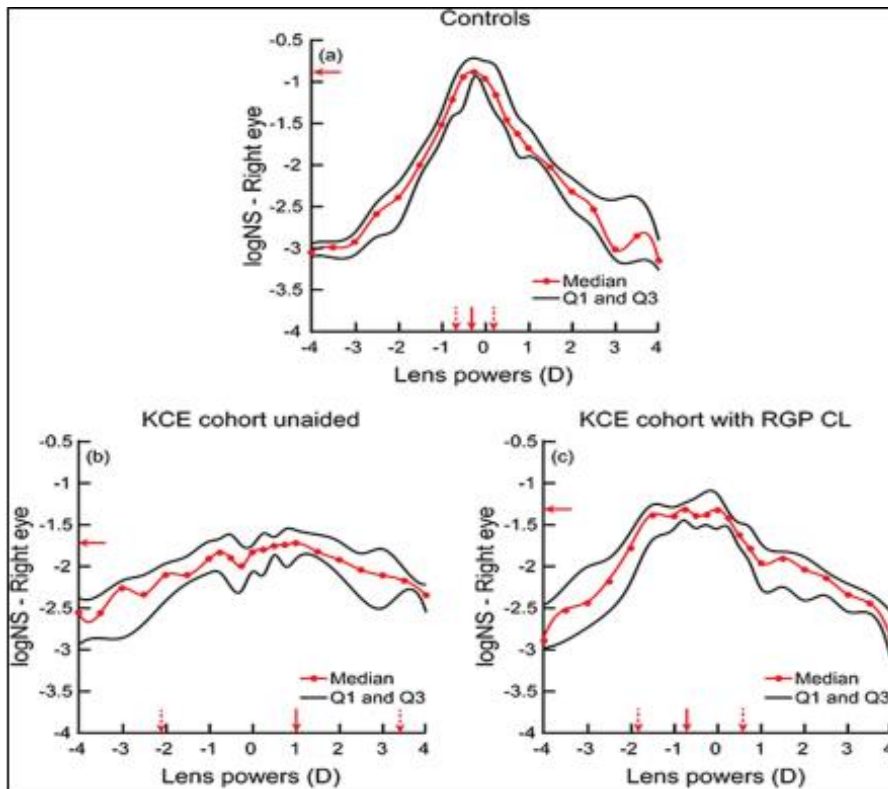


Figure 2.10: The computationally analysed through focus curve depicted the peak IQ (horizontal red arrow) and the depth of focus (Vertical solid and broken arrows) for 20 control eyes (a), right eyes of 12 bilateral keratoconus eyes under unaided condition (b) and the same keratoconus eyes with RGP CLs (c). Results indicated a narrowing down of depth of focus in keratoconus eye after using RGP CLs, however, unable to reach the level of the controls (Adapted from Nilagiri et al. (2020)).

2.2.2. Visual performance of eyes with keratoconus

As a consequence of impaired retinal image quality in keratoconus (section 2.2.1), visual function can become compromised. On average, the HOAs of eyes with mild-to-moderate keratoconus are five to six-fold higher than age-similar controls (Nilagiri et al., 2018). Therefore, achieving a complete restoration of visual performance with spectacles or conventional soft contact lenses (SCLs) is expected to be challenging. A deterioration of high

contrast visual acuity has almost always been reported in the literature (Davis et al., 2006, Lee et al., 2013, Belin and Duncan, 2016). Nilagiri et al. (2018) showed that high contrast visual acuity with best corrected spectacles was on average two to three-fold poorer in a cohort of mild to moderate keratoconics compared to age similar controls (Figure 2.11). This drop in performance is expected to scale with more severe forms of the disease as the influence of the HOAs increase.

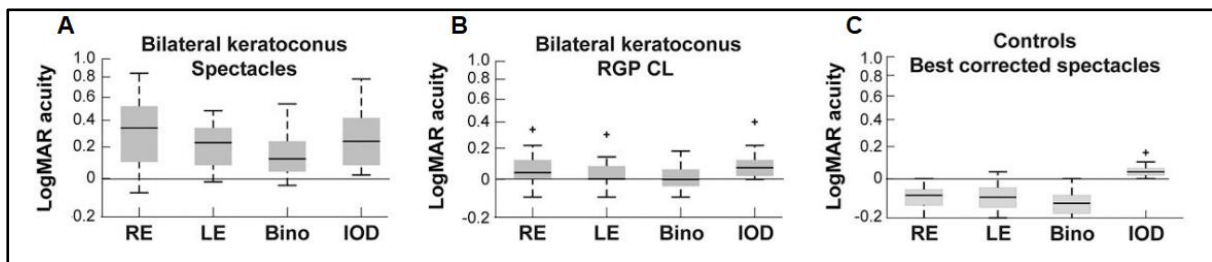


Figure 2.11: High contrast visual acuity of each eye individually as well as binocularly for a cohort of bilateral keratoconus subjects, with their best corrected spectacles (A) and RGP contact lenses (B) along with the performance of the age-similar controls with their best corrected spectacles (C) (Adapted from Nilagiri et al. (2018)).

Despite its widespread use in the literature, high contrast visual acuity has been considered a “shallow” measure of visual performance, which may not comprehensively explain the visual deficit experienced by the patient (Carney, 1982, Bullimore et al., 1991). This is evident from a significant decrease in self-reported quality of life in patients with good levels of high contrast acuity compared to controls (Kandel et al., 2020). As a result, the spatial contrast sensitivity function has been proposed as a more comprehensive measure of visual performance. Shneor et al. (2021) have reported a drop in contrast sensitivity in a cohort of patients with keratoconus who otherwise possessed 0.00 logMAR high contrast acuity.

Until recently, reports of binocular visual performance have been rarely mentioned in the literature. Studying this function is useful for two reasons: first, the natural day to day operation of an individual is usually dependant on binocular performance; and, second, the usual presentation of keratoconus is asymmetric with a significant inter-ocular difference in higher

order aberration and subsequently retinal image quality (Nilagiri et al., 2018, Nilagiri et al., 2020). Since binocular visual function is predominantly dependant on the ability to overlap the information gathered by individual eyes, this is expected to be affected in keratoconus. Nilagiri et al. (2018) has reported a 12-to-15-fold deterioration in stereo performance in a mild to moderate keratoconic cohort with best corrected spectacle correction (Figure 2.12).

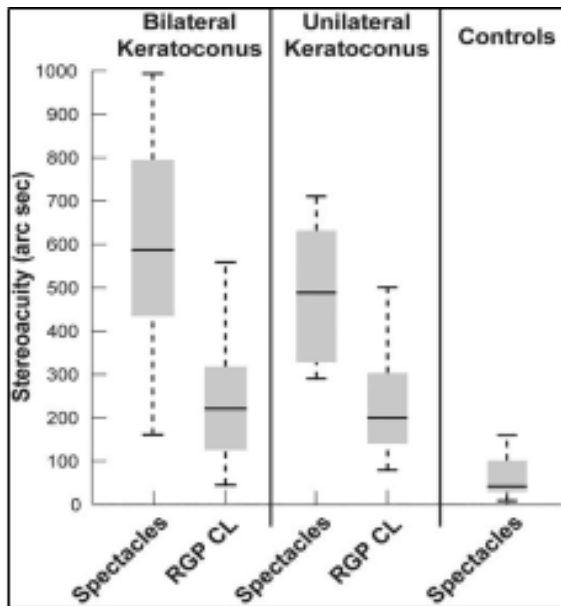


Figure 2.12: Box and whisker plots showing the stereoacuity results for a cohort of unilateral and bilateral keratoconus with mild to moderate disease severity, with their best corrected spectacles and with the RGP contact lenses. The results show a significant improvement in performance with the lenses, although it does not reach the level of the controls (Adapted from Nilagiri et al. (2018)).

Two reasons have been proposed to explain the loss in stereoacuity. The first is a failure in correspondence matching. Metlapally et al. (2019), through a cross-correlation model, have shown that the presence of higher order aberration, and in particular, high inter ocular difference in retinal image quality, results in a reduced ability to detect small amounts of disparity (Metlapally et al., 2019). Another reason was recently suggested by Marella et al. (2021), who explored the concept of suppression of the weaker eye when the two eyes are presented with significantly disparate retinal image quality. Although, similar phenomena in the spatial domain have been explored in conditions such as amblyopia (Holopigian, 1989), the

depth of suppression in the weaker eye (more severe) has been discussed for the first time for keratoconus. This report proposed that the poor image contrast in the weaker eye is the reason for the inability to successfully combine the retinal images from both eyes resulting in a loss of stereoacuity (Marella et al., 2021).

Although traditional measures of threshold visual function could recognize the general impact of the disease, these metrics alone fall short of capturing the full impact on a patient's functional abilities in managing their day-to-day activities. This is because they fail to take into account the individual's personal characteristics, emotional responses, social interactions, experiences, expectations during specific tasks conducted throughout the day and importantly, the strategies individuals might employ to manage their condition. Therefore, the results obtained from visual tests may not be directly extrapolated to the quality of life (QOL) of keratoconic patients. This has led to increased use of questionnaire based QOL outcome measures. Questionnaires such as the National Eye Institute-visual function questionnaire (NEI-VFQ) (Panthier et al., 2020), impact of vision impairment (IVI) (Kandel et al., 2022), and contact lens impact on quality of life (CLIQ) (Erdurmus et al., 2009) have been used to assess QoL in patients with keratoconus. The reports are in agreement that there is a disproportionate loss in QOL when compared to conventional measures of visual function. However, one of the major limitations with these questionnaires is the lack of disease specificity, as they were not primarily designed for keratoconus. To overcome this, Khadka et al. (2017) proposed the Keratoconus Outcome Research Questionnaire (KORQ), which is disease-specific, and successfully demonstrated the loss in QOL in keratoconus.

2.2.3. Threshold Vs suprathreshold performance in keratoconus

The studies reported in the previous section all assessed visual performance at a threshold, or, at the detection level. However, many of our daily activities are supra-threshold visual tasks that may not relate to threshold level performance. Assessing suprathreshold performances may therefore be very relatable to the daily activities. Georgeson and Sullivan (1975) measured the perception of contrast by a technique of subjective contrast matching and compared that with the sensitivity defined by the threshold assessments. The results demonstrated a systematic difference between the threshold and suprathreshold level function. In addition, they suggested that the visual system develops a compensatory mechanism to adjust the neural noise that are responsible for a drop in contrast sensitivity at the threshold level, a phenomenon they termed ‘contrast constancy’ (Figure 2.13) (Georgeson and Sullivan, 1975).

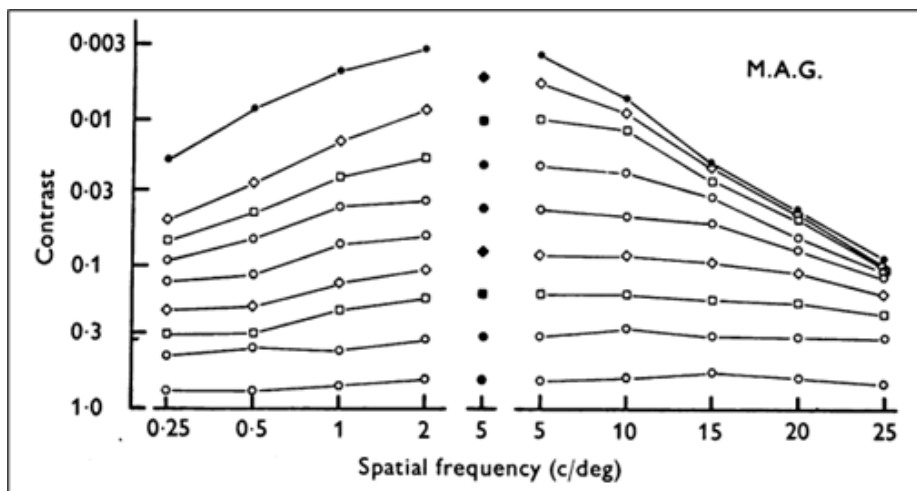


Figure 2.13: The perception of contrast at threshold (outer most curve of the graph) and different suprathreshold levels (inner curves) for a particular subject (M.A.G). A systematic deviation from the trademark inverted “U” pattern (threshold) was noted for the suprathreshold space as the curves appeared to be increasingly straightened as the contrast level increased, indicating the invariable perception of contrast across the spatial frequencies. (Taken from Georgeson and Sullivan (1975)).

A similar relationship between the threshold and suprathreshold level performance was investigated by Patel et al. (2009) in the field of binocular depth perception. The results concurred with those seen at a spatial level and a systematic difference between the two was

noted. Since, the threshold level function significantly deteriorates in keratoconus, it would be intuitive to think that the effect of this will also translate to the suprathreshold space. In other words, there will be a disruption noted in the above-mentioned compensation process. On the other hand, however, if the keratoconic system still shows a compensatory mechanism, that would indicate an adaptation of the visual system in these eyes that is overriding the optical limitation posed by the structural change in the cornea. To date, there is only one recently published report by Ng et al. (2022), that has looked into the performance of four keratoconic eyes in suprathreshold space and they reported the presence of contrast constancy for a range of spatial frequencies that the eyes were habitually accustomed to (Ng et al., 2022). However, there remains a lack of literature investigating supra-threshold visual performance in keratoconus.

2.2.4. Response of visual system to optical blur in keratoconus

Webster et al. (2002) investigated how neural adaptation plays a role in human perception of an image. Their studies have shown that an individual's judgement of blur heavily depends on the state of adaptation of the visual system. Mon-Williams et al. (1998) has further revealed that an extended period of viewing through a myopic blur improves the visual acuity when the blur is removed although, this was not necessarily accompanied by a corresponding improvement in the contrast sensitivity function. With the help of an adaptive optics (AO) system, Artal and Guirao (1998) particularly focussed on understanding the level of neural adaptation to the blur created by a normal individual's innate higher order aberrations. Results revealed the subjects preferred the level of blur induced by their own set of HOAs compared to their phase rotated counterparts, clearly demonstrating the fact that an individual's visual system is calibrated and adapted to its own subset of optical aberrations.

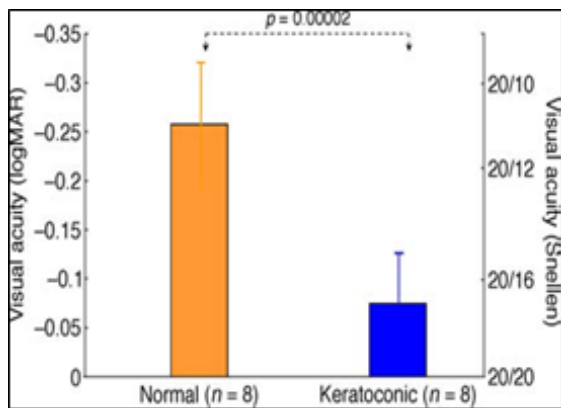


Figure 2.14: In spite of maximum optimization in image quality in both the keratoconus and normal cohorts, high contrast visual acuity in the keratoconus group did not reach the level of controls, proposing the presence of neural insensitivity due to the visual system getting exposed to chronic optical blur (adapted from Sabesan and Yoon (2009)).

Keratoconus is characteristically progressive in nature which leaves the visual system exposed to a progressive deterioration of retinal image quality. Sabesan and Yoon (2009) proposed two different theories as to how the visual system can respond when exposed to chronic losses in image quality: “neural insensitivity”: a negative phenomenon that limits visual performance from reaching its maximum potential akin to amblyopia; and “neural compensation”: a positive phenomenon that helps the visual system to adapt to the innate aberrations enhancing its performance akin to neural deblurring to optimize visual performance. With a closed-loop AO system, they optically corrected eight keratoconus and eight age-matched control eyes to their diffraction limited level and checked their visual performance with the correction in place. In spite of matching the optical image quality of keratoconic eyes to the controls, the keratoconus group had a relatively poorer visual acuity, suggesting a component of ‘neural insensitivity’ in the visual system due to the chronic exposure to blur (Figure 2.14) (Sabesan and Yoon, 2009).

In a follow up study, the same group studied the effect of neural compensation in four keratoconics and four age matched control eyes (Sabesan and Yoon, 2010). The ocular aberrations of both cohorts were first measured using a Shack-Hartman aberrometer. This was followed by a single step where the aberrations of the normal eyes were corrected to produce

diffraction limited retinal images and then the ocular aberrations that were measured from the keratoconus eyes were induced in those normal eyes. Subsequently visual performance of the ‘induced keratoconus’ normal eyes were compared to the performance of the keratoconus cohort. The results showed the performance in the keratoconus eyes was better than the controls with ‘induced’ keratoconus wavefront aberrations (Figure 2.15). This suggested the ability of the keratoconus eyes to counter some of the detrimental effect of higher order aberrations on the visual performance by some compensatory mechanism (Sabesan and Yoon, 2010).

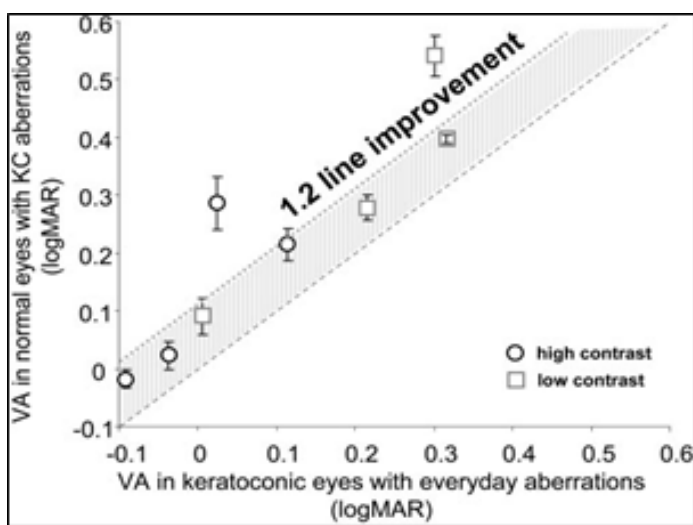


Figure 2.15: The 1:1 plot compares the performance of keratoconic eyes with their habitual aberration and the normal eyes performance, when the keratoconic aberrations are induced in them. The diagonal line in the figure indicates the point of equality, i.e., data points falling on this line suggests that the performance from both the cohort are similar. This study shows that the visual acuity in habitually keratoconic eyes were better (data points are above the line of equality) in comparison to normal eyes where keratoconus aberrations were induced (Taken from Sabesan and Yoon (2010)).

2.3. Management strategies in keratoconus

2.3.1. Optical management strategies

As evident from the sections 2.2.1 and 2.2.2, the visual deficit in keratoconus is largely driven by the HOAs of the eye. As a result, correction with spectacles or soft contact lenses only offers limited visual rehabilitation. Rigid gas permeable CLs have played a central role in the management of keratoconus due to their ability to create a regular refracting surface (Griffiths et al., 1998, Wagner et al., 2007). A timely intervention with contact lenses, and dispensing the

correct form of lens, can significantly delay major surgical interventions such as penetrating keratoplasty. Smiddy et al. (1988), in one of the early prospective observational reports on 190 eyes of 115 keratoconic subjects, showed that 87% of the patients could be fit successfully with bi-spheric RGP contact lenses. In addition, for 69% of the patients, keratoplasty could be delayed successfully. Over the years, the manufacturing techniques and contact lens designs have improved significantly and there are now several options available to practitioners to deal with the whole spectrum of the disease (see Figure 2.16). Different types of lenses have evolved in an attempt to improve the anatomical fitting of the lenses on the cornea, improving lens tolerance by enhancing the on-eye lens stability and comfort, as well as to meet the visual demand across a range of disease severity.

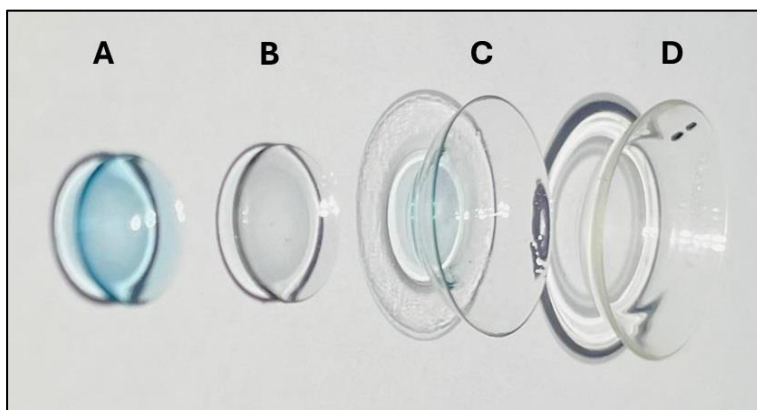


Figure 2.16: Images of different form of contact lenses available to the clinicians to optically manage a case of keratoconus. Image A and B are small diameter corneal GP lenses. The panel A shows a special design RGP lens, known as Rose K design lens, which also contains a visibility tint (blue). The panel C contains a hybrid lens with a combination of RGP lens in the centre, surrounded by a soft lens skirt in the periphery. The panel D contains a large diameter scleral contact lens.

RGP lenses have gone through significant changes, specifically in their back surface design, to improve their relationship with the anterior corneal surface. A strategic increase in the number of intermediate and peripheral curves in the back surface as well as the flexibility to alter the curvature of those curves has helped in increasing the stability of the lens on the corneal surface. A good example of this type of design is the Rose K lenses, which have improved on-

eye lens comfort significantly compared to the conventional RGP lenses (Jain and Sukhija, 2007, Mandathara Sudharman et al., 2010). Some of the other special design contact lenses include: the proprietary customized soft toric Kerasoft contact lenses; a piggyback system of using an RGP lens over a soft contact lens (lenses are placed on the eye separately); hybrid contact lenses (a single lens where a central RGP lens is surrounded by the peripheral skirt of a soft contact lens); and large diameter min-scleral and scleral lenses (see Figure 2.16). In spite of the large variety of lenses available, conventional RGP lenses are still the most widely used modality in clinical practice due to their ease of manufacture, availability and low cost (Zadnik et al., 1998, Kumar et al., 2019).

The premise of all the different contact lens designs has been for them to combine with the ocular tear-film layer effectively to regularize the anterior refracting surface of the eye. This regularization has been shown to have a significant impact on the optical as well as visual function of the eye (Wei et al., 2011, Jinabhai et al., 2012b, Nilagiri et al., 2018, Nilagiri et al., 2020). Nilagiri et al. (2018) observed that the median (interquartile range) higher order root-mean-square wavefront aberration (HORMS) of patients with keratoconus reduced from 1.96 μm (1.50 – 2.44 μm) to 0.62 μm (0.49 – 0.83 μm) unaided after using conventional RGP contact lenses, although the aberration remained significantly higher than age-similar controls. A follow up report from the same group (Nilagiri et al., 2020) explored the retinal image quality of these eyes with the help of a through focus analysis. With the help of RGP CLs, the otherwise flat image quality function (i.e., the neurally weighted Strehl ratio) started showing a pattern that is similar to the controls. An improved peak image quality and a relatively narrow depth of focus suggested a recovery of the visual system that had become relatively more sensitive to the changes in defocus. However, the recovery still remained partial and did not match the performance of the controls (Figure 2.10). Their reports on visual functions complimented the optical performance by showing a median improvement of three-to-four logMAR lines of high

contrast visual acuity. This performance, however, remained inferior to the controls, similar to the optical function assessment (Figure 2.11) (Nilagiri et al., 2018). Similarly, Jinabhai et al. (2014) reported a mean (± 1 SD) unaided HORMS error of $1.15 \mu\text{m}$ ($\pm 0.30 \mu\text{m}$) in a cohort of mild to moderate keratoconics that reduced to $0.50 \mu\text{m}$ ($\pm 0.18 \mu\text{m}$) with the help of RGP CLs, measured at a 4 mm pupil diameter (Jinabhai et al., 2014) (Figure 2.17). The visual function results confirmed the superior performance of these lenses compared to conventional spectacles and toric soft contact lenses.

In spite of the obvious visual benefits that the RGP lenses offer, they also pose notable challenges such as instability of the lens on the corneal surface and intolerance with the lenses (Weed et al., 2007). As the disease severity and corneal irregularity increases, the anatomical fit of a corneal RGP lens becomes increasingly difficult (Zadnik et al., 1996). The need to attain a lens fit that compliments the altered cornea has led to the development of a range of specialty contact lenses with different materials and design features compared to conventional GP lenses. Large diameter intra-limbal RGP lenses (Mandathara et al., 2017), customized corneal RGP lenses (Betts et al., 2002), customized soft toric lenses (Kerasoft) (Fernandez-Velazquez, 2012), a combination of a RGP lens at centre and soft lens at periphery (Hybrid) (Nau, 2008, Hashemi et al., 2014), miniscleral lenses (Severinsky et al., 2013) and large diameter scleral lenses (Schornack, 2015, Shorter et al., 2018) are some of the examples that are used in the management of keratoconus.

Given that the conventional RGP contact lenses have been the most widely used modality in keratoconus, the performance of specialty lenses is often tested against RGP contact lenses. The general consensus that prevails in the literature is that the specialty lenses produce performance at least comparable or better than that produced by RGP CLs. Betts et al. (2002) assessed the performance of Rose K lenses in keratoconus. Their results showed a marginal improvement compared to habitual conventional RGP lens wear in terms of high contrast visual

acuity. However, the subjects' self-reported preferences were skewed heavily towards the Rose K lenses. In a retrospective report, (Fernandez-Velazquez, 2012) compared the performance of Kerasoft lenses and compared them to Rose K contact lenses in eyes with mild and moderate keratoconus. The results suggested a highly comparable visual acuity with both the lenses. The studies by Hashemi et al. (2014) and Lee et al. (2013), showed a superior performance of hybrid lenses and scleral contact lenses respectively. Recent literature indicates a growing popularity of scleral contact lenses due to their unique design and less reliability on corneal shape for fitting.

In view of higher order aberrations being the major detrimental factor in keratoconus, recent investigation have tried to explore the possibility of developing custom-designed contact lenses where the keratoconic eye's wavefront aberration can be matched as closely as possible. This provides an opportunity to eradicate the major source of visual discomfort and potentially enhance the retinal image quality of the eye. Jinabhai et al. (2014) compared the performance of custom designed wavefront corrected soft toric contact lenses against the habitual RGP CLs for moderate keratoconic individuals. Although, optical performance was similar for the custom-designed lenses, the visual performance still remained significantly inferior to the RGP CLs. Sabesan et al. (2013) developed a custom-designed scleral contact lens and compared its performance against a conventional scleral lens. Results showed both the optical and visual performance was better with the aberration corrected device (Figure 2.18).

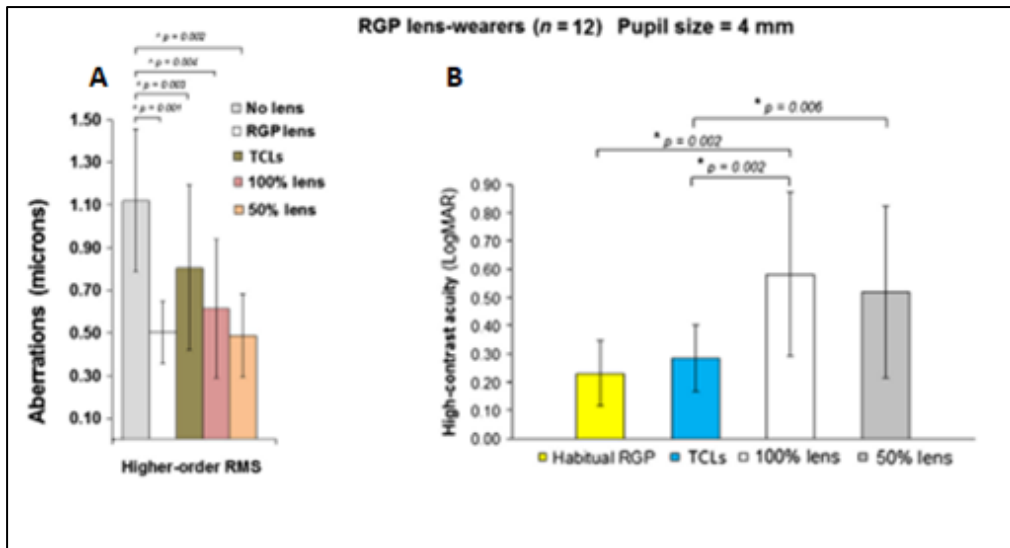


Figure 2.17: The histogram shows optical performance (A) and visual performance (B) with habitual RGP lenses as well as two different forms of aberration corrected contact lenses (ACCLs). Results suggested all forms of contact lenses improved optical quality compared to unaided condition. Furthermore, both the 50% and 100% ACCLs improved optical quality to comparable level as the habitual RGP contact lenses. However, the visual performance with the RGP lenses remained superior to that of the ACCLs (Adapted from Jinabhai et al. (2014)).

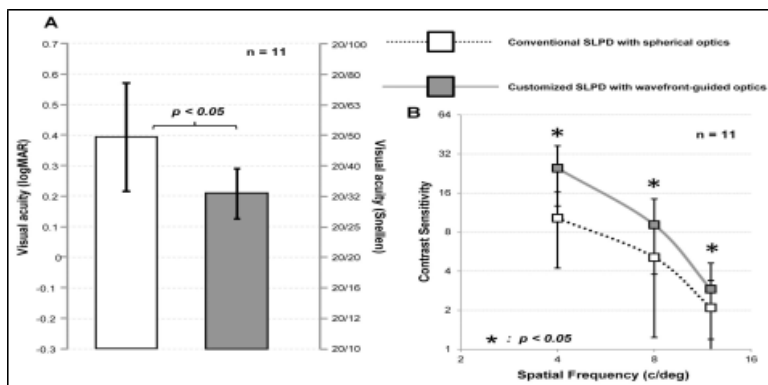


Figure 2.18: Histogram shows the performances of aberration corrected scleral lens prosthetic device (SLPD) compared to the conventional scleral lenses. Both high contrast visual acuity (A) and contrast sensitivity function (B) was relatively superior with the customized scleral lenses (Taken from Sabesan et al. (2013)).

Marsack et al. (2014) used the same technology to test the optical and visual performance of wavefront corrected scleral contact lenses. Although, the resultant ocular aberration and the retinal image quality could be corrected to match that of the control population, the psychophysical assessment of visual performance could not achieve a similar level of improvement, giving rise to the hypothesis of the possible insensitivity at a neural level in these

eyes as a result of chronic exposure to optical blur (discussed in detail in section 2.2.4) (Marsack et al., 2014).

2.3.2. Surgical management strategies

A comprehensive approach for managing keratoconus would need to consider the severity and the progressive nature of the disease. In addition to providing visual rehabilitation, the rate of progression needs to be arrested by strengthening the cornea through additional medical / surgical procedures. The surgical procedures comprise three different types: First, additive procedures, where external material is implanted in the eye such as the intracorneal ring segments (ICRS) or phakic intraocular lens implantation. The primary goal of these procedures is to improve the unaided and corrected visual performance of the keratoconic eyes. An ICRS implant improves the acuity by flattening the central cornea and reducing the overall asymmetric astigmatism. The thickness and the number of ring segment can be varied depending on the severity and the asymmetry of the topography map. This procedure has been shown to be very useful in refractive improvement and contact lens tolerance of keratoconus patients (Colin et al., 2001, Colin and Malet, 2007). Implantation of a phakic IOL is largely beneficial in stable keratoconus where there is a large refractive error present. Reports in the literature are usually in agreement on the predictive accuracy of the surgical outcome on the high contrast visual acuity, spherical and cylindrical refractive error (Leccisotti and Fields, 2003, Kamiya et al., 2008). Nonetheless, both the procedures come with their respective risks and potential complications. In their longitudinal report, Alio et al. (2006) showed that the central corneal flattening effect, gained through the ICRS implant, can start deteriorating with a progressive increase in keratometry starting from six months post-surgery. For phakic IOLs, there have been reports of endothelial cell loss (Moshirfar et al., 2006) and repositioning and exchange of IOL (Jaimes et al., 2011). Second, biomechanical strengthening procedures such as collagen cross linking (CXL). CXL utilizes a combination of riboflavin (vitamin B2) and

ultraviolet-A (UVA) light to strengthen the corneal tissue through a process of photosensitization and chemical cross-linking (Wollensak et al., 2003). Riboflavin acts as a photosensitizer, absorbing the UVA radiation and effectively controlling the treatment's depth into the corneal tissue (Wollensak, 2010). During photosensitization, the production of free radicals initiates the formation of chemical bonds within the corneal stroma, resulting in the reinforcement of the cornea (Spoerl and Seiler, 1999). The fundamental objective of CXL is to prevent further degradation of corneal shape. There are extensive reports on corneal tomographic and refractive parameters' changes after the CXL procedure. There is a consensus in the literature about the flattening of corneal curvature (Wollensak, 2010, Caporossi et al., 2010, Greenstein et al., 2011, Hersh et al., 2011) along with a reduction of refractive error (Vinciguerra et al., 2009, Caporossi et al., 2010) and corneal irregularity index (Caporossi et al., 2010, Greenstein et al., 2011). In one of the initial prospective trials, Wollensak et al. (2003) documented a reduction of the maximum keratometry value by 2.01 ± 1.74 D and a reduction of refractive error by 1.14 ± 2.18 D after a mean follow up period of 2 years following CXL. These results were confirmed by Caporossi et al. (2010) and Hersh et al. (2011).

While the primary objective of the collagen cross-linking procedure is not to enhance visual function, high contrast acuity has consistently been reported in the literature as an outcome measure along with the structural changes. The prevalent trend observed is an initial drop in high contrast acuity within the first month of surgery, followed by a notable improvement thereafter (Wollensak, 2010, Caporossi et al., 2010, Greenstein et al., 2011, Hersh et al., 2011). CXL is the most widely used surgical procedures in keratoconus so far due to the minimum risk involved in the procedure. Third, is corneal transplantation, where the keratoconic cornea is removed completely (full-thickness transplant) or partially (lamellar keratoplasty) and replaced by a healthy cornea. This option is usually chosen when all the other modalities fail.

2.4. Relationship between structure and function in keratoconus

Anatomical structures are meant to subserve functions. The biological system at large and the visual system specifically are no exception to this general rule. The cornea is the major refracting element of the eye contributing 70% of its overall power. Changes in the structure of the cornea will therefore have an impact on the visual function of the eye, hence corneal structure and visual function cannot be considered as isolated parameters. While structural changes in keratoconus are well-documented, their effect on visual function are less established. The only large-scale report that has measured the natural course of the visual function changes, comes from the CLEK study group (Wagner et al., 2007). Their results showed a very slow rate of decrease in high contrast visual acuity (mean of 2.03 Snellen letters) and low contrast visual acuity (mean of 4.06 Snellen letters) during the eight years of study period. In a recent meta-analysis, Ferdi et al. (2019) suggested that although high contrast acuity is an important parameter to consider, this may not be susceptible to progression of the disease.

There are sporadic reports that have tried to find correlations with structure and function, in an attempt to explain the natural course of the disease. Kanellopoulos and Asimellis (2013) have shown a moderate association between topometric indices from Scheimpflug imaging and high contrast visual acuity in keratoconus, with the best correlation being for the index of surface variance (ISV) ($r=0.75$). Xian et al. (2023) have recently published similar correlation models that focussed on the contrast sensitivity function. Compared to the previous literature, this report used the quick CSF paradigm (Lesmes et al., 2010) to register a comprehensive assessment of contrast sensitivity function of the participants. Their results showed a variable range of association with different topometric indices. Similar to the report by Kanellopoulos and Asimellis (2013), the ISV index had the maximum correlation ($r=0.69$) compared to all the other topometric indices.

Comparison between these studies is not straightforward, given the diverse nature of keratoconus, with a possible difference in morphology (e.g., extent and location of the cone) as well as the robustness of the neural system (e.g., exposure of visual system to a chronic blur) existing across the study cohorts. Therefore, a more systematic approach to develop a structure-function relationship is required on a specific cohort of keratoconus, analogous to other progressive ocular disease conditions such as glaucoma (Medeiros et al., 2012).

2.5. Lacuna in the literature

In an attempt to have a comprehensive understanding of the impact of keratoconus on the visual system, a review of the literature indicates the following areas need strengthening:

First, by and large, the literature has used high contrast acuity as the surrogate to represent visual performance in the presence of keratoconus as well as with the means of best possible optical correction (contact lenses) or post-surgical intervention (collagen cross-linking). However, recent reports have emphasized the importance of parameters such as contrast sensitivity function and stereopsis. Therefore, an in-depth assessment of high contrast acuity, contrast sensitivity and stereoacuity would significantly add to our understanding of the disease complexity.

Second, the structural and the functional changes in keratoconus are often studied in isolation and studies investigating the impact of structural change on visual function are scarce. Given the progressive nature of the disease condition, it is of value to assess changes in visual performance as a function of structural changes in the cornea. Through this thesis, a structure-function relationships will be created to help practitioners predict the functional loss from the state of corneal structure.

Third, literature assessing visual performance often reports a detection level (threshold) task, which may not represent the daily activities that, to a large extent, involve suprathreshold level

vision. Research has suggested a difference in sensitivity for a supra-threshold level task when compared to a threshold level task for normal individuals. Although, a recent study has reported the suprathreshold level contrast performance in keratoconus, this area needs to be explored in greater detail.

Fourth, while we consider the optical strategies to manage keratoconus, contact lenses perform better than spectacles. The superiority of different contact lenses has been documented in isolation. This often puts the practitioners in a dilemma as to what could be the lens of choice from a whole array of lenses available. One aim of the work in this thesis is to provide good evidence of the performance of the different lenses used to manage keratoconus.

2.6. Aims

The overarching aims of the thesis are:

- 1) To establish a structure-function relationship in keratoconus that could be used to predict functional loss from corneal structural parameters. The visual function measurements will include visual acuity, contrast sensitivity and stereoacuity.
- 2) To compare the optical and visual performance of different contact lenses used to manage keratoconus. This will enable eye care professionals to have an evidence-based rationale for identifying the ideal contact lenses and to design an optimum plan to deliver optical management to a patient with keratoconus.
- 3) To assess the suprathreshold performance of keratoconic eyes and compare that against visual performance at threshold. This will enable us to understand to what extent the impact seen at threshold level is translated to the suprathreshold real world tasks.

3. Chapter 3: Structure-Function relationship in keratoconus: Spatial and depth vision

3.1. Introduction

Keratoconus brings about changes in corneal structure such as curvature, thickness and elevation, compared to the normal controls (Belin et al., 2022). These changes are quantified using several corneal tomographic indices, with the general understanding (as noted in chapter 2) that multimetric indices that are based on a combination of factors, are more reliable at identifying the disease and/or its progression than unimetric indices (Duncan et al., 2016, Shajari et al., 2019). While structural changes in keratoconus are well-documented, associated losses in function are relatively less understood. Alteration in corneal shape in keratoconus can result in increased higher order aberrations and a consequent loss in retinal image quality, relative to age-similar and pupil matched controls (Nilagiri et al., 2020, Shneor et al., 2021). Research has shown that a significant deterioration of peak image quality is evident, even with the best correction in place (Nilagiri et al., 2020). This poor optical performance consequently has an impact on visual performance. High contrast visual acuity has been the most commonly used metric to evaluate visual functions in this disease condition (Nilagiri et al., 2018). This parameter tends to progressively deteriorate with increasing disease severity (Ferdin et al., 2019), and it tends to be better with rigid contact lens wear than uncorrected or spectacle-corrected conditions (Nilagiri et al., 2018). In spite of being widely reported as a measure of visual performance, high contrast visual acuity may fail to represent the daily visual experience of an individual. There is an increasing body of evidence of a lack of correlation between high contrast acuity and quality of life in keratoconus patients (Kandel et al., 2020), suggesting that the day-to-day visual experience can be better explained by other measures such as the contrast sensitivity function. A recent report by Shneor et al. (2021) found reduced contrast sensitivity

performance in a cohort of keratoconus patients who otherwise possessed logMAR acuity of 0.00 units.

An additional dimension of visual performance in keratoconus, which has previously received limited consideration, is binocular visual function. Assessing binocular vision in keratoconus is important for two important reasons: first, the natural day to day operation of an individual is usually dependent on binocular visual performance; and, second, the usual presentation of keratoconus is asymmetric producing a difference in retinal image quality between the two eyes (Vazirani and Basu, 2013). Stereoacuity is routinely used as a measure of binocular performance by calculating the minimum disparity that the eye requires to identify depth.

A few recent studies have investigated changes in contrast sensitivity (Shneor et al., 2021, Xian et al., 2023) and stereoacuity (Nilagiri et al., 2018, Marella et al., 2021) in keratoconus. While all these studies provide insights into the gamut of visual function loss in keratoconus, they do not describe the exact nature of the structure-function relationship in this disease condition. A structure-function relationship may allow clinicians to predict the vision loss experienced by the keratoconic patient at their presentation to the clinic and also predict their future rate of vision loss with disease progression. The most comprehensive report on this topic to date comes from the Collaborative Longitudinal Evaluation of Keratoconus (CLEK) study that has documented a slow decline in uncorrected and best corrected visual acuity with increasing disease severity (Wagner et al., 2007). In this report, a mean deterioration of 2.03 letters of high-contrast acuity and 4.06 letters of 10% low-contrast acuity with Bailey-Lovie acuity chart was noted over a study period of eight years. Kanellopoulos and Asimellis (2013) tried to find the association between different topometric indices from Scheimpflug imaging and high contrast acuity. Their results showed that a global curvature-based metric, called the index of surface variance (ISV), had a high correlation with visual acuity (Pearson correlation, $r=0.75$) (discussed in detail in section 2.1.3). The same ISV metric was also shown to have a good

correlation with the contrast sensitivity function (Pearson correlation, $r=0.69$) by Xian et al. (2023). A direct comparison of the different functional elements between the different study cohorts are not straightforward due to the heterogenous nature of the disease that could arise from the morphology (e.g., location or type of cone) or the state of the neural system that drives the visual performance along with the optical quality. The state of the neural system can be influenced by factors such as the age of the patient, duration of the disease or the duration and magnitude of exposure to optical blur. These elements are not necessarily consistent across the different study population. One way to address this concern is to create the structure-function relationship for different measures of visual function on the same subset of keratoconic subjects. Structure-function relationships in general may show one of four trends (Figure 3.1). First, visual function can deteriorate linearly with structural loss (Figure 3.1, red line). Second, visual function may remain immune to structural loss at the beginning of the disease (the ceiling effect), following which it may deteriorate monotonically with further losses in the structure (Figure 3.1, green curve). The ceiling effect may also reflect the insensitivity of the visual function per se or its measurement to the underlying loss of structure. Third, the visual function may deteriorate monotonically with structural loss but may saturate beyond a certain disease severity (the floor effect) (Figure 3.1, blue curve). The floor effect may represent the absolute minimum value that may be possible for that visual function (e.g., no form perception for visual acuity) or a certain level above the absolute minimum where the function asymptotes to. Fourth, the structure-function relationship may be a combination of the ceiling effect, followed by a monotonic deterioration phase and finally a floor effect thereafter (Figure 3.1, black curve). The present study systematically investigated the presence of such trends in keratoconus for two monocular measures of spatial vision (high-contrast visual acuity and contrast sensitivity) and for one measure of binocular vision (stereoacuity). Based on contrast sensitivity being a more sensitive marker of vision loss in ophthalmic disease, including keratoconus, than high

contrast acuity (Shneor et al., 2021, Bullimore et al., 1991), it was hypothesized that the structure-function relationship will show a more prominent ceiling effect and a slower rate of loss thereafter for monocular visual acuity than contrast sensitivity. Stereoacuity, on the other hand, is determined by both the overall decrease and interocular difference in retinal image quality of the two eyes (Westheimer and McKee, 1980, Schmidt, 1994). The latter is more potent at causing a deterioration in stereoacuity than the former in normal individuals (Westheimer and McKee, 1980), especially, when the stereo processing is driven by lower spatial frequencies (i.e., more deteriorated retinal image) than higher spatial frequencies (i.e., less deteriorated retinal image; the contrast paradox) (Cormack et al., 1997). Based on this background, it was hypothesized that stereoacuity will be relatively better in individuals with early and bilaterally similar keratoconus than those with advanced disease severity with or without similarity in the disease presentation between the two eyes.

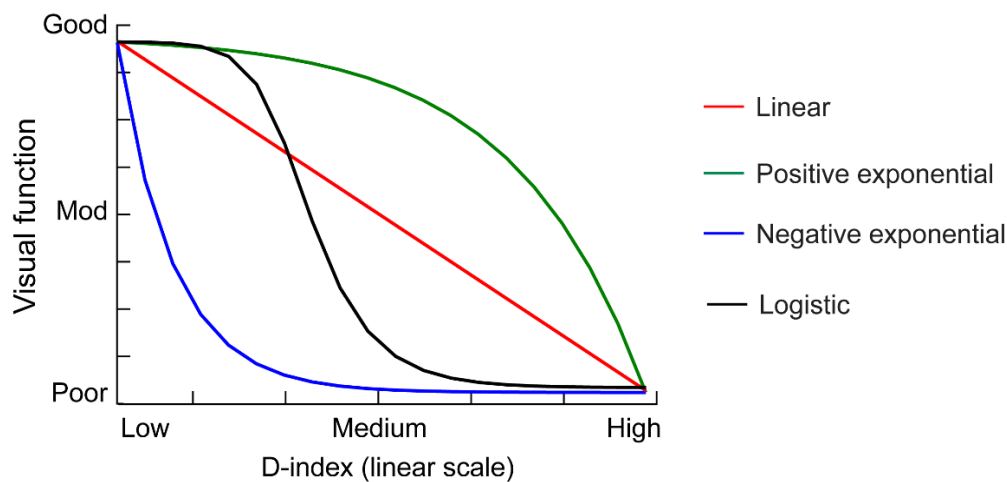


Figure 3.1: Schematic of the four trends of structure-function relationship envisaged for spatial vision and depth vision in keratoconus. The four trends were quantitatively described using regression equations described in the Methods section. The abscissa is plotted in linear scale.

3.2. Methods

3.2.1. Patient selection, inclusion, and exclusion criteria

Subjects with mild to severe keratoconus, visiting the out-patient services of the L V Prasad Eye Institute, Hyderabad, India, for the first time, between January 2021 and April 2022 were

included in this cross-sectional and observational study. The study adhered to the tenets of the Declaration of Helsinki, and it was approved by the Institutional Review Boards of LVPEI and City, University of London (LEC-BHR-P-07-20-467). All subjects signed a written informed consent form prior to initiation of data collection. All subjects underwent a comprehensive eye examination prior to being inducted into the study and those with a diagnosis of bilateral keratoconus, as confirmed by an experienced clinician, were inducted into the study. For inclusion, subjects needed to demonstrate one or more signs of keratoconus, including: scissoring reflex in retinoscopy; Munson's sign; cornea ectasia; Fleischer's ring and Vogt's striae; (Zadnik et al., 1998); steep curvature, asymmetry and/or skewing of the bow-tie pattern on topographic maps; increased elevation points in the Belin-Ambrosio enhanced ectasia display; and relative thinning of the cornea in Scheimpflug imaging tomography (Belin and Duncan, 2016). Subjects with apical corneal scars, superficial punctate keratitis, presence of retinal pathology, strabismus and oculomotor pathology, previous history of contact lens wear or any form of ocular surgery or any other ocular co-morbidity were excluded from the study. In cases where the subjects had difficulty in understanding the tests, the data were excluded from the final analysis. Comparison data from visually healthy control subjects were obtained from the students and staff pool of LVPEI. The study methodology is outlined in Figure 3.2.

A prospective, longitudinal assessment of corneal structure and visual function was the original study design to create the structure-function model. However, this could not be implemented for the following reasons: first, keratoconus is known to be a slow progressing disease and to establish a structure-function relation for larger degree of structural change, a significant amount of time would be needed. For instance, Choi and Kim (2012) reported an average 3.5 years for observing a change in central corneal curvature of at least 1.5 D. In addition, significant structural change would have warranted some form of surgical intervention (such as collagen cross linking procedure) under local clinical practice standards. Finally, this study

was conducted largely within the time frame of the COVID-19 pandemic and therefore, a significant resistance was expected from convincing the participants to return to the clinic for repeated visits. A cross-sectional (pseudo-longitudinal) study design was therefore considered appropriate to pursue this study question. The initial sample size calculation for the longitudinal study design, with the alpha-error set at 5% and the study power set at 90%, required 72 participants. The aim was to recruit double the number of participants in the cross-sectional model, from what was calculated for the longitudinal study design, in an attempt to retain the power of the study. The sample size of the cases and the controls were significantly asymmetric. The visual optics laboratory in the study site has been consistently addressing questions regarding visual functions over the past decade (Devi et al., 2022) and the same functions have been assessed in this study. The results have always been shown to be highly repeatable for the controls. Keeping that as a reference, data from a smaller number of control subjects were recruited in this study to minimize the redundancy in data collection process.

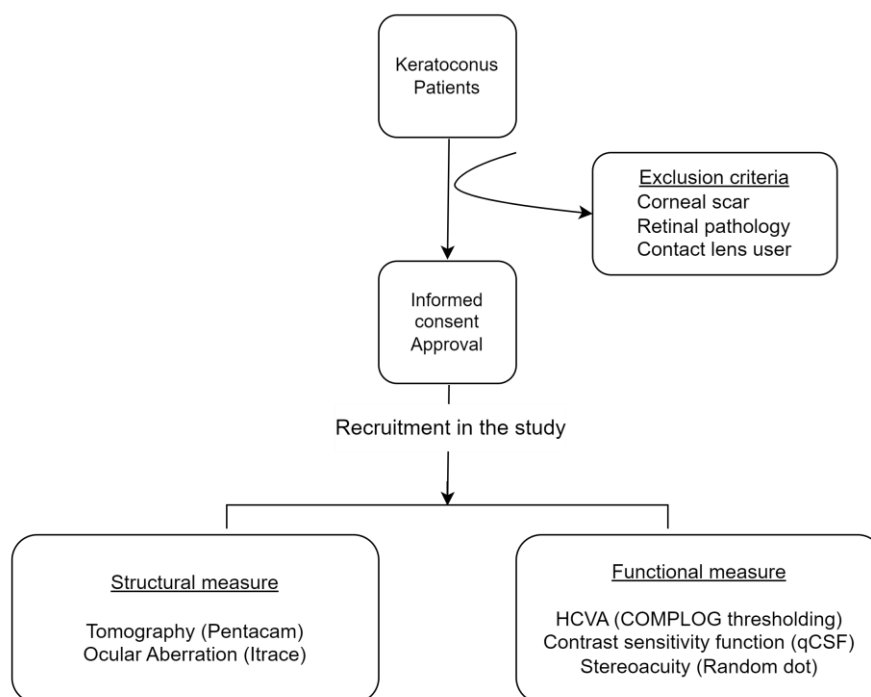


Figure 3.2: The flow chart provides an overview of the methodology used in this study

3.2.2. Assessment of corneal structure

The corneal structure of cases and controls were assessed using Scheimpflug imaging (Pentacam HR[®] (Oculus Optikgeräte GmbH, Wetzlar, Germany)) (Hashemi et al., 2016). The multimetric D-index was derived from both eyes of cases and controls using the Belin-Ambrósio enhanced ectasia display map (Belin and Duncan, 2016). This index includes deviations of front and back surface elevations of the cornea, pachymetric progression, thinnest corneal point, and deviation of maximum Ambrósio relational thickness. For keratoconus, higher D-index values indicated greater disease severity. Seven different indices from the tomographic map was obtained from the tomographic map (Hashemi et al., 2016). A detailed comparison of these indices for the present cohort of cases can be found in Appendix I. The D-index was considered as the primary outcome measure of corneal structural deformation in this study, based on evidence that this metric has good reliability for the diagnosis and progression of keratoconus (Duncan et al., 2016, Shajari et al., 2019).

3.2.3. Assessment of visual functions

3.2.3.1. High contrast visual acuity and the contrast sensitivity function

All psychophysical measurements were conducted for the subject's natural pupil size and with their best-corrected refraction at the spectacle plane. The sphero-cylindrical refractive error with spectacles was finalized using the maximum plus for maximum visual acuity criterion of clinical subjective refraction for each subject. The monocular high contrast visual acuity of each eye was assessed using an electronic projection chart (Complog Clinical Vision Measurement Systems Ltd, London, UK) (Laidlaw et al., 2008). Each level of acuity assessment comprised five Sloan letters, randomly selected from the complete range of Sloan optotypes. The letters were displayed on an LCD monitor (1680 × 1050 pixels) at 3-meter distance from the subject, with a calibrated screen luminance of 80 cd/m² luminance. The acuity was determined using a thresholding algorithm that terminated when three out of five

letters were incorrectly identified. The acuity value was quantified as the cumulative number of optotypes that were correctly identified by the subject, with 0.02 logMAR units assigned per optotype (Nilagiri et al., 2018) (Figure 3.3).

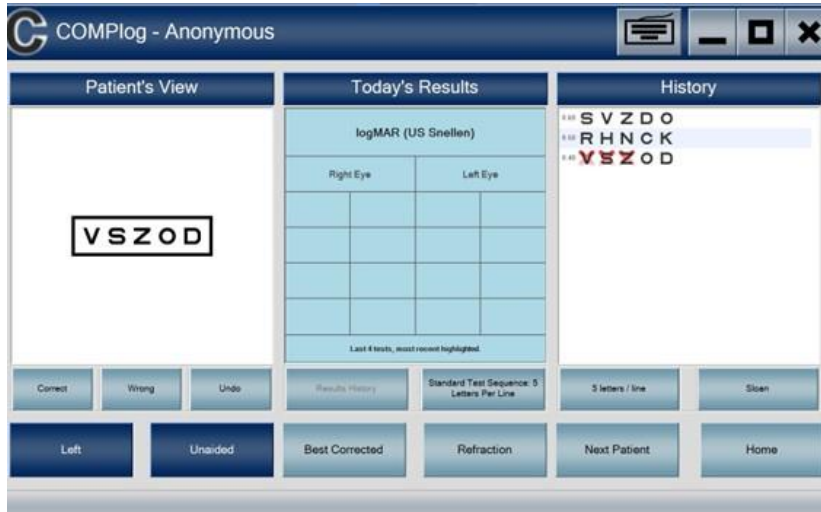


Figure 3.3: Figure shows the computer screen registering the response of an individual during the thresholding technique for assessing high contrast visual acuity. The letters that are marked with red cross indicates a wrong response from the subject. Three out of five such wrong response would terminate the procedure and quantify the acuity based on the total number of optotypes read.

The monocular contrast sensitivity function (CSF) of each eye was measured using a modified version of the quick CSF (qCSF) experimental paradigm, implemented using Psychtoolbox-3[®] in Matlab[®] (Mathworks Inc, Natick, MA, USA) (Brainard, 1997, Lesmes et al., 2010, Pelli, 1997, Rosen et al., 2014). In this paradigm, subjects made two-alternate forced choice judgments of the Gabor stimulus orientation presented at 45° or 135° on a luminance-calibrated CRT monitor (1280 × 1024 pixels; 85 cd/m²) from 1m viewing distance. The Gabor stimuli subtended 4° × 4° at the eye's nodal point from the 1m viewing distance (Figure 3.4). The algorithm determined the contrast sensitivity function for a range of spatial frequencies from 1 to 50cycles/degree (cpd) by varying the grating spatial frequency and contrast in an adaptive thresholding manner, which included a one-step-ahead search algorithm to evaluate the next trial's possible results. This effectively allowed an assessment of the contrast threshold for the visible range of spatial frequencies to be estimated within 100 trials. The bit-depth of the

stimulus display on the CRT monitor was enhanced to facilitate fine contrast measurements using the Bits# stimulus processor (Cambridge Research System Ltd, Kent, UK) that was synchronized with Psychtoolbox-3[®]. The area under the CSF (AUCSF) was considered to be the primary outcome parameter from this analysis. To understand the relative contribution of each component (sensitivity and spatial frequency) independently on the restriction of overall contrast sensitivity function, two additional parameters were derived- cut-off spatial frequency (to explain changes along the abscissa of a CSF) and the contrast sensitivity at 3 cpd spatial frequency (to explain changes along the ordinate of a CSF) (Rosen et al., 2014). To understand the impact on the sensitivity parameter, it could be argued that the sensitivity at the peak spatial frequency could have been captured. However, there are two important aspects that are pertinent to mention in this regard- first, the peak spatial frequency does not remain constant across the subjects. Consequently, the inter-subject comparison of sensitivity becomes ambiguous. Therefore, the attempt was made to compare the sensitivity performance at a given spatial frequency. Second, the peak spatial frequency of the normal individuals ranges from 2 to 4 cpd (Campbell and Green, 1965, Campbell and Robson, 1968). Lower values of visual acuity and higher values of the three different parameters from the contrast sensitivity function (AUCSF, cut-off frequency and sensitivity at 3 cpd), indicated better spatial resolution and a larger “visible area” for spatial vision, respectively (Chung and Legge, 2016).

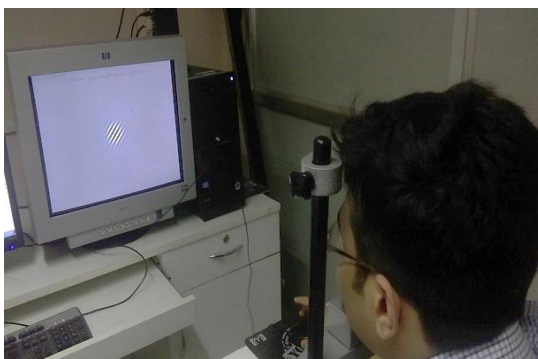


Figure 3.4: Figure shows the experimental set up for assessment of the contrast sensitivity function. The subject is positioned at 1 meter distance from the CRT monitor and fixates at the centre of the

screen. The Gabor stimulus projected at the centre of the screen with the sinusoidal gratings oriented at either of the oblique directions (45° or 135°). Subjects' response is registered as a 2-AFC procedure.

3.2.3.2. Stereoacuity

Stereoacuity was measured using random-dot stereograms implemented in Psychtoolbox-3 interface of Matlab[®] (Brainard, 1997). The random-dot field subtended $7^\circ \times 7^\circ$ at 60 cm distance on the LCD monitor (1280×1024 pixels resolution). Subjects viewed these stereograms through a mirror stereoscope from 50 cm viewing distance and made two-alternate forced choice judgments of the orientation of a rectangular bar appearing in crossed disparity (appears elevated from the surface of the computer screen) within the random-dot field (Figure 3.5). The stimulus disparity was created by spatially displacing the positions of the random dots and was scaled to the subject's interpupillary distance. The viewing distance and the angle of the mirror in the stereoscope was adjusted to overcome any horizontal heterophoria of the subject. Based on prior knowledge of the stereoacuties being poor in keratoconus (Nilagiri et al., 2018), the initial disparity value of the adaptive staircase was set at 800 arc sec for these subjects and at 100 arc sec for controls. The disparity values were subsequently modulated in a 2-down-1-up fashion, with the step-size ranging from 50% to 0.5% of the initial disparity value. The staircase terminated after 16 reversals and the average of the last 13 reversals was considered as the stereoacuity of the subject. Smaller values of averaged disparity indicated a better depth detection capability.



Figure 3.5: Figure shows the experimental set up for stereoacuity assessment. The subject is seated 50 cms from the screen, fixated at the random-dot pattern at the centre of the screen. The purpose of the stereo viewer (subject is holding at the spectacle plane) is to fuse the random-dot images perceived separately with each eye, with the help of prisms located inside the mirror.

3.3. Assessment of the structure-function relationship

Four putative trends in the structure-function relationship for keratoconus were hypothesized, as described in the introduction section (Figure 3.1). These trends were quantitatively assessed for each visual function tested here using a linear regression equation (Eq. 1; Trend 1 in Figure 3.1), an exponential equation with a positive exponent value (Eq. 2; Trend 2 in Figure 3.1), an exponential equation with a negative exponent value (Eq. 3; Trend 3 in Figure 3.1) and a logistic sigmoid-shaped equation (Eq. 4; Trend 4 in Figure 3.1). The mathematical forms used were:

$$y = y_0 + ax \text{ ----- Eq. 1}$$

where, y = normalized visual function, y_0 = y-intercept of the fit, a = rate of loss of visual function and x = D-index.

$$y = y_0 - a[1 + e^{\left(\frac{x}{b}\right)}] \text{ ----- Eq. 2}$$

$$y = y_0 + a[1 + e^{\left(-\frac{x}{b}\right)}] \text{ ----- Eq. 3}$$

where, y = normalized visual function, y_0 = y-intercept of the fit, a = amplitude of change in visual function, x = D-index and b = rate of loss of visual function. And

$$y = y_0 + \frac{a}{[1 + e^{b(x-x_0)}]^c} \text{ ----- Eq. 4}$$

where, y = normalized visual function, y_0 = lower asymptote of the logistic fit, a = height of the sigmoid between the asymptotes, b = rate of loss of visual function, x = D-index, x_0 = midpoint of the logistic fit, and c = sharpness of the edge roll-offs.

These trends were also additionally evaluated for the cut-off spatial frequency and the sensitivity at 3cpd parameters of the CSF to determine how each of them contributed to the overall loss of the AUCSF. Curve fitting was performed in Matlab 2017a using the *fminsearch* algorithm that optimized the values of the three free parameters using the Nelder-Mead multidimensional, unconstrained, nonlinear minimization process (Liu et al., 2011). The goodness of fit of each equation was assessed using the R^2 values and the pattern of the residual errors obtained with the best-fit equation. The first derivative of the best-fit equation described the rate of change of the given visual function per unit increase in D-index value.

To enable comparison of the structure-function relationship between the different measures of visual functions, all raw data were normalized against the corresponding values of controls before curve fitting. Normalization was achieved by dividing the visual function value of cases by the median value of that visual function obtained from controls. Therefore, a normalized value of unity indicated that the performance of cases equalled that of controls while values less than unity indicated a deterioration in visual function of cases relative to controls for high contrast acuity and contrast sensitivity performances. Worsening of stereoacuity was indicated by normalized values of stereoacuity greater than unity. While the normalization was straightforward for AUCSF and stereoacuity, it was rendered ambiguous for visual acuities recorded in the logMAR scale (e.g., 0logMAR value corresponding to 20/20 acuity will become a meaningless entity during the normalization process). To overcome this challenge, all values of visual acuity were first converted into decimal acuity and then normalized against the corresponding values of controls.

3.4. Statistical analysis

All data were analyzed using Matlab[®] R2017a and IBM SPSS statistics v20.0[®] (SPSS, Chicago, IL, USA). Although visual acuity and CSF data were obtained from both eyes of the subject, only data from the right eye was used for the analysis here. Data from the left eye showed near-identical trends and hence is not reported here. The Shapiro-Wilk test was used to determine the normality of the dataset and appropriate parametric or non-parametric tests were applied for analysis subsequently.

3.5. Results

3.5.1. Demographic, refractive and topographic and visual parameters

A total of 155 subjects (310 eyes) with keratoconus (age range: 15 to 38 years) were recruited for the study (Table 3.1). Visual acuity, CSF and stereoacuity data were successfully collected from all subjects. However, fifteen subjects reported difficulty in understanding the stereoacuity test. Therefore, data for 140 of the 155 subjects with keratoconus were included for the analysis. Since the data were not normally distributed, all outcome parameters are reported as median values along with appropriate measures of data dispersion in Table 3.1. Sphero-cylindrical refraction values were converted into standard power vectors using formulae described in detail by Thibos et al. (1997).

Data were collected from 10 age-similar controls were used for the aforementioned normalization process. For the control group, the median high contrast acuity was -0.06 logMAR (range -0.02 to -0.12 logMAR) and area under contrast sensitivity function curve was 2.35 units (range 2.3 to 2.55 units). The median cut-off spatial frequency was 26 cpd (range 25.2 to 35.2 cpd) and the sensitivity at the peak spatial frequency was 2 units (log sensitivity) (range 1.95 to 2.3 log sensitivity). The median stereoacuity of the control group was 32 arc sec (range 25.3 to 73.4 arc sec).

Age (yrs)	21 (18 to 25)	
Gender (M: F)	93: 62	
	RE	LE
Topographic measures		
<i>Steep keratometry (D)</i>	51.1 (47.4 to 55)	51.4 (47.3 to 56.7)
<i>Flat keratometry (D)</i>	46.9 (44.4 to 50)	46.8 (44.5 to 51.3)
<i>Maximum keratometry (D)</i>	57.5 (51.1 to 62.9)	57.5 (49.9 to 64.2)
<i>D-index (unitless)</i>	9.02 (5.7 to 11.6)	8.8 (5.1 to 12.7)
Refractive measures		
<i>M (D)</i>	-3.0 (-1.5 to -5.5)	-2.9 (-1.25 to -5.6)
<i>J0 (D)</i>	0.0 (+0.9 to -0.5)	0.25 (+1.3 to -0.4)
<i>J45 (D)</i>	-0.9 (0.0 to -1.9)	0.6 (+1.8 to 0.0)
Spatial-related visual functions		
<i>HCVA (logMAR)</i>	0.23 (0.44 to 0.06)	0.22 (0.47 to 0.04)
<i>AUCSF (unit area)</i>	1.1 (0.77 to 1.47)	1.1 (0.73 to 1.66)
<i>Cut-off frequency (Cpd)</i>	10.6 (7.5 to 13.8)	10.2 (6.8 to 16.7)
<i>Sensitivity at 3cpd</i>	1.3 (1.0 to 1.7)	1.3 (0.9 to 1.7)
Depth-related visual functions	487.4 (324.4 to 618.3)	
<i>Stereoacuity (arc sec)</i>		

Table 3.1: Demographic, refractive and topographic details of study participants. The values indicate median (interquartile range) for each parameter described in the study. The *M*, *J0* and *J45* terms represent the spherocylindrical refractive error in power vectors, wherein *M* = spherical equivalent of refraction and *J0* and *J45* represent the regular and oblique astigmatic components of refraction (Thibos et al., 1997).

3.5.2. Overall trend in the structure-function relationship

The overall trends in the structure-function relationship for high contrast visual acuity and contrast sensitivity were rather different from that of stereoacuity. Therefore, the results for the former two functions will be described first followed by a description of the results for the latter function.

3.5.2.1. Visual acuity and contrast sensitivity function

Figure 3.6A and B show scatter diagrams of the normalized high contrast visual acuity (panel A) and the AUCSF (panel B) plotted as a function of the D-index in the present study cohort. Both functions deteriorated with increasing disease severity, with a prominent phase where the functional loss was proportional to the structural deterioration followed by the ‘floor’ effect

(Figure 3.6). A ‘ceiling’ effect was also prominent for high contrast visual acuity, with several data points lying around the unity line during the initial stage of the disease (Figure 3.6A). Such a ‘ceiling’ effect was not apparent for AUCSF, with all data points (except one) lying well below the unity one even for early disease severities (Figure 3.6B). Additionally, qualitative differences in the rate of loss of visual acuity and AUCSF were also apparent in these plots, with the former variable showing a faster rate of deterioration than the latter, for equivalent ranges of D-indices (Figure 3.6).

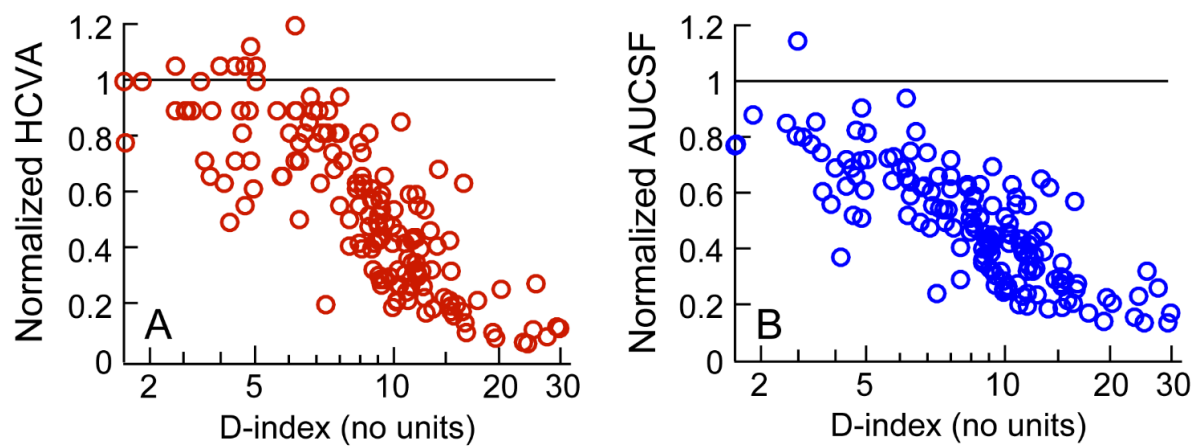


Figure 3.6: Scatter diagram of normalized spectacle-corrected high contrast visual acuity (panel A) and normalized area under the CSF (AUCSF; panel B) plotted as a function of the D-index for all study subjects. The abscissa is plotted in logarithmic scale in both panels. Data points lying along the horizontal unity line indicate that the visual acuity and AUCSF of these subjects were equal to those of age-similar controls.

These qualitative trends were further investigated by fitting the raw data to the four patterns of structure-function relationship described in Equations 1 – 4 (Figure 3.7). The adjusted R^2 for all fits ranged from 0.54 to 0.69 for high-contrast visual acuity ($p < 0.001$) and from 0.54 to 0.65 for AUCSF ($p < 0.01$) (Figure 3.7). Of the four fits, the linear regression equation had the smallest R^2 for both visual acuity and AUCSF (Figure 3.7 A and I) while the negative exponential equation and the logistic equation had the maximum R^2 for both outcome variables (Figure 3.7 C, D, K and L). The fit’s residual errors for both visual acuity and AUCSF showed a prominent underestimation bias for the mid-range of D-indices (D-index from 10 – 20) and a prominent

overestimation bias for the high range of D-indices (D-index >20) for the linear regression equation and the positive exponential equation (Figure 3.7 E, F, M and N). These biases were less prominent for the negative exponential equation for both outcome variables (Figure 3.7G and O) and least for the logistic equation, more so for visual acuity than for AUCSF (Figure 3.7 H and P).

The logistic equation was meant to identify the ‘ceiling’ and ‘floor’ effects in the data more prominently than the exponential equations (Figure 3.1, Eq. 2 – 4). That the performance of the logistic equation was marginally superior to the negative exponential equation for visual acuity but not for AUCSF reinforced the qualitative observation of the presence of a ceiling effect in the former but not in the latter (compare Figure 3.7 C and D and Figure 3.7 K and L). Both functions predicted the floor effect seen in the raw data (Figure 3.6). The logistic equation, whose coefficients are shown in Table 3.2, was deemed the most appropriate mathematical description of the structure-function relationship for spatial vision in keratoconus. Therefore, only this equation was used for exploring additional dimensions of the structure-function relationship in keratoconus. Coefficients for the logistic equation for the four outcome variables are given in Table 3.2.

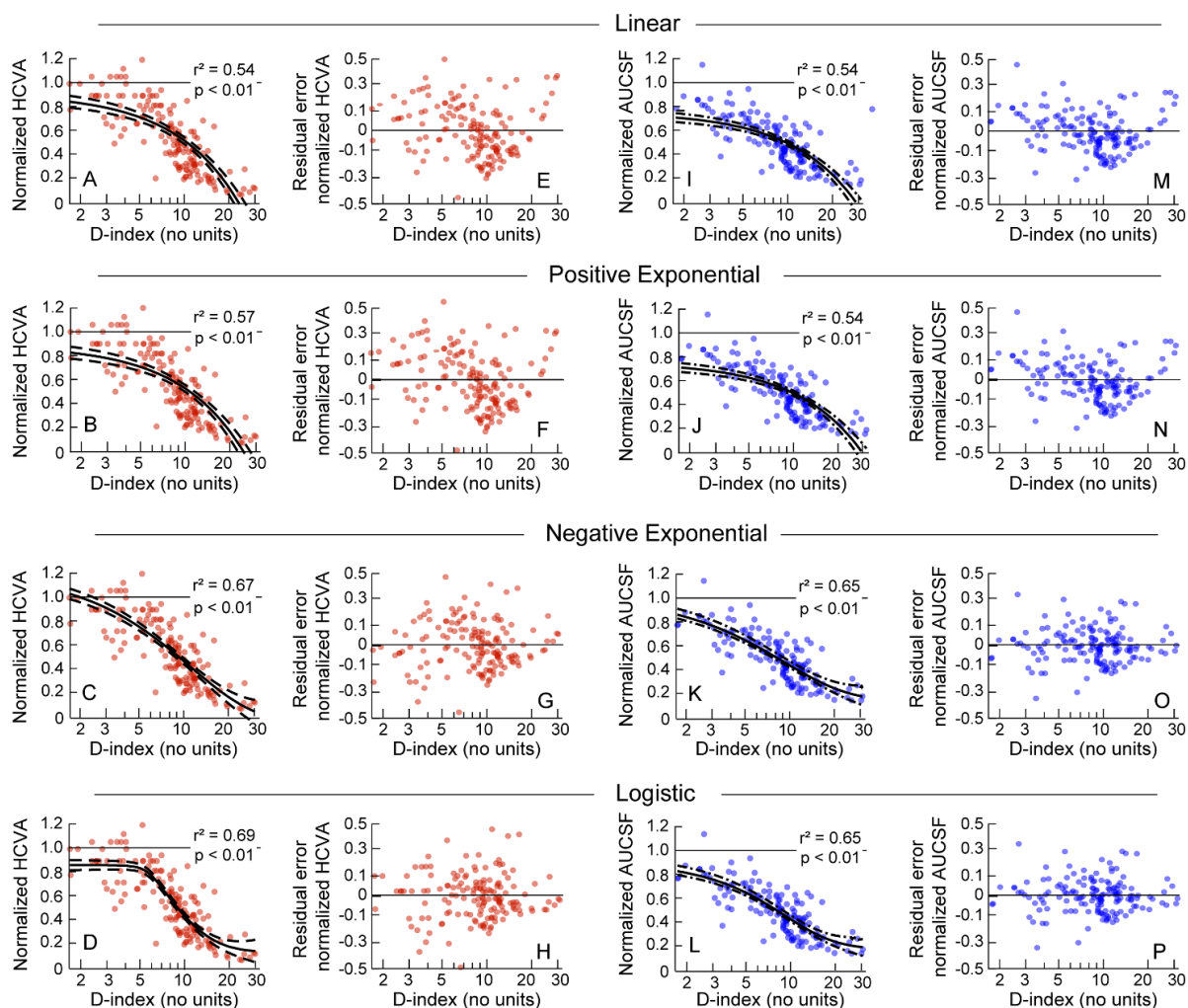


Figure 3.7: Same data as Figure 3.6 plotted along with the best-fit regression equations describing the pattern of structure-function relationship for high-contrast visual acuity (Panels A – D) and area under CSF (AUCSF; Panels I - L). The dashed curves around the best-fit curve indicate $\pm 95\%$ confidence interval of the fit. The residual errors of the fit are shown for visual acuity (Panels E – H) and AUCSF (Panels M – P). Other details are the same as Figure 3.6.

	x_0	y_0	y_1	a	b	c
High contrast visual acuity	5.52	0.14	0.87	0.73	1.816	0.11
Area under CSF (Area units)	0.92	0.19	1.22	1.03	0.27	0.57
Cut off spatial frequency (cpd)	-5.39	0.17	4.4	4.23	0.09	1.84
Sensitivity at 3cpd	-13.14	-0.23	2.33	2.56	0.25	0.18

Table 3.2: Coefficients of the best-fit logistic regression equation for the different spatial vision parameters considered in this study (Eq. 4). x_0 = midpoint of the fit, y_0 = lower asymptote of the fit, a = height of the sigmoid between the asymptotes, b = rate of loss of visual function, and c = sharpness of the edge roll-offs. An additional parameter, y_1 , describes the value at the upper asymptote of the function. This parameter is derived by simply adding the lower asymptote (y_0) to the height of the function (a).

The first derivatives of the logistic fits for visual acuity and AUCSF further distinguished the patterns of loss in these two parameters with increasing D-index on two counts (Figure 3.8). First, unlike visual acuity, the derivative plot for AUCSF was negative from early disease severity, reflecting a lack of a ceiling effect for AUCSF (Figure 3.8). Second, unlike AUCSF, the derivative plot for visual acuity showed a more prominent negative peak in the mid-range of D-indices (D-index from 7 – 12), reflecting a faster decline in visual acuity once the loss is initiated, relative to that of AUCSF (Figure 3.8).

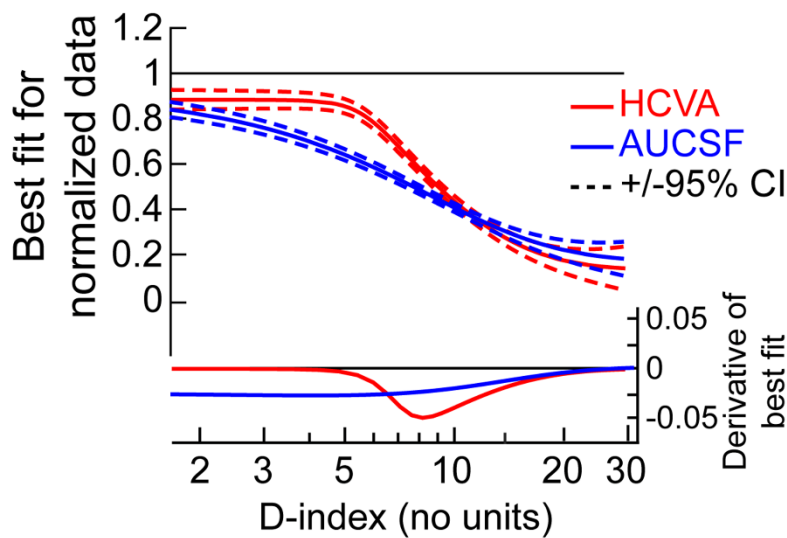


Figure 3.8: The best fit logistic equation shown in Figure 3.7D and L for high-contrast visual acuity and area under CSF, respectively, shown along with their first derivative to describe the rate of change of the visual function with per unit change in D-index. Negative values of the derivative indicate a worsening of the visual function with increasing D-index while positive values of the derivative indicate the opposite trend.

3.5.2.2. Cut-off spatial frequency and peak sensitivity at 3cpd

The cut-off spatial frequency describes the highest resolvable spatial detail while the sensitivity at 3cpd describes the sensitivity with which spatial details at that frequency can be resolved by the visual system. Both parameters have been shown to be poorer in keratoconus, via-a-vis, controls (Figure 3.9A) (Nilagiri et al., 2018, Shneur et al., 2021). Figure 3.9B and C confirmed these trends by showing a progressive decline in both parameters with increasing values of D-

index. The logistic regression equation had an adjusted R^2 value of 0.53 and 0.64 for the cut-off spatial frequency and sensitivity at 3cpd, respectively ($p < 0.001$).

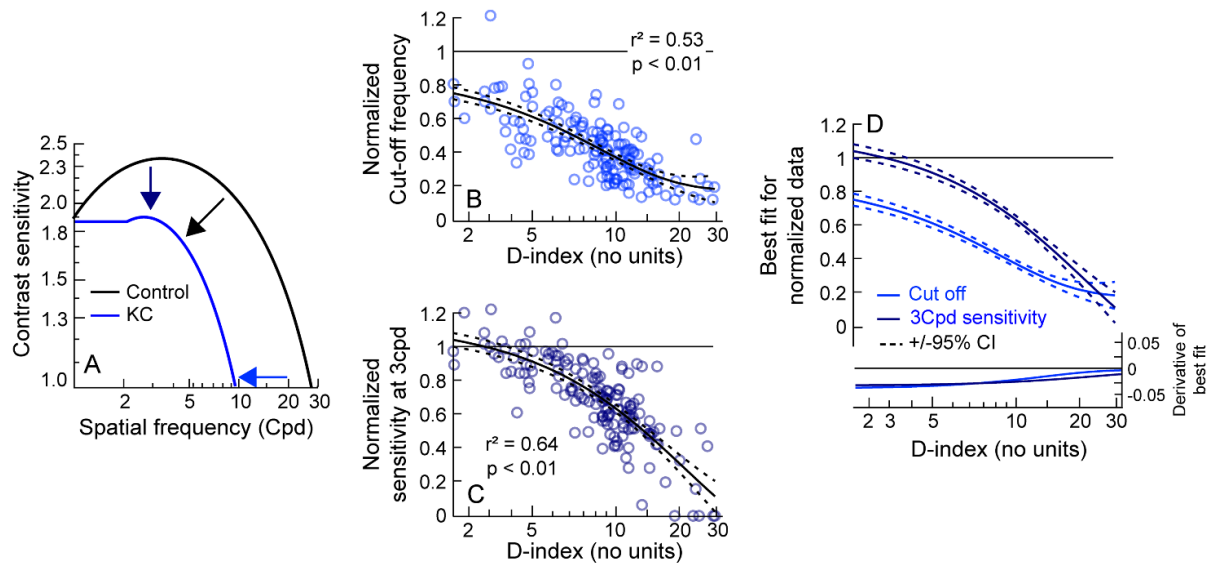


Figure 3.9: Panel A shows representative contrast sensitivity functions (CSFs) from a control subject and a case with keratoconus. The attenuation of the CSF can occur solely from the loss of high spatial frequency information (i.e., cut-off spatial frequency; horizontal arrow) or from the loss of sensitivity at relatively low spatial frequencies (i.e., sensitivity at 3cpd; vertical arrow) or from both (diagonal arrow). Panels B and C shows scatter diagram of the normalized cut-off spatial frequency and sensitivity at 3cpd plotted as a function of the D-index for the present cohort. The best-fit logistic regression equation along with the $\pm 95\%$ confidence interval is shown in these panels. All other details in these panels are the same as Figure 3.7. Panel D shows the two best-fit logistic regression equations along with their first derivative to determine the rate of change of performance per unit change in D-index. All other details are the same as Figure 3.8.

The best-fit equations showed no apparent ‘ceiling’ effect and a monotonic decline from early severities of the disease with similar loss rates for both parameters (Figure 3.9 B – D, Table 3.2). In addition, the regression fit along with the data points for the latter reached the level of the controls at an early form of the disease severity in comparison to the former, where all the points were well below the unity line (Figure 3.9 B – D). This perhaps indicate the impact of the disease on the contrast sensitivity function starts early on with an attenuation from the cut-off spatial frequency parameter (Figure 3.9A, horizontal arrow). The cut-off spatial frequency showed a ‘floor’ effect at advanced disease severities while such an effect was absent for the peak sensitivity at 3cpd (Figure 3.9 B – D). These results indicated that both parameters

contribute to the overall attenuation of the AUCSF from the beginning of the disease with the impact on the cut-off frequency preceding the sensitivity parameter. With advancing disease severity, the loss in cut-off spatial frequency asymptotes while losses in the sensitivity of low spatial frequencies continue to attenuate the AUCSF.

3.5.2.3. *Stereoacuity*

Unlike monocular visual acuity and contrast sensitivity, stereoacuity is dependent on both the overall image quality and the interocular difference in image quality available for the processing of retinal disparity in the random-dot patterns used in this study (Schmidt, 1994). In keratoconus, the image quality in the two eyes available for the purposes of stereo calculations is defined by the overall structural loss in the cornea due to a given disease severity and the difference in the structural loss between the two eyes due to interocular difference in disease severity (Metlapally et al., 2019, Marella et al., 2021). The statistical independence of the two structural variables were confirmed through a poor correlation between these variables (Spearman's ρ : -0.27; $p < 0.01$). Therefore, the normalized stereoacuity was plotted independently as a function of the D-index of the better eye and the interocular difference in D-index in Figures Figure 3.10 A and B to explore this relationship in detail. Overall, the stereoacuity of the keratoconic cohort [median (minimum to maximum range: 487.4arc sec (60.7arc sec to 1667.9arc sec))] was significantly poorer than in controls [32 arc sec (25.3 arc sec to 73.4 arc sec)], resulting in the normalized values of stereoacuity falling well above the unity value along the ordinate axes in Figure 3.10 A and B. Both scatter diagrams showed significant intersubject variability in the data, even though the normalized stereoacuties were significantly correlated with the D-index of the better eye (Spearman's ρ : 0.42; $p < 0.01$) and the interocular difference in D-index (ρ : 0.23; $p = 0.006$) (Figure 3.10 A and B). The four regression equations described earlier all gave poor fits to the data ($R^2 \leq 0.26$; $p \geq 0.2$), and therefore, it was not possible to determine a structure-function relationship for stereoacuity. In

that regard, it was fair to conceive that the null-hypothesis had to be accepted for stereoacuity performance.

Qualitatively, the stereoacuity data of some cases was found to be significantly better than the median values noted above. To better understand this trend, a different analytical approach was chosen to explore the relationship between the two independent variables that define bilateral image quality in the keratoconic eye (the D-index of the better eye and the interocular difference in D-index) and stereoacuity. The bubble plot shown in Figure 3.10 C plots the stereoacuity of individual subjects as a function of both the D-index of the better eye and the interocular difference in D-index. In general, the smaller and lighter colored bubbles, which represent better stereoacuity, were very few compared to the larger and darker colored bubbles, which indicate an overall poor stereoacuity in the keratoconus cohort (Figure 3.10 C).

The data points in the bubble plot were further divided into separate groups of mild, moderate, and severe keratoconus in the better eye, as described using the Amsler-Krumeich classification scheme for keratoconus severity (Krumeich et al., 1998) (Figure 3.10 C). The data points were further sub-divided into those with lower-than- and higher-than-median IOD in D-index within each severity group (Figure 3.10 C, Table 3.3). The smaller and lighter-colored bubbles were placed in the group containing subjects with mild keratoconus in the better eye and with smaller IOD in disease severity, indicating better stereoacuity in this group, relative to the other groups (Figure 3.10 C, Table 3.3). A pair-wise comparison between the subgroups indicated that the cohort containing stereoacuity data from subjects with mild keratoconus and low IOD in disease severity was significantly different from all the other groups (Mann-Whitney U test, $p \leq 0.007$) (Figure 3.10 D). The stereoacuity of those with moderate severity of keratoconus in the better eye and low IOD in disease severity was significantly different from those with severe keratoconus and low or high IOD in disease severity (Figure 3.10 D). All other comparisons were not statistically significant, indicating an upper-limit saturation of

stereoacuity in these groups (Figure 3.10 D). Taken together, these findings indicate that stereoacuity is very vulnerable to the loss of optical structure in keratoconus and it tends to reach the floor level of performance much earlier in the disease than its spatial vision counterparts.

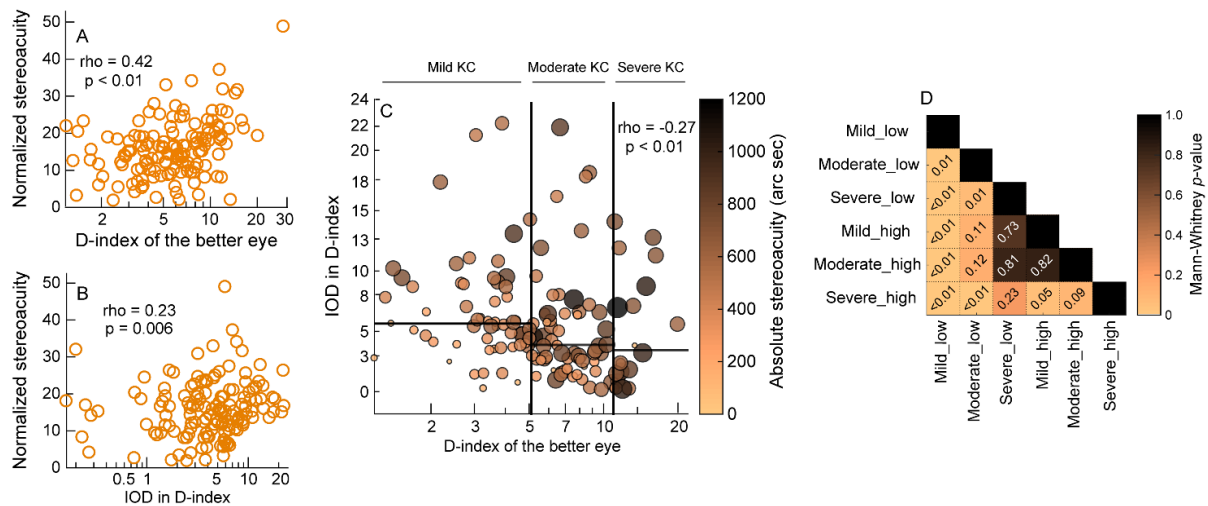


Figure 3.10: Panels A and B shows scatter diagrams plotting the normalized stereoacuity as a function of the D-index of the better eye and interocular difference (IOD) in D-index. Panel C presents the bubble plot showing the distribution of stereoacuity as a function of both the D-index of the better eye and the IOD in D-index. The stereoacuity value of each subject is indicated by the size and the color of the bubble, with smaller sizes and lighter colored bubbles indicated better stereoacuity. The colormap relating the individual bubbles to the stereoacuity values is included in this panel. Data points in this bubble plot are divided into separate groups of mild, moderate, and severe keratoconus in the better eye, as described using the Amsler-Krumeich classification scheme for keratoconus severity (Krumeich et al., 1998) (vertical lines in Panel C). The data points are also divided into lower-than-median (*_low) and higher-than-median (*_high) IOD in D-index for each severity group (horizontal lines in Panel C). Panel D shows a heatmap representing the statistical significance of the difference in stereoacuties between any two groups identified in Panel C. Lighter colored boxes indicate smaller p-values, as derived from the non-parametric Mann-Whitney U-test. The black boxes indicate self-comparison of groups and can be ignored. See Table 3.3 for actual values of stereoacuity in the different groups.

		D-index of the better eye		
		Mild	Moderate	Severe
IOD in D-index	Lower-than median	n=21 247.6 (181.6 to 376.0)	n=27 427.1 (288.9 to 538.7)	n=25 547.6 (341.2 to 707.0)
	Higher-than median	n=18 490.9 (406.8 to 600.5)	n=26 500.6 (381.4 to 638.2)	n=23 618.6 (487.7 to 758.9)

Table 3.3: Median (interquartile range) of stereoacuity (arc sec) for the subjects with mild, moderate, or severe keratoconus in the better eye and with lower-than median or higher-than median interocular difference (IOD) in disease severity.

3.6. Discussions

3.6.1. Major findings from the study

The results of this study may be summarized as follows:

i) Spatial- and depth-related visual functions show a non-linear pattern of decline with increasing deterioration of optical structure in keratoconus (Figure 3.7 and Figure 3.9). The pattern of loss differs across the different visual functions evaluated in this study.

ii) High-contrast visual acuity shows a distinct ceiling and floor effect that surrounds the region of proportional loss with increasing disease severity (Figure 3.7D and Figure 3.9A and Table 3.2). Unlike acuity, contrast sensitivity lacks this ceiling phase and shows a steady decline from early stages of the disease severity until saturation (Figure 3.7L and Figure 3.8 and Table 3.2). The rate of loss of contrast sensitivity is, however, lower than that of visual acuity (Figure 3.8 and Table 3.2).

iii) The reduction in the cut-off spatial frequency and the loss of sensitivity at lower spatial frequencies contribute equally to the loss in the CSF with increasing disease severity. However, the loss in the cut off spatial frequency appears to precede the loss in sensitivity at lower spatial frequencies (Figure 3.9B - D).

iv) Stereoacuity is reduced in keratoconus compared to controls; mild forms of the disease that is symmetric in the two eyes show slightly better stereoacuity than moderate and advanced forms of the disease with or without interocular symmetry (Figure 3.10 and Table 3.3). The decline in stereoacuity may thus be steeper than the corresponding decline in spatial vision in this disease condition.

v) These patterns of loss in spatial and depth vision are not unique to the metric used here to describe changes in structure with disease severity (D-index). Instead, the structure-function

relationship appears comparable across several other indices of corneal distortions that veridically capture the progression of keratoconus (Appendix, Figure A1).

3.6.2. Implications of these results for the clinical management of keratoconus

The study findings clearly highlight the complex nature of the structure-function relationship in keratoconus. Several features of this relationship indicate the need to evaluate multiple visual functions and at multiple time points during disease progression to obtain a comprehensive understanding of vision loss in keratoconus (Figure 3.6 to Figure 3.10) (Ferdin et al., 2019, Kandel et al., 2020, Belin et al., 2022). The following three features are of relevance here. First, that this relationship is non-linear suggests that a given quantum of deterioration in optical structure does not result in an equal proportion of loss in function at all disease severities (Figure 3.6 to Figure 3.10). Second, that the pattern of this relationship was dissimilar across visual functions indicates that different visual functions have different levels of vulnerability to the same loss of optical structure in keratoconus (Figure 3.6 to Figure 3.10). Consequently, the loss observed in one visual function at a given stage of the disease cannot be extrapolated to other visual functions in any meaningful manner. Third, even while the pattern of the structure-function relationship may be broadly similar across different tomographic indices (Figure A1), the differences observed between them suggest that switching between indices to determine the changes in visual functions of a patient at different stages of disease is not straightforward and not recommended for clinical practice. With all these factors considered, the structure-function relationships derived in this study may be used by eye care practitioners to make meaningful inferences about the nature of visual functions loss experienced by patients at different severities of the disease.

The present study showed that AUCSF deteriorated in early keratoconus, even while high contrast visual acuity remained relatively intact (Figure 3.6 to Figure 3.8, Table 3.2). These results agree with Shneor et al. (2021) and (Xian et al., 2023) who observed significant losses in the

discrete spatial frequencies they probed within the CSF in patients with forme-fruste or sub-clinical keratoconus with intact visual acuities. This result can be interpreted in two ways. One, the loss of optical fidelity in early keratoconus is not large enough to deteriorate resolution of high spatial frequency optotypes used in the assessment of visual acuity, but they are large enough to impact contrast detection that attenuate the AUCSF. This explanation is counter-intuitive because the cut-off spatial frequency in the CSF, an oft-used surrogate of visual resolution limit (Chung and Legge, 2016, Xian et al., 2023), showed no such “ceiling” effect in our cohort (Figure 3.6 B). Perhaps, the “ceiling effect” in high contrast visual acuity arises from the keratoconic eye’s ability to correctly interpret a slightly blurred image, even while the associated retinal image quality loss produces deficiencies in contrast processing at threshold (Marsack et al., 2007, Marella et al., 2021). Two, the measurement resolution of visual acuity is not as fine as that of contrast sensitivity, leading to a spurious “ceiling” effect for this visual function. Typically, the clinical assessment of visual acuity involves a line-by-line allocation of acuity score that offers allowance for the entire line even when a few optotypes may be incorrectly identified (Ng and Wong, 2022). A letter-by-letter allocation of acuity scores, as performed in this study, improves resolution and reduces the chances of such spurious patterns. That the ceiling effect was observed despite this protocol being followed suggests that the ceiling effect is either not spurious or that the measurement resolution needs further refinement to avoid such challenges. Additionally, visual functions were assessed in this study with the reduced aperture trial lenses in place. In cases of keratoconus with significantly high astigmatism, this can pose challenges and could possibly affect the results. However, the visual angle of the stimulus (4° for the spatial tasks and 7° for the stereoacuity task) were too small to possibly impact the study results. What resolution of acuity measurement is acceptable for such purposes, however, remains to be defined. Whatever the reason for this effect, the eye care practitioner should not rule out disease progression or visual functions loss if visual acuity

remains unaltered – instead, visual acuity assessment should be complemented with assessments of CSF and stereoacuity in all patient visits. The study also observed that the acuity loss, once initiated beyond the ceiling phase, occurs at a rate that is steeper than AU-CSF (Figure 3.8, Table 3.2). The result of this is that the “floor” phase of both functions is reached at more or less the same magnitude of disease severity, even while the acuity loss started happening at a later level of disease severity (Figure 3.8). This is somewhat unexpected, for the distinct “ceiling” phase and an ability to recognize optotypes despite a loss of optical fidelity would have predicted the opposite trend. Alternately, this loss rate may indeed be what is predicted by optical quality loss, and that the shallower loss rate of AU-CSF reflects some form of active recalibration in contrast processing to optimize the “visible area” constituted by the CSF. Recently reports on suprathreshold contrast processing certainly allude to the presence of such a recalibration in the keratoconic visual system (Ng et al., 2022). A detailed analysis of how the retinal image quality varies with D-index and its comparison with psychophysical measures of visual performance is needed in all these patients for definitive answers.

3.6.3. Modelling the structure-function relationship data

Mathematical modelling of the raw data using regression analysis allows a determination of the extent to which the independent variable (structural measure of D-index, in this case) explains the variability seen in the dependent variable (visual functions, in this case) (Figure 3.7 to Figure 3.10) (Kanellopoulos and Asimellis, 2013, Medeiros et al., 2012). The residuals plot indicates the presence of systematic biases in the way the regression fit explains the relationship between the dependent and independent variables (Figure 3.7) (Liu et al., 2011). Ideally, the independent variable should be free from any measurement error and all the variance in the data is attributable only to the dependent variable. If not, as was the case in this study wherein the D-index may also contain measurement variability from the corneal tomography scans (Shetty et al., 2017), an orthogonal regression that even distributes the error

between the dependent and independent variables ought to be performed (Perin et al., 2014). That only an ordinary regression analysis was performed is a limitation of this study. Orthogonal regressions typically result in slightly higher R^2 values than ordinary regressions and, therefore, performing the former analysis would have only increased the strength of the regression analyses shown in this study (Figure 3.7, Figure 3.9 and Figure 3.10). This limitation notwithstanding, distinct differences were observed between the four regression models tested in this study. The linear and positive exponential regressions had relatively lower R^2 values and could not veridically represent the transition of visual acuity and AUCSF into their respective floor phases with increasing D-index values (Figure 3.7). The other two functions –the negative exponential and the logistic regression equations – explained more of the data variance, with little or no bias in the residual plots (Figure 3.7). Between these two functions, the logistic regression fared marginally better than the negative exponential function owing to its potential ability to delineate the three distinct phases in the structure-function relationship – the ceiling phase at early disease stages, the intermediate phase where functional loss is proportional to the structure loss and the floor phase at advanced disease stages. Both functions are equally well-suited to explain the latter two phases of the structure-function relationship, but the negative exponential is less suited to explain the ceiling effect relative to the logistic regression function (Figure 3.1). That the superiority of the logistic model was only marginal relative to the negative exponential model [that too, only for visual acuity (Figure 3.7)], suggest that the early ceiling phase of this structure-function relationship is not as robust as the other two phases and may be subject to change with sample size and data variance.

Piece-wise linear regression analysis may be a simpler and more intuitive alternative to the logistic regression function fit to the raw data of spatial vision in this study (Ochab and Puszynski, 2020). The hypothesis of the structure-function relationship having three distinct phases could be potentially examined using a tri-linear regression equation. The expectation

would be that the slopes of the linear pieces corresponding to the ceiling and floor phases would be near-zero and their y-intercepts would indicate the magnitude of the visual function in these phases. The intermediate zone would have a non-zero slope which would indicate the loss rate of the visual function with increasing structural deformation. The intersection points of the linear pieces would indicate the D-index values that mark the end of the ceiling phase and the other marking the beginning of the floor phase. While this model might be useful from a clinical perspective to bin patients into one of the three phases, it artificially breaks a biological variable that is inherently continuous into discrete phases. The natural course of keratoconus progression (and for that matter, any disease) involves a spectrum of structural changes that occur gradually over time. The continuous nature of this may be veridically represented by a model that accounts for the subtle transitions and ongoing modifications in the cornea. The tri-linear equation, characterized by abrupt transition between phases, may therefore oversimplify the complex structure-function relationship in this disease condition. Taken together, despite its complexity, the ability of the logistic regression function to retain the continuous nature of the independent variable makes it more attractive over its piece-wise linear regression counterparts to model the structure-function relationship in keratoconus.

3.6.4. Explaining the structure-function relationship from the optical quality of the eye

The losses in spatial and depth vision observed in this study may be explained by the underlying loss of retinal image quality in the two eyes. Retinal image quality may be derived from the wavefront aberrations of the eye and quantified in terms of the modulation and phase transfer functions (MTF and PTF) using standard Fourier optics techniques. The ensuing analysis will describe the relationship between the losses in retinal image quality and visual functions using only the MTF derived only from higher-order aberrations of the eye (lower-order aberrations are assumed to be fully corrected) over 3mm pupil diameter and for 555nm light (Figure 3.11) (Thibos et al., 2004). Little is known about the PTF in keratoconus and hence its impact on the

retinal image quality is presently ignored. Also, the MTF's were rotationally averaged in this analysis, ignoring the asymmetries commonly observed in highly-aberrated eyes like keratoconus (Marsack et al., 2007). For all these reasons, the following analysis may only be considered as an overall framework for how the retinal image quality determines spatial and depth vision in keratoconus.

As shown in Figure 3.11, the low-pass filtering of the MTF progressively increases with disease severity, intersecting the neural transfer function (NTF) at progressively lower spatial frequencies (Figure 3.11). The visual acuity (Figure 3.6A and Figure 3.7D) and the cut-off spatial frequency of the CSF (Figure 3.9B) are determined by this intersection point (intersection of NTF and the highest lobe in the case of phase shifts in the retinal image quality (Thibos et al., 2004); see MTF of severe keratoconus in Figure 3.11 and that are clearly shifted to lower spatial frequencies with increasing disease severity (Figure 3.11 A). The “visible” area for spatial vision, described empirically using the AUCSF parameter in this study (Figure 3.6 B and Figure 3.7 L), also gets progressively attenuated with increasing disease severity (Figure 3.11 A). The contrast energy available for the lower spatial frequencies, except for the very low ones, also reduces with advancing disease severity (Figure 3.11 A), reflecting the empirical loss of sensitivity at the 3cpd spatial frequency (Figure 3.9 C).

Stereoacuity loss is dependent on both the overall and interocular difference in keratoconus severity (Westheimer and McKee, 1980, Schor and Wood, 1983). For symmetric disease severities in the two eyes, the highest spatial frequency available in the retinal images for correspondence matching and subsequent calculation of retinal disparity for stereo progressively shifts to lower frequencies with increasing disease severity (Figure 3.11B). Stereo thresholds mediated through lower-spatial frequencies are poorer than when mediated through higher-spatial frequencies (Schmidt, 1994), thus predicting worse stereoacuity with increasing keratoconus severity (Figure 3.11B).

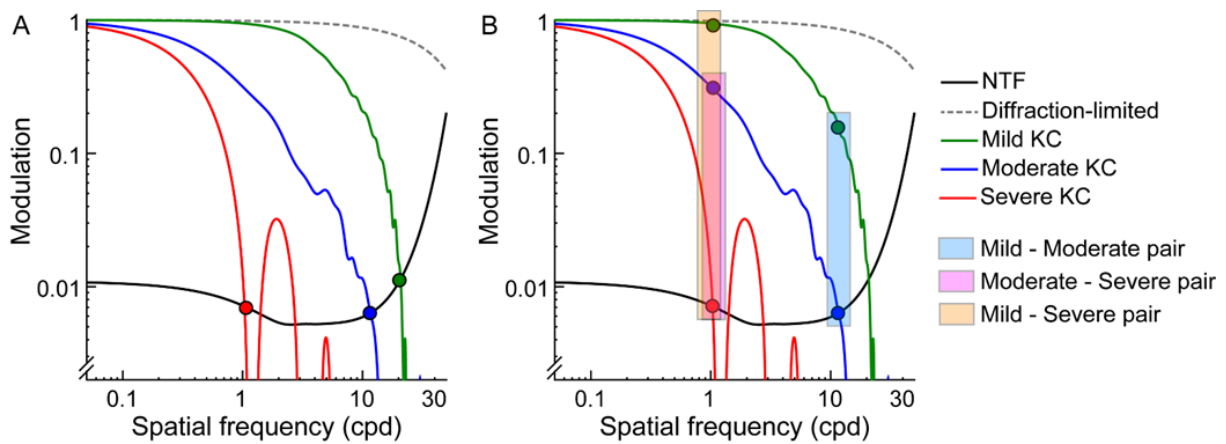


Figure 3.11: Rotationally averaged modulation transfer functions (MTFs) for diffraction-limited optics and for representative subjects with mild, moderate, and severe keratoconus (KC). The MTF's derived from the ocular higher-order wavefront aberrations for 3mm pupil diameter at 555nm and the neural transfer function (NTF) for a 25-yr old subject at 400Td of retinal illuminance, as described by Hastings et al. (2020), are plotted in this figure. Multiple lobes in the MTF (see for severe KC) represent the effect of phase shifts in the retinal image. Panel A highlights the intersection point between the MTF and NTF for different severities of keratoconus (filled circles). Panel B depicts the matching spatial frequency and the associated interocular difference in contrast for three asymmetry pairs of keratoconus (mild-moderate, mild-severe and moderate-severe). The filled circles where the MTF and NTF intersect represent the highest spatial frequency available for stereo processing in these eyes.

This relationship is, however, more involved for bilaterally asymmetric disease severity. The highest spatial frequency available for correspondence matching and disparity processing is defined by the eye with greater disease severity in a given asymmetry pair (Figure 3.11B). This frequency is relatively lower for the mild-severe and moderate-severe pairs compared to the mild-moderate pair, thus predicting lower stereoacuity in the former two cases compared to the latter (Figure 3.11B). This loss is compounded by the well-known contrast paradox effect in stereoacuity, wherein interocular differences in contrast are more potent at deteriorating stereoacuity than overall losses in contrast (Schmidt, 1994, Cormack et al., 1997). The interocular difference in contrast for the mild-severe pair is larger than that of the mild-moderate or the moderate-severe pairs (Figure 3.11B), thus predicting lower stereoacuties for the former than the latter two cases. Given that the contrast paradox is more prominent for lower- than higher-spatial frequencies (Cormack et al., 1997), the mild-severe pair may

experience a double-whammy for stereoacuity by having a large interocular difference in contrast at a relatively low matching spatial frequency (Figure 3.11B). The moderate-severe asymmetry pair and the mild-moderate asymmetry pair experience similar interocular difference in contrast, with its effect on stereoacuity likely to be greater for the former pair than the latter owing to the contrast paradox phenomenon (Cormack et al., 1997). All these predictions were more or less observed in the empirical data shown here – stereoacuities progressively worsened with increasing disease severity for all sub-cohorts of keratoconus (Table 3.3). Stereoacuities were also relatively better in sub-cohorts with lower-than-median IOD in D-index, than in those with higher-than-median IOD's (Table 3.3). Despite these trends, the stereoacuity differences did not reach statistical significance for the moderate and severe sub-cohorts, reflecting the floor effect for stereoacuity in keratoconus (Figure 3.10D).

3.7. Summary

Vision loss in keratoconus is critically dependent on the overall disease severity in the two eyes, the symmetry of disease between eyes (for binocular visual functions), the type of visual function being evaluated, and the psychophysical measurements adopted to evaluate this visual function. Amongst the visual functions commonly evaluated in the clinic, stereoacuity may be the first to deteriorate significantly, followed by contrast sensitivity and then high contrast visual acuity. Losses in functional depth vision and contrast sensitivity may therefore be early symptoms of keratoconus, prior to perceptible losses in optical resolution. The logistic regression equation described in this study for cross-sectional data of visual acuity and contrast sensitivity may be used in the future for predicting longitudinal losses in these functions with advancing keratoconus or following optical/surgical interventions to limit its progression.

4. Chapter 4: Comparative analysis of different optical management strategies in keratoconus

4.1. Introduction

The subjects that participated for the experiments in chapter 3, were neophytes and were visiting the clinic for the first time. As per the standard clinical protocol, all these cases are expected to be managed optically with the help of contact lenses (CLs). The optical management of keratoconus using CLs depends greatly on finding the lens that provides the best visual performance. It is well-established that visual performance is enhanced with CL wear in keratoconus relative to spectacles (Naroo et al., 2022, Santodomingo-Rubido et al., 2022), but there is no clear consensus for the superiority of one CL design over another in improving the patient's visual performance. While the early form of the disease can be still managed with spectacles or conventional soft toric contact lenses, different forms of special design contact lenses are preferred as the disease severity increases (Mandathara et al., 2017, Kumar et al., 2019, Santodomingo-Rubido et al., 2022). In terms of optical management of keratoconus, conventional RGP CLs are the most widely used lens modality among the available options. However, poor wearing comfort and the process of adapting to the lenses have been a major hindrance in considering them for long-term usage (Schornack and Patel, 2010, Weed et al., 2007). The newer modalities of CLs (e.g., Rose K CL, Kerasoft CL and scleral CL) theoretically offer improved lens designs and materials (Mandathara et al., 2017). Given the expanded range of CLs available currently for keratoconus management, two inter-related issues become pertinent to answer. First, whether there is an objective paradigm available to the practitioner regarding the selection of final choice of CL to be dispensed to the patients. Second, how does the performance efficacy of different CL designs compare relative to each other. In the end, the practitioner needs to employ a systematic evidence-based approach for choosing one design over another for their patient.

At present, the rationale for determining the choice of CL dispensed to a patient with keratoconus largely depends upon: the anatomical fit of the CL on the cornea/sclera; the comfort of the CL; ease of lens care; cost of the lens; and, the patient's quality of vision as assessed through their monocular high-contrast visual acuity (Mandathara et al., 2017). While these are perfectly acceptable metrics to evaluate the CL's performance, as the results show in Chapter 3, high contrast visual acuity does not satisfactorily represent the full complexity of the patient's day-to-day visual experience (Wandell, 1995). The improvement in monocular high-contrast visual acuity with CLs in keratoconus is well-established but there is limited evidence on the impact of CLs on contrast sensitivity (Negishi et al., 2007, Montalt et al., 2018), binocularity (Sherafat et al., 2001, Nilagiri et al., 2018, Metlapally et al., 2019) and optical quality (Nilagiri et al., 2020, Gumus et al., 2011) with different CL modalities, compared to spectacle correction. Moreover, previous studies do not necessarily compare the visual functions across different CL designs in keratoconus. There is, therefore, a need for a more systematic investigation of the performance of different CL designs in patients with keratoconus.

Comparison of the relative performance of different CL designs for managing keratoconus reported in previous cross-sectional studies has not found clear evidence for the superiority of one CL design over another (Fernandez-Velazquez, 2012, Montalt et al., 2018). There are several possible reasons for this: first, given the disease heterogeneity of keratoconus, it is practically impossible to closely match all parameters of the keratoconic eye (e.g., topographic changes in the cornea and the morphologic changes in the cornea such as the location and the type of cone) in a cross-sectional study; Second, in addition to the optics, visual function may also be influenced by the subject's neural system, which may vary in keratoconus owing to the subject's age, disease longevity and duration of exposure to blurred vision. All these factors would also influence the outcomes of these cross-sectional studies. These differences can be taken care of with a cross-over study design, wherein the outcome variables are evaluated across

different CL designs in the same subject, as the disease state will have a uniform impact on all the outcome measures reported here.

The aim of the study reported in this chapter was to use a cross-over design to evaluate the visual (high-contrast logMAR acuity, contrast sensitivity and stereoacuity) and optical performance (higher-order wavefront aberrations) of four commercially-available CL designs: conventional RGP[®], Rose K2 GP[®], Kerasoft IC soft[®] and Scleral[®] CLs (see chapter 2) in the same cohort of subjects with bilateral keratoconus.

4.2. Methods

4.2.1. Patient selection, inclusion, and exclusion criteria

The study adhered to the tenets of Declaration of Helsinki and was approved by the Institutional Review Board (LEC-BHR-P-07-20-467). All subjects participated after signing a written informed consent form. All controls were recruited from the staff or students at LVPEI. All subjects with a clinical diagnosis of keratoconus and who were neophytes to CL wear were recruited from the cornea and contact lens services of LVPEI. The diagnosis of keratoconus was established after confirmation of clinical and topographic signs (Kanski and Bowling, 2015) and disease severity was graded using the Amsler-Krumeich classification system (Krumeich et al., 1998). Eyes with previous history of CL wear or surgery, presence of an apical corneal scar, or significant superficial punctate keratitis and sensory and motor binocular vision abnormality (e.g., tropia, receded near point of convergence, suppression and amblyopia) were excluded. Subjects who reported their inability to understand the experimental paradigm and provide reliable responses were also excluded from the study. Standard clinical management was followed for all subjects, with no influence of the study protocol on their subsequent care in the Institute.

4.2.2. Study protocol- contact lens fitting

Overall, the keratoconic subjects visited the study site for six different visits. In the first two visits, contact lens fitting was finalized for four CLs by a single experienced optometrist (two CL fits were scheduled on a given visit). Conventional RGP and scleral CLs were sourced from Purecon McAsfeer (Silver line laboratory Pvt. Ltd, Delhi, India), special design Rose K corneal GP lens were sourced from Rose K2 (Menicon Co. Ltd., Nagoya, Japan) and KeraSoft IC[®] CLs were sourced from Ultravision (Ultravision^{CLPL} international Limited, Bedfordshire, UK). For the conventional RGP and Rose K2 CLs, the base curve of the initial trial lens was selected based on the best-fit sphere parameter from the topography map. The CL fit on the eye was then assessed for appropriate centration and movement using standard clinical procedures and the endpoint of the CL fit was determined by the lens base curve and diameter that resulted in a feathery apical touch on fluorescein staining (Zadnik et al., 1998). For the KeraSoft CL, the fitting was initiated using the company recommended guidelines and the endpoint was determined by the lens parameters that produced a well-centered optic zone, adequate lens movement (no more than 3 mm in the primary gaze), minimal lag on up-gaze, vertical orientation of the laser mark and no subjective fluctuation in vision after each blink (Fernandez-Velazquez, 2012). For scleral CLs, the endpoint of the fit was determined as having a sufficient fluid reservoir underneath the lens back surface along with minimal compression of the peripheral curves of the lens on the sclera and the overlying conjunctiva (Vincent et al., 2018). Each subject's sphero-cylindrical refractive error with spectacles or over-refraction with the different CL modalities was finalized using standardised subjective refraction procedures as documented in chapter 3 above. Customized CLs were ordered for each subject and data collection commenced on receipt of all lenses. Subjects attended for an assessment with one optical correction (spectacles or one of the four CLs randomly selected per visit), with at least one week gap between visits (Jinabhai et al., 2012a, Kumar et al., 2020). The final CLs were

dispensed to the subject at the end of the study period free of cost and the remaining CLs were added to the institute's library stock of lenses.

4.2.3. Study protocol- ocular aberration and psychophysical testing

All psychophysical measurements were made with the subject's spectacle and over-refraction corrections incorporated using trial lenses and a trial frame. Monocular and binocular high-contrast logMAR acuity was determined at a 3m viewing distance using COMPlog[®] (Clinical Vision Measurement Systems Ltd, London, UK) (Laidlaw et al., 2008). The monitor characteristics, procedure and the steps of data acquisition were similar to those described in the previous chapter (Section 0 above). The monocular and binocular contrast sensitivity functions (CSF) were determined using a modified version of the quick CSF program developed in Matlab[®] (Lesmes et al., 2010, Rosen et al., 2014). The experimental setup and the steps of data acquisition were the same as documented in chapter 3 (section 0, above). Stereoacuity was measured using a custom-designed Howard-Dolman apparatus at 3 m viewing distance where subjects aligned two thin rods presented in depth against a monocular-depth cue-free background. The axial separation between the two rods where subjects no longer perceived a depth difference provided a measure of the subject's stereoacuity (Bandela et al., 2016, Howard, 1919). This setup was capable of producing disparities ranging between 1.5arc sec to 2260arc sec for a 60 mm interpupillary distance (Bandela et al., 2016). In the random-dot stereogram used in the chapter 3, disparity threshold is usually detected by the amount of spatial displacement (X and Y dimension) between the random dots on the computer monitor (Section 3.2). However, estimating the axial separation (Z- dimension) between the rods in the Howard-Dolman apparatus provides an opportunity to directly assess depth performance and makes the task more inclined towards assessment of functional depth performance.

Wavefront aberrations were measured using the irx3[™] wavefront aberrometer (Imagine Eyes, Orsay, France) three times in each eye for the subject's natural pupil diameter and scaled to a

3 mm pupil diameter using standard computational techniques and averaged (Campbell, 2003, Visser et al., 2011). The eye's optical quality was described in terms of the overall Higher Order Root Mean Squared (HORMS) deviation of the 3rd to 8th order wavefront aberration terms.

4.3. Data analysis and hypothesis

Statistical analyses were performed using SPSS[®] v.20.0 (SPSS, Chicago, IL, USA) and Matlab R2016a[®] (The MathWorks, Inc, Nantucket, MA). The sphero-cylindrical refractive error data were represented using power vector notation M, J0 and J45 (Table 4.2) (Thibos et al., 1997). The Shapiro-Wilk test indicated that the outcome variables were not normally distributed and therefore, all data were analyzed using non-parametric statistics. The Wilcoxon signed rank test was used to determine the statistical significance of the inter-ocular difference in results of the cohort with the significance (type 1 error) threshold set at 5%. The Friedman test determined the overall statistical significance of an outcome variable across different management options and post-hoc Wilcoxon signed rank test with Bonferroni correction used to determine the significance of subsequent pair-wise comparisons.

In this study, the subject's D-index value, derived from the Scheimpflug imaging using Pentacam HR[®] (Oculus Optikgeräte GmbH, Wetzlar, Germany) was used as a surrogate measure of disease severity (as described in chapter 3) (Shajari et al., 2019). For monocular outcome measures, the corresponding eye's D-index value was used for analysis while for binocular outcome measures, the average D-index of both eyes was used. Two types of analyses were performed in this study. The first analysis used the entire dataset obtained across all subjects to determine if there was a significant difference in visual performance between different optical corrections in keratoconus. The second analysis divided the subjects into two broad categories, mild to moderate keratoconus and severe keratoconus. This categorization was performed using the well-established Amsler-Krumeich classification (Krumeich et al., 1998). Steep keratometry values $\leq 53D$ were used to define the former group whereas,

keratometry values $> 53D$ were used for the latter group. This analysis used keratometry as a structural measure for the classification for two reasons: first, there is no existing literature at present that can grade the severity of keratoconus on the basis of D-index; second, the keratometry value is used in the Amsler Krumeich classification, which is currently the most widely used grading scale and therefore, the results would be easy to interpret and apply in clinical practice (Belin et al., 2022). The analysis determined if the CL designs tested here had a differential impact on the subject's visual performance and optical quality depending on disease severity. It was hypothesized that: 1) all four CL designs would produce better visual performance than spectacles, independent of disease severity, and 2) there would be a differential impact of the CL design on visual performance and optical quality in advanced keratoconus but not in mild to moderate keratoconus.

The fold-change of performance in logMAR acuity, contrast sensitivity and stereoacuity with CL wear, relative to spectacles, was calculated as the outcome value wearing CLs divided by the corresponding value with spectacles. For logMAR acuity, the data were converted into a decimal scale due to the convenience of calculating the fold change, while the data were retained as is for contrast sensitivity and stereoacuity. A fold-change of unity indicates no change in performance with CLs while a fold-change greater than unity indicates improvement in performance with CLs, both relative to spectacles.

A multiple regression analysis was further undertaken to determine how the monocular and binocular fold-change of performance was influenced by the following factors: severity of keratoconus as determined by the subject's D-index, modality of CL correction (coded as 1 for conventional RGP CL, 2 for Kerasoft CL, 3 for Rose K2 CL and 4 for scleral CL), location of the cone in keratoconus (coded 1 for central cone and 2 for paracentral cone), self-reported duration of keratoconus (in years) and subject's age (in years). For monocular visual performance, results from the right and left eyes were very similar to each other and hence data

from only the right eye was used. Since the location of the cone in both eyes of keratoconic subjects was similar, the data of the right eye was considered as the independent variable in the binocular analysis.

4.4. Results

4.4.1. Demographic and refractive features

Twenty-eight subjects with bilateral keratoconus and 10 control subjects participated in the study. Data were successfully collected in 27 subjects with keratoconus and in all controls. Data from one keratoconic subject were excluded as the assessments could not be completed for all the CLs due to logistical reasons.

Table 4.1 provides the median (interquartile range) of the CL parameters for the keratoconic subjects in this study. For the baseline measurements (i.e., without the contact lenses), there was no statistically significant difference in the D-index, keratometry, HORMS and the M and J0 values of the power vector between the two eyes ($Z \geq 1.1$; $p \geq 0.05$) (Table 4.2). The J45 component was however statistically significantly different between the two eyes ($Z = 3.9$; $p < 0.05$) (Table 4.2). For over-refraction with CLs, the data between the two eyes were not significantly different for all power vector components ($Z \geq 1.1$; $p > 0.05$), except J0 in conventional RGP and Kerasoft CLs ($Z \geq 2.1$; $p < 0.05$) (Table 4.2).

There was a statistically significant difference in the M and J0 values of over-refraction between CLs in both eyes ($\chi^2 \geq 10.2$; $p \leq 0.05$) (Table 4.2). The M values when wearing the Kerasoft CLs were significantly different from all others in both eyes ($Z \geq 2.6$; $p \leq 0.01$) (Table 4.2). The J0 values in the right eye were significantly different between the Scleral and RGP CLs ($Z = 2.1$; $p = 0.03$) and between Scleral and Rose K2 CLs ($Z = 2.27$; $p = 0.02$) (Table 4.2). The J0 component in the left eye was significantly different between Kerasoft and all other

CLs studied here ($Z \geq 2.2$; $p \leq 0.02$) (Table 4.2). There was no statistically significant difference in the J45 values across different CLs in the two eyes ($\chi^2 \leq 6.9$; $p \geq 0.07$) (Table 4.2).

	BC (mm)	BVP (D)	Diameter (mm)	Vault (mm)
RGP CL	7.0 (6.6 – 7.3)	-5.0 (-7.6 to -3.6)	9.1 (8.9 – 9.20)	NA
Rose K2 CL	6.8 (6.4 – 7.15)	-6.0 (-10.5 to -4.0)	8.9 (8.70 – 9.10)	NA
Kerasoft CL	8.0 (7.9 – 8.4)	-5.5 (-9.0 to -3.25)	14.5 (14.5 – 14.75)	NA
Scleral CL	8.0	-3.0 (-6.5 to -2.0)	16.0	4.9 (4.8 – 5.2)

Table 4.1: Median (interquartile range) base curve (BC), back-vertex power (BVP), diameter and vault values for the four different CLs that were finalized across the keratoconic subjects that participated in this study. All scleral lenses used in this study had a central base curve of 8.0 mm and a diameter of 16.0 mm.

Overall population (n=27)		
Age (yrs)	24 (20 - 28)	
Duration of keratoconus (yrs)	3 (2 - 5)	
Male: Female	15: 12	
	RE	LE
D-index (no units)	11 (7.6 – 15)	10.1 (7.0 – 15.6)
Steep keratometry (D)	53 (50 – 58.5)	52 (48.9 – 65.1)
Flat keratometry (D)	47 (45.9 – 52.4)	48 (44.4 – 56.5)
HORMS at 3 mm pupil	0.4 (0.23 – 0.52)	0.34 (0.22 – 0.50)
Uncorrected subjective refraction		
M (D)	-6.00 (-9.25 to -2.00)	-4.12 (-12.25 to -2.25)
J0 (D)	-0.47 (-1.53 to 1.00)	-0.65 (-1.53 to 0.34)
J45 (D)	1.44 (0.85 to -2.21)	-1.12 (-1.72 to -0.01)
Kerasoft CL over refraction		
M (D)	-0.62 (-1.12 to 0.00)	-0.50 (-1.37 to -0.12)
J0 (D)	0.08 (-0.25 to 0.37)	0.24 (0.12 to 0.58)
J45 (D)	0.00 (-0.08 to 0.00)	-0.01 (-0.21 to 0.49)
Rose K2 CL over refraction		
M (D)	0.00 (-0.62 to 0.00)	-0.18 (-0.62 to 0.00)
J0 (D)	0.00 (0.00 to 0.01)	0.00 (0.00 to 0.01)
J45 (D)	0.00 (0.00 to 0.00)	0.00 (0.00 to 0.00)
RGP CL over refraction		
M (D)	0.00 (-0.40 to 0.06)	0.00 (-0.50 to 0.12)
J0 (D)	0.00 (0.00 to 0.12)	0.00 (-0.18 to 0.00)
J45 (D)	0.00 (0.00 to 0.01)	0.00 (0.00 to 0.00)
Scleral CL over refraction		
M (D)	-0.01 (-0.5 to 0.00)	-0.25 (-0.75 to 0.00)
J0 (D)	0.00 (0.00 to 0.00)	0.00 (0.00 to 0.00)
J45 (D)	0.00 (0.00 to 0.00)	0.00 (0.00 to 0.02)

Table 4.2: Overall demographics along with the median (interquartile range) D-index, keratometry, HORMS, uncorrected subjective refraction and over-refraction with different CL options in both eyes of subjects that participated in the study. The subjective refraction and over-refraction values are represented as M, J0 and J45 power vector components.

4.4.2. Individual trends in visual performance with CLs

The logMAR acuity, area under the CSF curve and stereoacuity of individual subjects that participated in this study are shown in Figure 4.1. Across all outcome variables, the spectacle correction resulted in the worst performance followed by correction with Kerasoft CLs in all subjects (Figure 4.1). The visual performance with the remaining three CLs – conventional RGP, Rose K2, and Scleral lenses – were better than spectacles and the Kerasoft CL, and comparable with each other, as suggested by their clumping relative to the other two corrections in all subjects (Figure 4.1). Some minor variations from this general trend were seen. The area under the CSF curve with Scleral CLs was worse than conventional RGP and Rose K2 CLs in subject 3 (panel B). The area under the CSF curve with Rose K2 CL correction was similar to spectacle correction in subject 15 (panel B) and stereoacuity with a Scleral CL was worse than conventional RGP and Rose K2 CLs in subjects 6, 15, 17 and 18 (panel C).

4.4.3. LogMAR acuity and contrast sensitivity function

Figure 4.2 and Figure 4.3 show scatter plots of the spatial vision parameters plotted as a function of the subject's D-index value for the different optical corrections. The interquartile range of controls is represented as a grey band in these and all subsequent figures. In general, the monocular and binocular logMAR acuity (Figure 4.2) and the area under the CSF (Figure 4.3) worsened with an increase in the D-index value across all correction modalities. As expected, the loss was greatest for spectacles and it was restored to different degrees with CL wear (Figure 4.2 and Figure 4.3). There was a significant difference in logMAR acuity and area under the CSF across different optical corrections ($\chi^2 = 143.3$; $p \leq 0.05$).

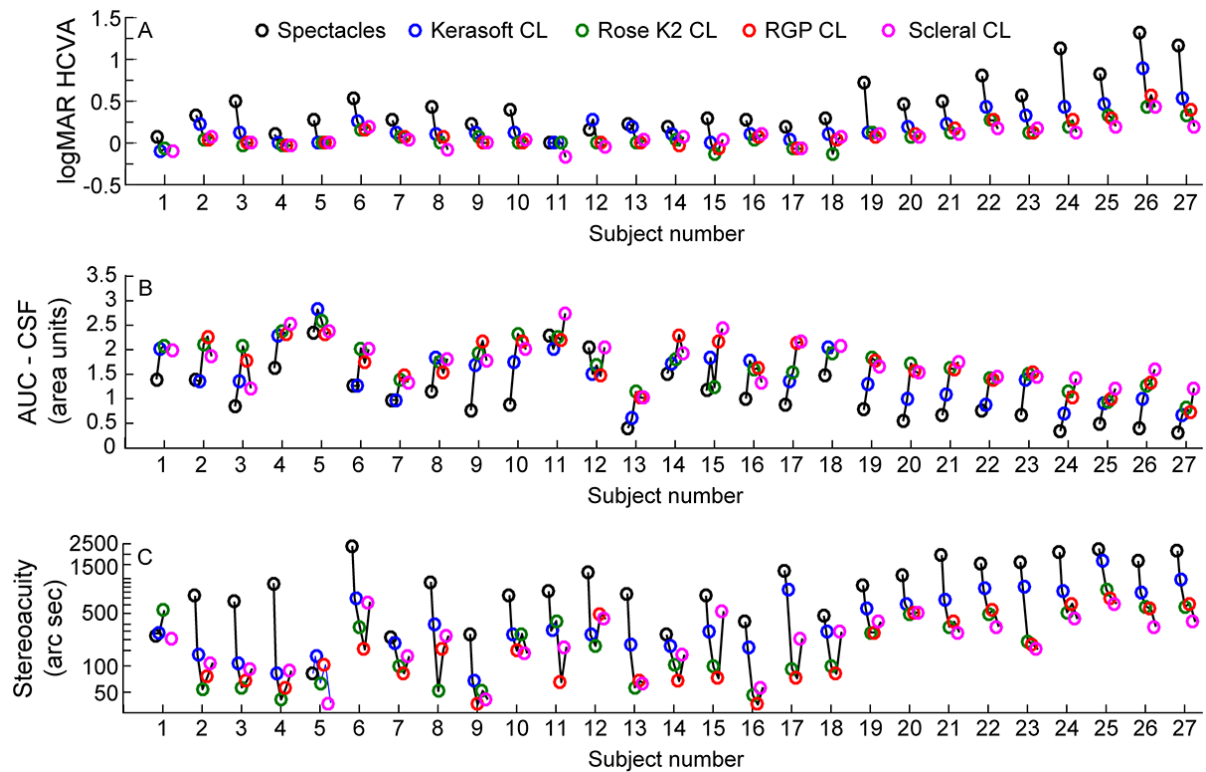


Figure 4.1: Data of binocular logMAR acuity (panel A), area under the CSF (panel B) and stereoacuity (panel C) for all 27 subjects on whom data was successfully collected in this study. Each coloured symbol represents data from a given type of correction, in the order of spectacles, Kerasoft CL, Rose K2 CL, conventional RGP CL and Scleral CL. Data from the uncorrected condition are not included here as they were significantly poorer than the data with correction and, including them will obscure the differences observed across various correction modalities. An increase in the ordinate values for logMAR acuity (panel A) and stereoacuity (panel C) indicates performance loss while an increase in the ordinate value for area under CSF curve indicates performance gain (panel B). The ordinate axis of panels A and B are plotted in linear scale while that of Panel C is plotted in logarithmic scale.

The results for spectacle correction were significantly poorer than all four CL designs ($Z \geq 5.9$; $p \leq 0.05$). Those obtained with Kerasoft CLs also showed a significant difference from the other three designs ($Z \geq 5.2$; $p \leq 0.05$) (Figure 4.2 and Figure 4.3). There was no significant difference in the outcomes obtained across Rose K2, conventional RGP and Scleral CLs ($Z \leq 1.5$; $p \geq 0.13$) (Figure 4.2 and Figure 4.3). The same trends were observed when the data was divided into the mild to moderate and advanced disease groups, except that the performance of Rose K2 and Scleral CLs were significantly better than the conventional RGP CLs in the latter cohort ($Z \geq 2.3$; $p < 0.02$) (Figure 4.2 and Figure 4.3). None of the spatial vision parameters

tested here reached the level of controls, with this effect being more obvious for the advanced forms than the mild and moderate forms of the disease (Figure 4.2 and Figure 4.3).

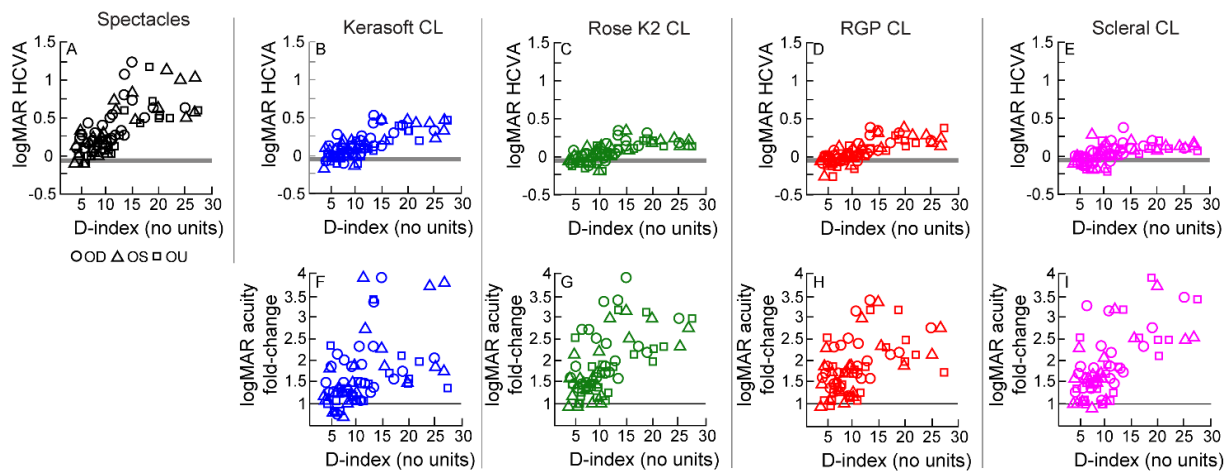


Figure 4.2: Scatter diagram of monocular (right eye: circles; left eye: triangles) and binocular (squares) logMAR acuity obtained with spectacles (panel A), Kerasoft CL (panel B), Rose K2 CL (panel C), conventional RGP CL (panel D) and Scleral CL (panel E) plotted as a function of the subject's D-index value. The gray band in panels A–E represents the interquartile range of the data of age-matched controls. An increase in the ordinate values of logMAR acuity in panels A–E indicates performance loss. Panel F to I plot the fold-change in logMAR acuity obtained with each of the CLs, relative to spectacles. The black horizontal unity line in each of these panels indicates no change in logMAR acuity with a given CL correction, relative to spectacles. An increase from the unity line indicates the magnitude of improvement in performance with CLs compared to spectacles.

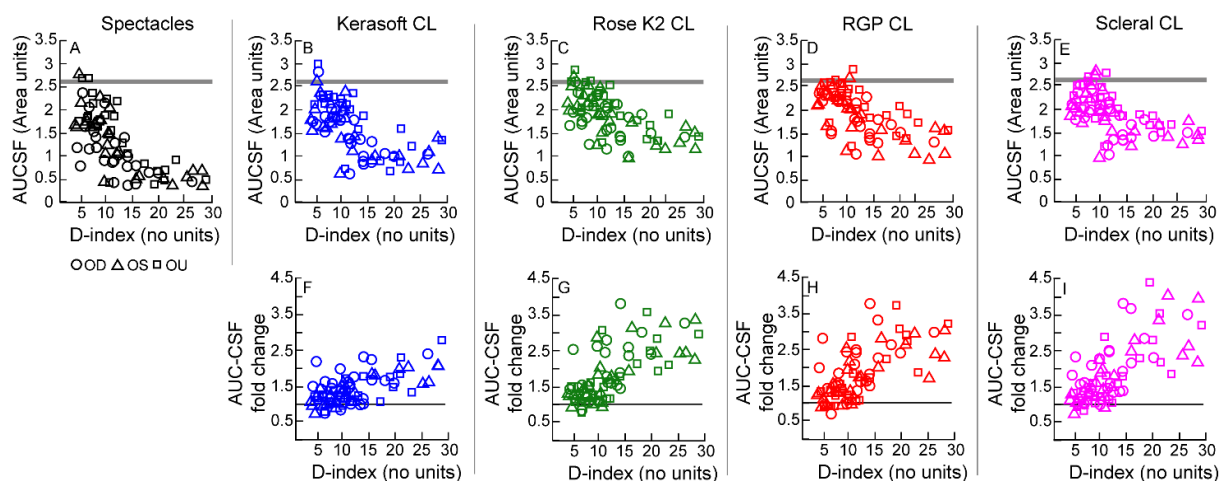


Figure 4.3: Scatter diagram of the area under CSF (AUC-CSF) obtained under monocular and binocular viewing conditions with spectacles (panel A) and different CL designs (panels B–E) plotted as a function of the subject's D-index value. An increase in the ordinate values of AUC-CSF in panels A–E indicates an improvement of performance. Panel F to I plot the fold-change in AUC-CSF obtained with each of the CLs, relative to spectacles. All other details are same as Figure 4.2.

4.4.4. Sub-analysis of the contrast sensitivity function

Shrinkage in the area under the CSF (Figure 4.3) could be either due to a reduction in the cut-off spatial frequency or to a reduction in the sensitivity of each spatial frequency that constitutes the CSF exclusively or to both. The peak spatial frequency of the CSF obtained in this study ranged between 3 and 6cpd across all subjects and optical corrections (data not shown). The sensitivity at the peak spatial frequency of the subject is taken as a representative measure of how this parameter contributed to the reduction of the CSF observed in Figure 4.3 above. Figure 4.4 and Figure 4.5 indicated that both the cut-off spatial frequency and the sensitivity at the peak spatial frequency contributed to the reduction of the CSF with increasing disease severity. For spectacle correction, the cut-off spatial frequency progressively shifted to lower spatial frequencies (Figure 4.4) and the sensitivity of peak spatial frequency progressively decreased (Figure 4.5) with an increase in the subject's D-index values, both relative to controls. Performance was partially restored with CL wear (cut-off spatial frequency: $\chi^2 = 90$; $p \leq 0.05$; sensitivity at peak spatial frequency: $\chi^2 = 79$; $p \leq 0.05$), with Kerasoft CLs producing the least improvement followed by comparable results between Rose K2, conventional RGP and Scleral CLs (cut-off spatial frequency: $Z \geq 3.7$; $p \leq 0.05$; sensitivity at peak spatial frequency: $Z \geq 3.9$; $p \leq 0.05$) (Figure 4.4 and Figure 4.5, panels A–E). For the subgroup analysis, only cut-off spatial frequency was significantly different between the Scleral and Rose K2 lenses in advanced keratoconus cohort ($Z = 2.32$; $p = 0.02$). The fold-change of improvement in the cut-off spatial frequency and sensitivity of the peak CSF were similar to what was reported above for the area under the CSF (Figure 4.4 and Figure 4.5, panels F–I).

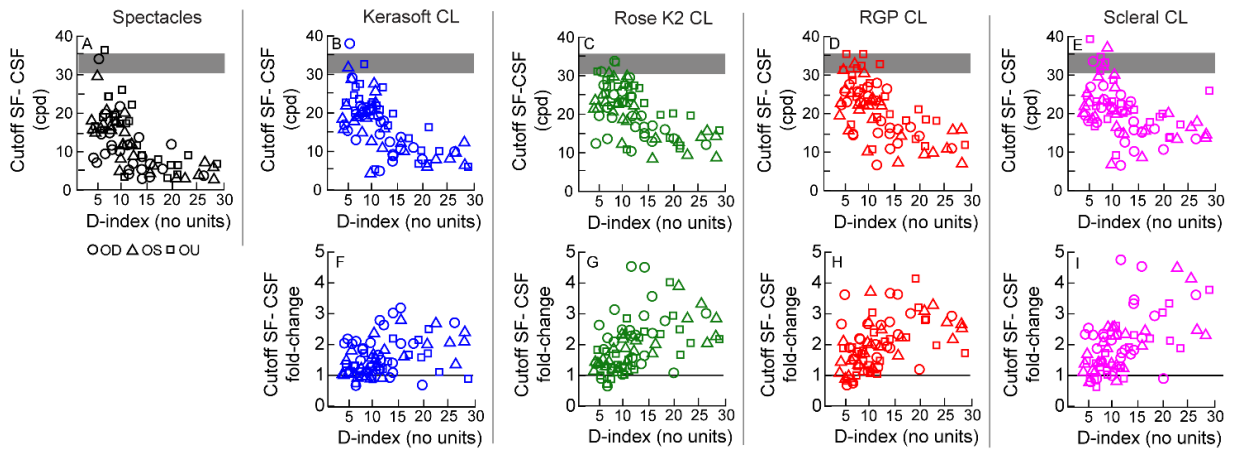


Figure 4.4: Scatter diagram of the cut-off spatial frequency of the CSF curve obtained under monocular and binocular viewing conditions with the spectacles (panel A) and different CL designs (panels B – E) plotted as a function of the subject’s D-index value. An increase in the ordinate values of the cut-off spatial frequency in panels A–E indicates an improvement of performance. Panel F to I plot the fold-change in the cut-off spatial frequency obtained with each of the CLs, relative to spectacles. All other details are same as Figure 4.2.

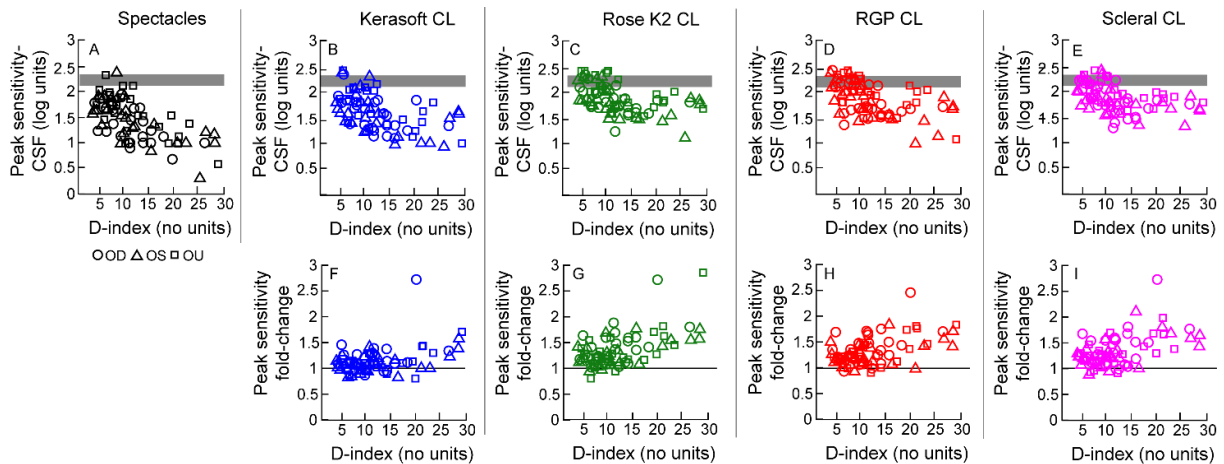


Figure 4.5: Scatter diagram of peak spatial frequency of the CSF curve’s sensitivity obtained under monocular and binocular viewing conditions with spectacles (panel A) and different CL designs (panels B–E) plotted as a function of the subject’s D-index value. An increase in the ordinate values of the peak spatial frequency’s sensitivity in panels A–E indicates an improvement of performance. Panel F to I plot the fold-change in the peak spatial frequency’s sensitivity obtained with each of the CLs, relative to spectacles. All other details are same as Figure 4.2.

4.4.5. Stereoacuity

Figure 4.6 plots the stereoacuity of subjects that participated in this study as a function of their interocular average D-index value. The unaided stereoacuity was immeasurable for most subjects with keratoconus while it was measurable but significantly poor relative to healthy controls with spectacles (Figure 4.6, panel A). There was also a trend for the stereoacuity to

worsen with an increase in the subject's interocular average D-index value with spectacles (Figure 4.6, panel A). Stereoacuities significantly improved with all CL designs ($\chi^2 = 73$; $p \leq 0.05$), with the values reaching the level of controls for the mild to moderate disease cohort ($\chi^2 = 40.2$; $p \leq 0.05$) (Figure 4.6, panel B–E). For the advanced cohort, Rose K2, conventional RGP and Scleral CLs produced a greater improvement in stereoacuity than the Kerasoft CL ($Z \geq 3.62$; $p \leq 0.05$) (Figure 4.6, panel B–E). This trend was also well reflected in the fold-change of stereoacuity relative to spectacles being greater with the Rose K2, conventional RGP and Scleral CLs than with Kerasoft CLs (Figure 4.6, panel F–I).

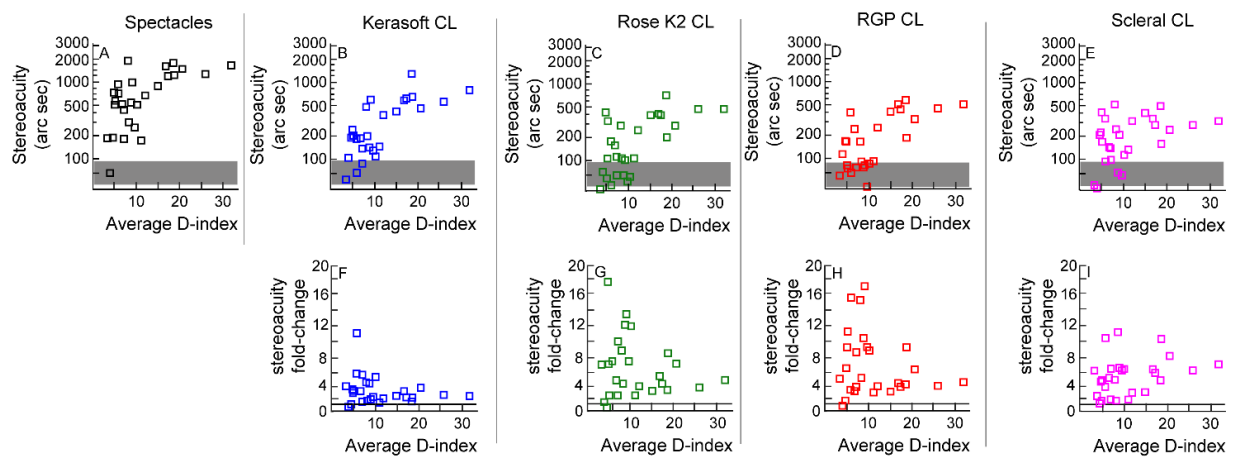


Figure 4.6: Scatter diagram of stereoacuity obtained with spectacles (panel A) and different CL designs (panels B–E) plotted as a function of the subject's average D-index value. An increase in the ordinate values of stereoacuity in panels A–E indicates a deterioration of performance. Panel F to I plot the fold-change in the stereoacuity obtained with each of the CLs, relative to spectacles. All other details are same as Figure 4.2.

4.4.6. Multiple regression analysis

The multiple regression analysis indicated that the fold-change in monocular logMAR acuity with CLs was only influenced by the D-index values [$r^2 = 0.38$, $F(5, 101) = 12.42$, $p < 0.001$] (Table 4.3). The same pattern was obtained for the area under curve of CSF [$r^2 = 0.34$, $F(5, 100) = 10.27$, $p < 0.001$] (Table 4.3). For both outcome variables, the comparison of the standardised beta coefficients (β), used to rank the contribution of the independent variables to the dependant variable, showed that D-index makes the largest contribution to the prediction

of acuity, compared to the other predictors. Similarly, other than the regression coefficient for D-index ($t \geq 4.9$; $p < 0.001$ for both), all other independent variables were not statistically significant ($p \geq 0.06$) (Table 4.3).

For binocular visual performance, logMAR acuity was influenced by both the inter-ocular average D-index as well as the self-reported duration of keratoconus [$r^2 = 0.40$, $F(5, 102) = 17.09$, $p < 0.001$]. Only the regression coefficients corresponding to interocular average of D-index ($t = 7.7$; $p < 0.001$) and self-reported duration of keratoconus ($t = -2.6$; $p = 0.01$) were statistically significant. However, the β analysis indicated that the contribution of the average D-index was the largest compared to the other predictors (Table 4.3). For the fold-change in area under curve of CSF, the average D-index alone, had the greatest contribution compared to the other variables (Table 4.3). For stereoacuity, only the y-intercept was statistically significantly different from zero (y-intercept = 12.5; $t = 3.7$; $p < 0.001$) but none of the independent variables successfully predicted the fold-change ($p > 0.1$) (Table 4.3).

		Variables	B	95% CI	β	t	p-value
Monocular	HCVA	D-index	0.04	0.02, 0.05	0.64	6.41	< 0.001
		CL modality	0.05	-0.02, 0.13	0.12	1.48	0.143
		Location of cone	-0.03	-0.28, 0.23	-0.02	-0.22	0.83
		Duration of keratoconus	-0.02	-0.06, 0.02	-0.09	-0.99	0.324
		Age of patient	0.006	-0.01, 0.02	0.05	0.63	0.53
	AUCSF	D-index	0.04	0.02, 0.06	0.51	4.93	< 0.001
		CL modality	0.04	-0.07, 0.14	0.05	0.65	0.52
		Location of cone	-0.18	-0.56, 0.21	-0.08	-0.91	0.36
		Duration of keratoconus	0.02	-0.04, 0.08	0.07	0.71	0.48
		Age of patient	-0.01	-0.04, 0.01	-0.09	-1.02	0.31
Binocular	HCVA	Average D-index	0.04	0.03, 0.05	0.75	7.65	< 0.001
		CL modality	0.05	-0.01, 0.11	0.11	1.5	0.14
		Location of cone	-0.01	-0.05, 0.03	0.03	-0.34	0.43
		Duration of keratoconus	-0.05	-0.08, -0.01	-0.25	-2.59	0.01
		Age of patient	-0.01	-0.02, 0.01	-0.09	-1.27	0.206
	AUCSF	Average D-index	0.08	0.06, 0.1	0.77	9.75	< 0.001
		CL modality	0.05	-0.05, 0.15	0.06	0.91	0.36
		Location of cone	-0.01	-0.11, 0.04	0.04	-0.5	0.54
		Duration of keratoconus	-0.006	-0.05, 0.06	0.02	0.18	0.85
		Age of patient	-0.02	-0.04, 0.004	-0.1	-1.67	0.09
Stereoaucuity	Average D-index	-0.09	-0.2, 0.02	-0.19	-1.61	0.11	
	CL modality	-0.12	-0.81, 0.57	-0.03	-0.34	0.73	
	Location of cone	0.05	-0.12, 0.08	0.03	-1.24	0.34	
	Duration of keratoconus	0.11	-0.28, 0.51	0.07	0.56	0.57	
	Age of patient	-0.09	-0.25, 0.06	-0.12	-1.2	0.23	

Table 4.3: Results of the multiple regression analysis for the outcome variables monocular and binocular high contrast logMAR acuity and area under the curve of CSF, as well as for stereoaucuity. B = the unstandardized beta, CI = confidence intervals for B , β = the standardized beta, t = the t -test statistic. The bold numbers in the table indicates the independent variables that had significant contribution to the predicted outcome variables.

4.4.7. Higher order wavefront aberrations

Of the 27 subjects that participated in the study, higher-order wavefront aberrations could be captured only in 19 subjects (i.e., 38 eyes). Subjects on whom data could not be collected, all belonged to the advanced keratoconus cohort, as the corneal distortion was outside the operating range of the aberrometer used in this study. The mean \pm 1SD pupil diameter over which the wavefront aberrations were captured was 5.1 ± 0.7 mm under unaided condition, 5.1 ± 1.1 mm with Kerasoft lenses, 4.9 ± 1.2 mm with conventional RGP lenses, 5.3 ± 1.3 mm with Rose K2 lenses and 5.7 ± 0.8 mm with scleral lenses. The wavefront aberrations were then

scaled to a constant diameter of 3 mm to maintain consistency in the data across subjects. The HORMS tended to increase with an increase in the subject's D-index value under unaided viewing conditions (Table 4.4). The HORMS values reduced significantly with all form of CLs compared to unaided conditions ($\chi^2 = 81$; $p \leq 0.05$). Relative to the unaided state, the magnitude of reduction in HORMS with Kerasoft CL was significantly lesser compared to the other forms of CLs ($Z \geq 3.2$; $p \leq 0.05$). HORMS remained comparable between RGP, Rose K2 and Scleral CLs in the mild to moderate and the advanced keratoconus cohorts ($Z \geq 1.6$; $p \leq 0.05$) (Table 4.4).

		Mild to moderate keratoconus	Advanced keratoconus	Overall population		
					Average HORMS (μm)	IOD (μm)
HORMS at 3 mm pupil (μm)	Controls	NA	NA	0.07 (0.04 to 0.14)	-0.01 (-0.02 to 0.01)	
	Unaided	0.32 (0.21 to 0.50)	0.43 (0.36 to 0.54)	0.4 (0.23 to 0.51)	-0.02 (-0.08 to 0.16)	
	Kerasoft CL	0.17 (0.13 to 0.25)	0.25 (0.20 to 0.30)	0.21 (0.14 to 0.26)	-0.02 (-0.06 to 0.08)	
	Rose K2 CL	0.14 (0.10 to 0.20)	0.1 (0.08 to 0.15)	0.13 (0.09 to 0.18)	0.02 (0.00 to 0.05)	
	RGP CL	0.13 (0.09 to 0.16)	0.1 (0.08 to 0.17)	0.12 (0.08 to 0.17)	0.02 (0.0 to 0.06)	
	Scleral CL	0.15 (0.12 to 0.19)	0.13 (0.12 to 0.18)	0.13 (0.12 to 0.18)	0.03 (0.0 to 0.07)	

Table 4.4: Median (interquartile range) HORMS obtained over 3 mm pupil diameter for controls and in the keratoconus cohort under unaided viewing conditions and with different CL designs. Data are shown for the overall population and separately for the mild to moderate and advanced keratoconus cohorts. For the overall population, the average and interocular difference (IOD) in HORMS between the two eyes are also shown.

4.5. Discussions

4.5.1. Overall clinical implication of the result

In the previous chapter, it was evident how the threshold values for different spatial and depth vision performances deteriorated in keratoconus across disease severity. This chapter captures how those functions improved with different contact lenses, which are often used as a first line treatment for keratoconus patients for visual rehabilitation. There is also a lack of clear

guidance in the literature for the choice of CL to be used to optically manage a given severity of keratoconus (Santodomingo-Rubido et al., 2022). The prevailing clinical wisdom is to correct mild and moderate keratoconus using conventional RGP or Kerasoft lenses and reserve the more complex lens designs like Rose K2 or Scleral CLs for advanced cases (Mandathara et al., 2017, Santodomingo-Rubido et al., 2022). This strategy is also driven by the clinical observation that the quality of CL fit achieved and the wearing comfort to the patient may be better with advanced CL designs for more complex disease forms (Mandathara et al., 2017). The study therefore hypothesized that the difference in visual performance and optical quality across CL designs would be minimal for mild to moderate keratoconus and it would become more obvious as the disease advances in severity. The results only partly supported this hypothesis – the visual performance and optical quality across CL designs remained largely similar across all disease severities, barring two small exceptions: logMAR acuity and contrast sensitivity fared slightly better with Rose K2 and Scleral CLs, than conventional RGP CLs (Figure 4.1 to Figure 4.6). The number of subjects with advanced keratoconus was, however, small in this study ($n = 9$) and the trends reported here may show some differences if the cohort size were to increase. The comparative analysis between the lenses showed that, despite the best effort to correct the lower order aberration with the lenses, a significantly higher residual refraction remains uncorrected for the Kerasoft lenses, which is negligible for the other lens modalities (Table 4.2). While this result can be a consequence of the elevated higher order aberrations with these lenses (Table 4.4), clinically it suggests that the masking of irregular astigmatism does not reach a satisfactory level and one might possibly face challenges finding the end point of refraction.

Keratoconus is a complex disease with various factors potentially determining the extent of improvement in visual performance that could be achieved with spectacle or CL wear (Santodomingo-Rubido et al., 2022). The multiple regression analysis revealed that only the

severity of the disease, as determined by the steep keratometry of the subject, to significantly predict the fold-change in visual performance while all other independent variables were not significant. The results of the CL modality not having a statistically significant influence on the fold-change of visual performance matches well the rest of the results showing no significant difference in visual performance of keratoconic subjects across different CL correction modalities (Figure 4.2 to Figure 4.6). For stereoacuity, only the y-intercept of the multiple regression analysis was significant, indicating that there was an overall magnitude of improvement in stereoacuity with CL wear in these subjects, but without any trends across the independent variables tested.

These results suggest that the choice of CL dispensed to the keratoconic patient may be determined more by non-visual factors like the quality of the CL fit, wearing-comfort and the cost of the lens, than by the magnitude of improvement in visual functions afforded by each lens design. Figure 4.7 summarizes this by graphically representing the various factors that needs consideration while dispensing a pair of CLs to the keratoconic patient. The visual functions and optical quality aspect of this figure are generated from the data collected in this study and the nonvisual factors are generated from the qualitative clinical experience of optometrists fitting these lenses at the study site (LVPEI, Hyderabad, India). The cost reflects the relative cost-price at which these CLs are sourced from the vendors at the study site. From a visual functions and optical quality standpoint, the performance of Kerasoft CLs is slightly worse than the other three designs (Figure 4.7). From the ease of lens fitting and the wearing comfort, scleral CLs fare better than Rose K2 and conventional RGP CLs (Figure 4.7). From a cost angle, conventional RGP's are the cheapest and Scleral CLs are the most expensive – there is about a 10 to 12-fold difference in cost price between convention RGP and Scleral CLs and about a 5-fold difference in cost price between convention RGP and Rose K2/Kerasoft CLs. Full-length scleral lenses like the Prosthetic Replacement of Ocular Surface Ecosystem

(PROSE) lenses were not included as part of the study protocol primarily due to their cost and the logistic challenges posed in procuring them from the manufacturer (~3–4 weeks for the lenses to reach study site from Boston Foundation for Sight (Boston, MA, USA) (Baran et al., 2012). Given that PROSE lenses are typically recommended for very severe keratoconus where other CLs are likely to fail, there is therefore little in the form of comparative analysis of visual performance and optical quality that can and needs to be performed. Additionally, the scleral lenses studied here have been shown to be optically as competent as the PROSE lenses and therefore the present results may be extrapolated to the latter as well (Fadel, 2017).

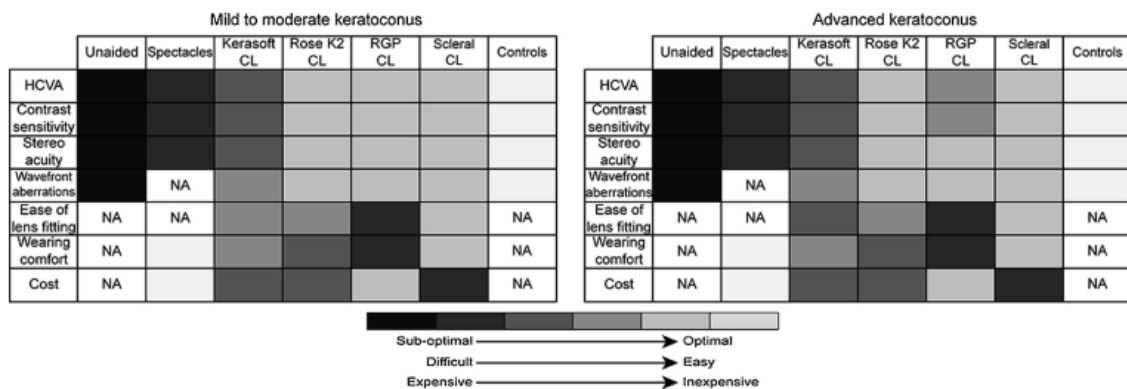


Figure 4.7: Summary chart describing the visual performance (HCVA, contrast sensitivity and stereoacuity), optical quality (higher-order wavefront aberrations) and nonvisual parameters that define lens wear with different optical corrections in subjects with mild to moderate (left panel) and advanced keratoconus (right panel), all relative to controls. The performance of each mode of optical correction is represented as a gray-scale value, with darker shades indicating poorer performance and lighter shades indicating better performance, relative to controls. The gray-scale ratings assigned to each optical correction for visual performance and optical quality are based on the data reported in this study (Figure 4.1 to Figure 4.6) while the gray-scale ratings of the non-visual parameters are based on clinical acumen gathered from experienced CL practitioners at the study site.

4.5.2. Magnitude of improvement in visual performance with CLs

On average, the improvement from spectacle-level performance was in the order of 1.5 to 2-fold for the mild to moderate keratoconus cohort and it increased to approximately 4 to 5-fold for the advanced cohort (Figure 4.2 to Figure 4.6, panels F–I). These results support the general clinical observation that patients with more advanced forms of the diseases tend to benefit more from CL wear than those with the milder forms of the disease. For stereoacuity, the

improvement from spectacle-level performance was in the order of 8 to 10-fold for the conventional RGP, Rose K2 and Scleral CL designs, indicating a greater benefit for depth perception in keratoconic subjects by wearing these designs of CLs. These results are in line with Nilagiri et al. (2018), who observed greater improvement in stereoacuity of keratoconic subjects with CLs than the improvement for logMAR acuity, both relative to spectacles. Possible reasons for these results including an improvement in disparity detection and oculomotor stability with improved optical quality of the eye are discussed in Nilagiri et al. (2020) and Metlapally et al. (2019). There is a possibility, albeit remote, that the orthoptic parameters of patients with keratoconus were worse than those of controls and this could have contributed to poorer stereoacuity in the former cohort. Only the presence of gross oculomotor abnormalities was excluded in the present study. This issue needs further investigation.

Interestingly, none of the CL corrections in keratoconic subjects reached the level of visual performance achieved with age-matched controls (Figure 4.2 to Figure 4.6, panels A–E). There could be two possible reasons for this finding. First, the optical fidelity of keratoconic eyes with CLs may not have reached the level of controls, as indicated from the magnitude of wavefront aberrations with CL wear, relative to controls, in this study (Table 4.4). Secondly, the slow and progressive nature of the disease may have resulted in some form of amblyopia in these subjects that may impose a limit on the magnitude of improvement in visual performance with CL correction (Sabesan and Yoon, 2009). Further studies involving a more complete correction of the eye's higher-order wavefront aberrations need to be conducted to test this hypothesis.

4.5.3. Inter-subject variability in the results

In addition to the overall improvement in spatial and depth-vision across CL designs compared to spectacles (Figure 4.1 to Figure 4.6), there was also a reduction in the inter-subject variability of visual performance with these lenses (see, distribution of data points in Figure 4.1 to Figure

4.6). This was most obvious for contrast sensitivity and least obvious for stereoacuity. These results are similar to the findings of Nilagiri et al. (2018) for high-contrast logMAR acuity and stereoacuity between spectacles and conventional RGP CLs in keratoconic eyes. The wide inter-subject variability in visual performance with spectacles possibly reflects the heterogeneity of the disease manifestation in the keratoconus cohort recruited for this study. An improvement in the results along with a reduction in the inter-subject variability indicates that the visual performance becomes better and more predictable across subjects with CL wear. This may allow CL practitioners to set more realistic expectations about the visual function outcomes for a given CL design in keratoconic subjects. This reduction in inter-subject variability is perhaps achieved by the restoration of regularity of the cornea surface and associated improvement in the eye's optical quality with CL wear in these eyes. This idea is supported by the overall reduction in the magnitude and inter-subject variability of wavefront aberrations seen in this study following CL wear, relative to spectacles (Table 4.4).

A direct comparison between the magnitude of reduction in wavefront aberrations and improvement in visual functions, however, cannot be made as the measurement conditions for these outcome variables were not uniform in this study. For instance, all visual functions were measured with the subject's natural pupil size between 5–6 mm under mesopic viewing conditions, while the wavefront aberration measurements were all made over a constant 3 mm pupil diameter. Further, psychophysical measures of visual performance could be influenced by neural factors that will not be captured in measures of optical quality derived from the aberration measurements. No attempt was made to equalize the viewing conditions for these measurements, as, such a correlation between optical structure and visual functions was not the primary focus of this study. Lastly, there was no definitive trend for the inter-subject variability to reduce more with one CL design than another in this study (Table 4.4), further indicating a similarity in visual performance across CL designs. In this study, the wavefront aberrations are

reported for 3 mm pupil diameter, representing the average mesopic pupil diameter of young adults. The magnitude of these aberrations, their differential impact on retinal image quality and the loss in visual performance with the different CL designs are therefore likely to be greater when the pupils dilate under low mesopic to scotopic viewing conditions (Campbell, 2003).

4.5.4. Study limitations

First, the cross-over design, in addition to the range of parameters measured here on multiple occasions made the study rather lengthy and cumbersome for the participant. Participant fatigue and learning effect could have therefore adversely affected the results presented here. The study however minimized these effects by allowing sufficient breaks for the participant as desired and by randomizing the order of CLs tested to evenly distribute any impact of fatigue or learning effect across CLs. Second, the lack of differences in visual performance across CL designs in the advanced keratoconus cohort could be related to the smaller sample size ($n = 9$), relative to the mild to moderate keratoconus cohort ($n = 18$). While every attempt was made to recruit subjects in this cohort, the cumbersome nature of the study was not attractive to many participants thus resulting in an uneven sample size. Third, this study did not include subjects with unilateral keratoconus or dissimilar severities of keratoconus in the two eyes. Previous studies have observed differences in binocular spatial-vision and depth-vision strategies between the bilateral and the unilateral disease cohorts (Nilagiri et al., 2018). The results observed here may therefore apply only to the bilateral keratoconus cohort. Any extrapolation to the unilateral cohort must be done with caution. Fourth, the claims of non-visual parameters playing a significant role in the decision-making process for the CL dispensed to the subject come from a rather qualitative and unstructured analysis (Figure 4.7). Future studies could use more structured patient-reported outcome measures to provide evidence for such claims (Khadka et al., 2017).

4.6. Summary

As has been previously reported, visual performance and optical quality in bilateral keratoconus improves with CL wear, relative to spectacles. The present study additionally shows no major differences in the performance of the four commonly used CL designs. The performance efficacy of Kerasoft CL is somewhat inferior to those of conventional RGP, Rose K2 and Scleral CLs, across disease severity. Non-visual factors such as the quality of CL fit, wearing comfort and cost may therefore drive the choice of CL dispensed in keratoconus more than relative performance efficacy of these lenses. Visual performance of keratoconic subjects remains poorer than age-matched controls even with the advanced designs of CLs available commercially, possibly indicating an element of neural insensitivity in these eyes.

5. Chapter 5: Assessment of suprathreshold contrast perception in keratoconus

5.1. Introduction

Chapter 3 and chapter 4 showed a significant deterioration in optical quality loss and threshold-level function in keratoconus. These results are in alignment with the present literature (Devi et al., 2022, Nilagiri et al., 2018, Nilagiri et al., 2020, Shneor et al., 2021). However, these measures do not provide a complete description of the patient's vision because the bulk of humans' visual experience occurs at suprathreshold levels (Haun and Peli, 2013, Jarvis et al., 2022, To et al., 2011). For instance, the perception of a naturalistic scene involves processing contrasts that are significantly higher than detection thresholds and at spatial frequencies that are significantly lower than the acuity limit (Haun and Peli, 2013, Jarvis et al., 2022). Perceived contrast matches at suprathreshold levels occur at similar physical contrast levels in humans with normal vision even though their contrast detection thresholds vary by several orders of magnitude across spatial frequencies (Georgeson and Sullivan, 1975, Brady and Field, 1995, Kulikowski, 1976, Smith, 2015). This "contrast constancy" might reflect an active normalization of suprathreshold visual inputs to compensate for threshold-level losses in performance (Georgeson and Sullivan, 1975). Alternatively, contrast constancy may also reflect uniform gains across spatial frequency channels, with sensitivity losses occurring due to a reduction in signal-to-noise ratio at threshold (Brady and Field, 1995). Irrespective of the model, threshold-level losses in contrast perception across spatial frequencies may not manifest as deficiencies at suprathreshold levels in visually healthy human observers.

It is evident from the Chapter 3 and chapter 4, that contrast sensitivity progressively degrades with increasing disease severity in keratoconus (Devi et al., 2022) and that these losses primarily arise from the underlying loss of retinal image quality from increased wavefront aberrations of the distorted cornea (Nilagiri et al., 2020, Metlapally et al., 2019, Devi et al.,

2022). However, very little is known about the status of suprathreshold contrast perception in keratoconus. It is important to address this issue for two reasons: first, it will determine if the loss of spatial vision in keratoconus is restricted only to the detection of fine details and threshold levels of contrast or whether the losses extend to stimuli typically encountered in day-to-day living. The latter may have an impact on the patient's quality of life beyond what is predicted from the deficit in visual acuity and contrast sensitivity. Second, losses in suprathreshold contrast perception may indicate that, like threshold level performance, the neural outputs of the different spatial frequency channels are also impacted at suprathreshold levels by the optical quality losses in keratoconus. Conversely, contrast constancy at suprathreshold may reflect recalibration of neural gains across spatial frequency channels to account for the exaggerated loss of contrast sensitivity in this disease condition (Georgeson and Sullivan, 1975). It could also reinforce the hypothesis that suprathreshold contrast gains are uniform across spatial frequency channels, regardless of the increased threshold level noise from optical degradation in the keratoconic visual system (Brady and Field, 1995).

The primary aim of the study in this chapter was to test the status of suprathreshold contrast perception in different severities of keratoconus, relative to age-similar controls. The well-established contrast matching paradigm previously employed to demonstrate the phenomenon of contrast constancy in visual healthy humans (Georgeson and Sullivan, 1975) was employed to evaluate suprathreshold contrast perception in this study (Experiment 1). The study tested the hypothesis that, unlike controls, contrast constancy in keratoconics will be impaired owing to the exaggerated loss of optical quality and that the deficiency may be predicted from the corresponding threshold-level losses in contrast sensitivity. As a corollary, the study also hypothesized that the quantum of loss in contrast constancy will be directly proportional to the severity of keratoconus. This study comprised three experiments.

Experiment 1

Figure 5.1 illustrates these predictions using data of a representative control and three keratoconic cases that participated in the present study. Relative to the control, the contrast threshold function of cases showed an overall constriction arising from an increase in contrast detection thresholds across all spatial frequencies and a shift in the trough of the contrast threshold function towards lower spatial frequencies (Figure 5.1A). The **fold-change** in contrast required to achieve a suprathreshold perceptual match between the test and reference stimuli was calculated from these curves by dividing the threshold contrast of the test stimuli by that of the reference stimulus (Figure 5.1B). Contrast constancy is absent if the empirical data from contrast matches yield the same fold-change as predicted from this figure – i.e., at a given suprathreshold level, the test stimulus required the same proportion of increased contrast as seen at threshold for a perceptual match with the reference stimulus. Conversely, contrast constancy is complete if the empirical fold-change was unity – i.e., a perceptual match was obtained between the test and reference stimuli at the same physical contrast level, indicating complete compensation for the lower contrast sensitivity of the test stimuli at threshold (Figure 5.1B). Ng et al. (2022) recently observed contrast constancy for spatial frequencies that are habitually experienced by keratoconic eyes. However, contrast constancy was not present for frequencies artificially made visible through adaptive optics manipulation (Ng et al., 2022). Based on this observation, this study hypothesized that contrast constancy will be present for spatial frequencies within the contrast sensitivity function in keratoconic eyes. A complete breakdown in contrast constancy was deemed as the null hypothesis of the study. It is worth acknowledging that, given the robustness of this phenomenon, the chance of accepting the null hypothesis was rather remote.

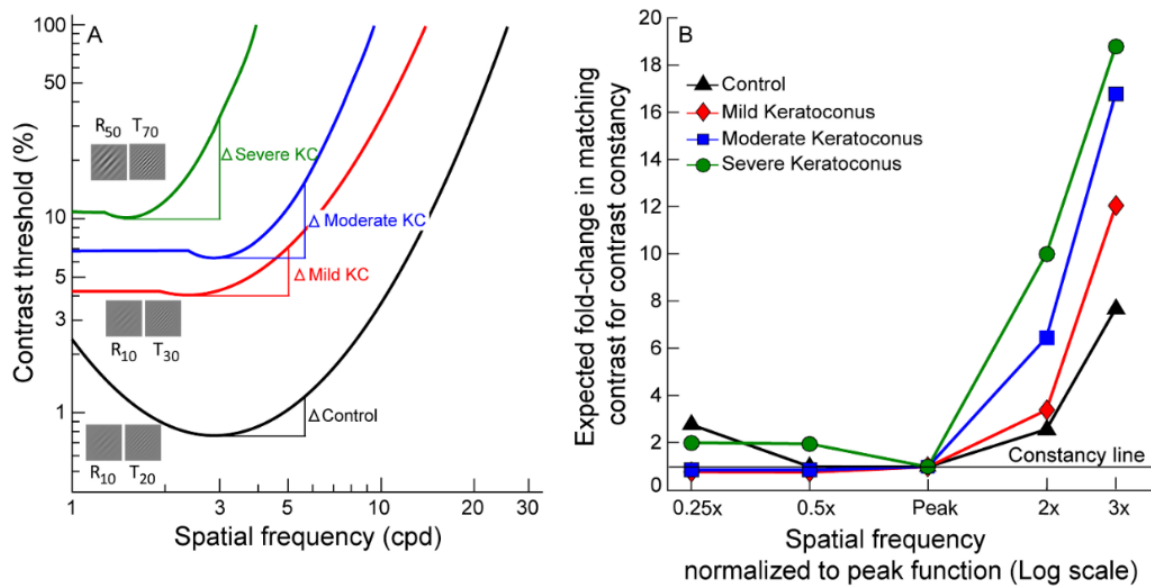


Figure 5.1: Panel A representative contrast threshold function for a control subject and three cases with mild, moderate, and severe keratoconus that participated in this study. Representative pairs of the test (T) and reference (R) grating patterns used in the contrast matching paradigm of this study are shown in this figure (see also Methods). Panel B shows Fold-change in suprathreshold matching contrast expected from the contrast threshold functions for the different spatial frequencies tested in this study. The abscissa plots \log_{10} values of spatial frequency, normalized to the peak values of the subject.

Experiment 2: impact of disease asymmetry

Two additional aspects of suprathreshold contrast perception that are relevant for the everyday visual experience of patients with keratoconus were evaluated. Experiment 2 addressed variations in suprathreshold contrast perception in bilaterally asymmetric keratoconus. This study hypothesized that contrast constancy will be impaired to a greater extent in the optically worse eye relative to the better eye and that the pattern of binocular contrast constancy will be dominated by the pattern observed in the better eye (Devi et al., 2022, Marella et al., 2021). This is because the suppressed stimulus appears to impact information processing in the higher cortical areas, potentially impacting contrast processing at suprathreshold levels in these eyes (Tong et al., 2006).

Experiment 3 impact of contact lenses v spectacle correction

The third experiment determined changes in contrast constancy when the viewing experience of patients with keratoconus changes from habitual contact lens wear to spectacle lens wear. While retinal image quality and threshold-level visual performance are known to be superior with rigid contact lens wear compared to spectacles in keratoconus (Devi et al., 2022, Nilagiri et al., 2018), equivalent changes in suprathreshold contrast perception have remained unexplored. This study hypothesized that the pattern of contrast constancy observed in a subject may be established over extended time periods. Any sudden alteration to this viewing experience, such as the degradation of image quality induced by switching from contact lenses to spectacles in keratoconus, or its restoration with contact lens wear within a short period of time, may lead to a break-down of contrast constancy.

5.2. Methods

5.2.1. Patient selection, inclusion, and exclusion criteria

Subjects were recruited at the L V Prasad Eye Institute (LVPEI), Hyderabad, India. Ethics committee approval was obtained from the Institute's internal review board and City, University of London, UK (LEC-BHR-P-07-20-467). The study protocol was in accordance with the Declaration of Helsinki and all subjects had the study explained to them before signing written consent forms. Twelve cases (age range: 20 – 32 years; 8 males and 4 females) with a confirmed diagnosis of bilateral keratoconus, using clinical signs (e.g., Vogt's striae, Fleischer's ring) and corneal tomography data (e.g., superior-inferior asymmetry in corneal curvature and elevation, asymmetric bow-tie pattern, relative corneal thinning etc.) were recruited from the patient pool of LVPEI. Patients with corneal scarring, retinal pathology or any other ocular co-morbidity that can affect contrast perception were excluded. Subjects who reported their inability to understand the experimental paradigm and provide reliable responses

were also excluded from the study. Twelve age-similar controls (23 – 27 years; 7 males and 5 females) were recruited from the post graduate students and staff pool at LVPEI.

5.2.2. Assessment of corneal structure

An assessment of the corneal structure of cases and controls was performed using a Scheimpflug imaging technique with Pentacam HR[®] (Oculus Optikgeräte GmbH, Wetzlar, Germany). The Belin-Ambrósio enhanced ectasia display map, derived from the tomography data, was used to obtain the D-index for all cases and controls (Duncan et al., 2016, Shajari et al., 2019). The D-index was obtained from both eyes of each subject. For those with similar disease severity in the two eyes, one eye was randomly allocated for psychophysical measurements. For those with interocular asymmetry in disease severity, the eye with greater disease severity was considered for the psychophysical measurements. This strategy ensured that a wide range of disease severities were included to test the study hypothesis. Unlike some previous studies, visual acuity was not considered for grading disease severity (Kanellopoulos and Asimellis, 2013).

5.2.3. Psychophysical measurements

All psychophysical measurements were carried out with the subject's best-corrected spectacles (cases and controls) or rigid contact lenses (only cases) in a dimly-lit room with their natural pupils. Keratoconic cases wore conventional tri-curve design rigid gas permeable contact lenses from Purecon McAsfer (Silver line laboratory Pvt ltd, Delhi, India) whose fitting was deemed appropriate by an experienced optometrist. Subjects were provided with sufficient breaks during the psychophysical procedures to avoid fatigue and boredom.

5.2.3.1. Assessment of threshold level performance

Monocular and binocular high contrast logMAR acuity was determined with best corrected spectacles and contact lenses at 3m viewing distance using COMPlog[®] (Clinical Vision

Measurement Systems Ltd, London, UK) (Laidlaw et al., 2008). The measurement process and quantification of acuity was similar, as discussed in chapter 3 (section 0).

Monocular and binocular contrast sensitivity functions (CSF) were measured using a modified version of the quick CSF program, executed using Psychtoolbox-3[®] in Matlab[®] (Mathworks Inc, Natick, MA) (Brainard, 1997, Lesmes et al., 2010, Pelli, 1997, Rosen et al., 2014). The contrast threshold assessment procedure was similar to that described in chapter 3 (section 0). The contrast sensitivity was summarised using three parameters: area under the curve, cut-off spatial frequency, and the contrast sensitivity at the peak of the CSF (Lesmes et al., 2010, Rosen et al., 2014).

5.2.3.2. *Assessment of suprathreshold level performance*

The contrast matching paradigm, implemented using Psychtoolbox-3[®], was adapted from the previous work of Georgeson and Sullivan (1975). For each trial, reference and test Gabor stimuli of different spatial frequencies were presented sequentially at the centre of the screen, each for 500ms duration. The reference grating had a spatial frequency corresponding to the peak of the CSF (R in Figure 5.1A) whereas the test grating, whose contrast changed during the procedure, had a spatial frequency set to a multiple of the spatial frequency of the reference grating (T in Figure 5.1A). Unlike the previous studies, where the spatial frequency of the reference grating was fixed (Brady and Field, 1995, Georgeson and Sullivan, 1975), this parameter was varied in this study to correspond to the peak spatial frequency of the CSF of each individual participant. This ensured that the reference and test gratings were resolvable by the subject, especially for cases with keratoconus. A fixation cross appeared at the centre of the screen during the exchange of stimuli to retain the attention of the subject. The order of presentation of the reference and test patterns were randomized across trials. Similarly, the orientation of the grating pattern was also randomized between 45° and 135° orientations across trials. The subject reported which of the two patterns was perceived with greater contrast

after both presentations. Like previous literature on the measurement of contrast constancy (Georgeson and Sullivan, 1975), subjects were specifically instructed to base their judgment on the contrast of the stimulus and avoid other confounding cues such as brightness and sharpness of the grating pattern. Based on the response after each trial, the contrast of the test grating was increased or decreased using a 2-alternate forced choice 2-down 1-up adaptive staircase procedure. The initial assignment of physical contrast of the test pattern was randomized and a given staircase was terminated after the completion of 8 reversals. The matching contrast for that test pattern, in comparison to the reference pattern, was calculated as the average contrast of the last 5 reversals.

Experiment 1

Contrast matching in Experiment 1 was assessed at 10% and 50% contrast for spatial frequencies that were 0.25x, 0.5x, 2x and 3x that of the reference pattern's spatial frequency (Figure 5.1B). For each set of contrast matching trials, the spatial frequency of the test pattern and the suprathreshold contrast level of the reference pattern (10% or 50%) were randomly allocated and kept constant until the end of the trial. All contrast matching trials were also repeated twice on each subject. Thus, an entire session of data collection on a given subject contained 16 contrast matching trials (4 spatial frequency combinations x 2 suprathreshold contrasts x 2 repetitions = 16). These measurements were all made monocularly for each eye of the participant while the fellow eye was occluded. In two cases with advanced keratoconus, the contrast threshold at the peak of the CSF was close to 10%. In such cases, the contrast matches were obtained at 20% and 50% supra-threshold contrast levels. One keratoconic subject could not perform the task at the 20% contrast level and hence the experiment was conducted only at 50% contrast.

The expected fold-change in contrast match for the 10% and 50% suprathreshold stimulus was calculated for each participant from their contrast threshold function by dividing the threshold

contrast of the test spatial frequencies by that of the reference spatial frequency. For instance, for the representative case shown in Figure 5.1A with moderate keratoconus, the test stimulus at 2x peak spatial frequency is predicted to be 6-times higher in contrast to achieve a perceptual match with the standard stimulus (Figure 5.1B). This resulted in an expected fold-change in contrast match of 6x for that spatial frequency, relative to the standard stimulus. The observed fold-change in contrast match was defined as the ratio of the physical contrasts of the reference and test stimulus at which a perceptual match was observed psychophysically. The observed and expected fold-changes were then compared to determine the presence/absence of contrast constancy. If the observed and expected fold-change in contrast matches were equal, it signalled the absence of contrast constancy. An observed fold-change in contrast match of unity signalled intact contrast constancy. Subjects will not be able to achieve a perceptual match for certain combinations of test and reference stimulus that required a large fold-change in the expected contrast match, in the event of a complete failure of contrast constancy. For instance, in the example given above, if the expected fold-change for a given test-reference stimulus combination was 6x, the test stimulus had to be presented at 300% contrast to achieve a perceptual match with the reference stimulus at the 50% suprathreshold contrast level. Since this is not physically possible, the subject would not be able to make a perceptual match for this combination of test and reference stimuli.

Experiment 2

Data for Experiment 2 were obtained by repeating the contrast matching paradigm on a subset of 5 subjects (20 – 32yrs; 2 males and 3 females) who participated in Experiment 1. These subjects had bilaterally asymmetric keratoconus determined from the D-index values. A minimum inter-ocular difference in D-index of five units was considered for this experiment. The eye with the higher of the two D-index values was designated the worse eye in these participants.

Experiment 3

Experiment 3 repeated the contrast matching paradigm on a subset of three subjects (23 – 26yrs; 2 males and 1 female) who had previously participated in Experiment 1. Data were obtained monocularly (right eye) at four different time points: with their habitual contact lens correction (data included in the analysis of main experiment), immediately after switching from contact lenses to spectacles, after one week of spectacle lens wear and after two weeks of spectacle lens wear. During this 2-week period, subjects did not use their habitual contact lenses.

5.3. Data analysis

Data analyses were performed using Matlab[®] R2016a and IBM SPSS statistics v20.0[®] (SPSS, Chicago, IL, USA). The Shapiro-Wilk test was used to determine normality and then data from cases and controls were compared using appropriate parametric or non-parametric tests. The impact of three independent factors – spatial frequency of the test pattern, suprathreshold contrast level and cohort type – on this fold-change in matching contrast was analysed using 3-factor repeated measures analysis of variance (RM-ANOVA). Spatial frequency of the test pattern and suprathreshold contrast level of the reference pattern were considered as independent factors to determine if, like previous studies (Georgeson and Sullivan, 1975, Brady and Field, 1995, Smith, 2015), their experimental manipulation produced predictable changes in the contrast constancy in cases and controls. The cohort type was considered as an independent factor to determine if the pattern of contrast constancy varied in subjects with and without the disease condition. Lack of statistical significance in this factor would indicate that contrast constancy is independent of the disease status. Post-hoc tests with Bonferroni correction for multiple comparisons were performed to determine the statistical significance of the pairwise differences in fold-change of matching contrast across different spatial frequencies. $P \leq 0.05$ was considered statistically significant. Effect size was quantified using the partial Eta-squared (η_p^2) statistic (Lakens, 2013). Since only a small number of subjects

participated in Experiments 2 and 3, their data were not subjected to any formal statistical analysis but described qualitatively, instead.

5.4. Results

5.4.1. Demographic and refractive features

The demographic details for the keratoconic subjects are shown in Table 5.1. Age and gender distribution were comparable to the controls that participated in this study. As expected, the corneal parameters such as the steeper and flatter keratometry values and the D-index, were significantly higher in cases compared to controls ($p < 0.001$) (Table 5.1). The D-index ranged from 1.3 to 6.9 in the better eye and from 9.1 to 33.3 in the worse eye of this cohort. For spherocylindrical refraction, the spherical equivalent (M) in power vector terminology (Thibos et al., 1997) was significantly higher in cases than in controls ($p < 0.001$) while the regular (J0) and oblique astigmatism (J45) components were not statistically different between the cohorts ($p = 0.4$ and $p = 0.7$, respectively) (Table 5.1). Habitual contact lens users were comfortable with their existing lenses. The corneal GP lenses had a mean base curve of 7.0 mm (± 1 SD, 0.4 mm) with a diameter of 9.2 mm (± 1 SD, 0.2 mm) and back vertex power of -5.0 D (± 1 SD, 2.5 D).

5.4.2. Experiment 1- visual acuity and contrast sensitivity

The mean spectacle-corrected high contrast logMAR visual acuity of cases was significantly poorer than the controls ($p < 0.001$) (Table 5.1). Figure 5.2 shows representative data of the contrast threshold function and contrast matches obtained for the 10% and 50% stimuli from one control participant (panel A) and individual keratoconic cases with mild, moderate, and severe disease (panels B – D). Contrast sensitivity was attenuated in all cases, relative to controls, with this attenuation progressively increasing with the disease severity (Figure 5.1 and Figure 5.2A – D). Table 5.1 shows three parameters of the contrast sensitivity function for the cases and controls that participated in this study. All the parameters showed significant

deterioration compared to controls ($p<0.001$). The area under the CSF parameter showed a significant negative correlation with the D-index ($r=-0.84$; $p=0.001$).

Cohort	Age Gender	Eye	Keratometry (D)		D-index (unitless)	Refraction (D)			HCVA (logMAR)	Contrast sensitivity function		
			Steep K	Flat K		M	J0	J45		Peak CS	Cut off SF (Cpd)	AUCSF (Unit area)
P1	25 M	LE	50.3	45.1	5.2	-3.0	-1.1	1.9	0.32	1.4	6.9	1.5
P2	26 F	RE	50.6	47.9	9.4	-6.6	-0.9	-0.7	0.22	1.8	18.4	1.9
P3	23 F	RE	53.9	49.7	8.0	-5.5	0.4	-1.9	0.14	1.4	15.4	1.3
P4	24 F	RE	72.6	61.2	17.4	-18.0	0	0	0.68	1.1	9.1	0.8
		LE	48.8	48	5.1	-6.5	0	0	0.06	1.9	16.9	1.8
		Bino	N/A						0.1	2.2	17.5	2.0
P5	25 M	LE	58.2	55.6	12.3	-19.3	-0.2	1.2	0.38	1.7	7.8	1.1
P6	24 M	RE	64.6	56	19.2	-2.0	-2.0	0	0.66	1.4	9.1	0.9
P7	24 M	RE	42.4	40.9	2.9	-0.5	0	0	0.0	1.5	18.2	1.5
		LE	50.5	46.3	9.1	-5.0	-1.5	1.3	0.22	1.0	6.9	0.8
		Bino	N/A						0.0	1.7	17.2	1.7
P8	25 M	RE	41.6	40	2.9	-2.1	-0.6	0	0.14	1.8	14.7	1.8
P9	28 M	RE	51	47.7	11.9	-1.5	1.4	-0.5	0.52	1.1	12.1	0.9
		LE	43.8	43.5	1.25	0	0	0	0.0	2.4	29.8	2.7
		Bino	N/A						0.0	2.4	36.6	2.8
P10	22 M	RE	55.4	52.2	13.3	-2.8	0.5	-0.8	0.5	1.2	5.2	0.6
P11	21 M	RE	45.8	45.1	2.9	-0.3	-0.2	-0.1	0.0	2.4	25.3	2.4
		LE	70.4	65.8	28.9	-9.0	0.5	2.9	0.8	1.8	7.4	0.5
		Bino	N/A						0.02	2.4	25.8	2.5
P12	32 M	RE	49	46.6	6.9	-4.4	-0.4	0.8	0.1	1.9	15.3	1.8
		LE	74.0	70.7	33.3	-11.3	0.3	1.5	0.9	0.9	3.4	0.4
		Bino	N/A						0.08	1.8	15.5	1.7
Controls	24.8±2.2 7 M 5 F	n=12	43.4±1.2	42.7±1.2	0.55±0.2	-1.6±3.7	-0.1±0.4	0.04±0.08	- 0.03±0.04	2.3±0.2	25.9±4.6	2.4±0.2

Table 5.1: Demographic and clinical details of study participants. Cases are presented individually while control data is represented as mean±ISD of the outcome variable. All cases participated in Experiment 1, cases P4, P7, P9, P11 and P12 participated in Experiment 2 and cases P3, P6 and P8 participated in Experiment 3. For participants in Experiment 2, data from each eye and from both eyes are noted in the table. The M, J0 and J45 terms represent the spherocylindrical refractive error in power vectors, wherein M = spherical equivalent of refraction and J0 and J45 represent the regular and oblique astigmatic components of refraction (Thibos et al., 1997). M: F = Male: Female; HCVA = spectacle corrected high contrast visual acuity; Cpd = cycles per degree; AUCSF = Area under curve of contrast sensitivity function.

5.4.3. Experiment 1- Suprathreshold contrast matching

The fold-change for 10% and 50% contrast stimuli were close to unity for spatial frequencies higher than the peak but greater than unity for spatial frequencies lower than the peak (Figure

5.2A–D). The main effects of spatial frequency and suprathreshold contrast on the fold-change in contrast match were statistically significant for cases and controls (Table 5.2, Figure 5.2E and F). The interaction between the two main factors was also statistically significant for cases and controls (Table 5.2, Figure 5.2E and F). Fold-changes of matching contrasts in controls and cases were significantly higher and farther away from the unity value for the 10% contrast than for the 50% contrast, indicating a departure from contrast constancy for the former than latter stimuli (Figure 5.2E and F). Fold-changes were also significantly larger for the lower two spatial frequencies than the higher two spatial frequencies for both cases and controls (Table 5.3, Figure 5.2E and F). The fold-change for 0.25x spatial frequency was significantly greater than the fold change for 0.5x spatial frequency, and more so for the 10% than 50% contrast (Table 5.3, Figure 5.2E and F). Fold-changes for the 2x and 3x spatial frequencies were not significantly different from each other (Table 5.3, Figure 5.2E and F).

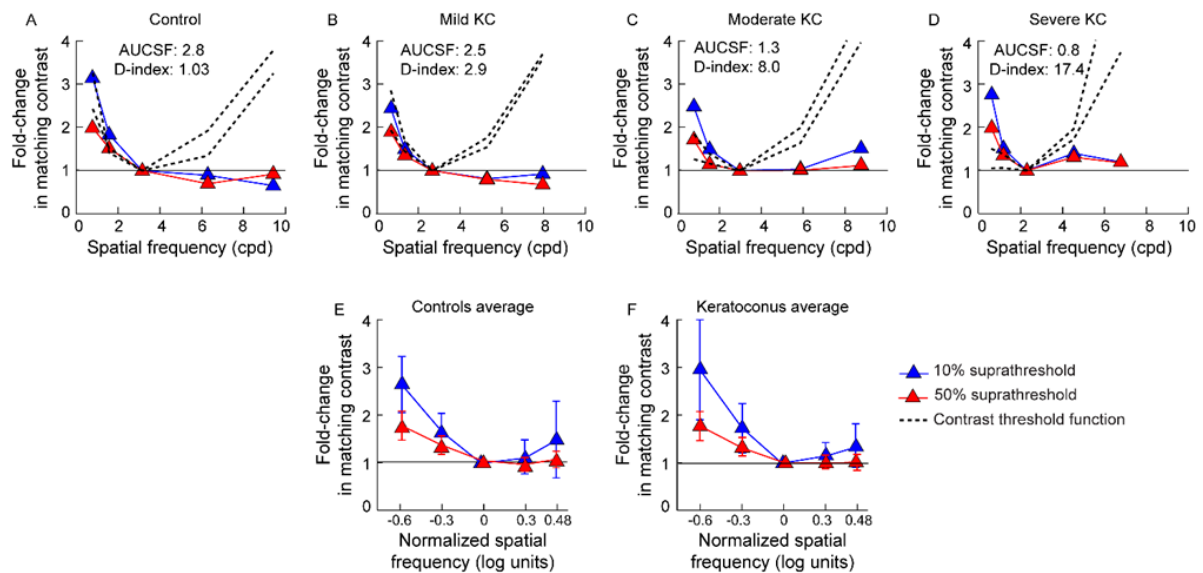


Figure 5.2: Panels A – D: Fold-change in contrast of test grating required to match the perceived contrast of the reference grating for one representative control subject (panel A) and three representative cases with different severities of keratoconus (panels B – D; these panels correspond to cases P11, P3 and P4 in Table 5.1, respectively). Threshold and suprathreshold data in all panels are normalized to the peak spatial frequency of that participant. Dashed curves indicate $\pm 95\%$ confidence interval of the fold-change for contrast detection thresholds. The area under the contrast sensitivity function (AUCSF) derived from the threshold function and the D-index of the participant as a measure of disease severity are also noted. Panels E and F: Average (± 1 SD) fold-change across all study participants in the controls and cases, respectively.

	F-value	P-value	η_p^2
Spatial frequency	F (4, 11) = 46.5	<0.001	0.81
Suprathreshold contrast	F (2, 11) = 41.9	<0.001	0.79
Cohort	F (2, 11) = 0.84	0.38	0.07
Spatial frequency x Cohort	F (4, 11) = 1.22	0.32	0.09
Spatial frequency x Suprathreshold contrast x	F (4, 11) = 14.5	<0.001	0.57
Suprathreshold contrast x Cohort	F (2, 11) = 0.81	0.38	0.07
Cohort x Suprathreshold contrast x Spatial frequency	F (2, 11) = 1.65	0.19	0.13
Post-hoc tests for spatial frequency			
0.25x – 0.5x	-	<0.001	-
0.25x – 2x	-	<0.001	-
0.25x – 3x	-	<0.001	-
0.5x – 2x	-	0.001	-
0.5x – 3x	-	0.12	-
2x – 3x	-	0.1	-

Table 5.2: Outcomes of the 3-factor RM-ANOVA and post-hoc Bonferroni test performed to evaluate the statistical significance of the fold-change in contrast match with test spatial frequency and suprathreshold contrast in controls and cases.

Table 5.3 shows the mean ($\pm 1SD$) expected fold-change from the contrast threshold function and the observed fold-change in contrast match for all test spatial frequencies in controls and cases. The p-values from t-tests performed to compare expected versus observed values are also included. The observed fold-change was similar to or higher than the expected fold-change for lower than peak spatial frequencies, relative to higher than peak spatial frequencies. This pattern was more exaggerated for the 10% contrast level compared to 50% contrast (Table 5.3). The observed fold-change in contrast match across spatial frequencies was poorly correlated with D-index (Pearson's correlation coefficient for 10% contrast: $r \leq 0.19$; $p \geq 0.38$, 50% contrast: $r \leq 0.3$; $p \geq 0.15$) (Figure 5.3).

Suprathreshold contrast level	Spatial frequency	Expected fold-change	Observed fold-change	P-value	Expected fold-change	Observed fold-change	P-value
		Controls			Cases		
10%	0.25x	2.32 (0.9)	2.73 (0.6)	0.13	1.69 (1.0)	3.28 (1.3)	0.003
	0.5x	1.53 (0.3)	1.69 (0.3)	0.29	1.52 (0.9)	1.89 (0.6)	0.03
	2x	1.92 (0.4)	1.13 (0.4)	<0.001	2.16 (0.7)	1.15 (0.3)	0.001
	3x	5.09 (2.7)	1.53 (0.8)	0.001	6.67 (3.7)	1.35 (0.6)	<0.001
50%	0.25x	2.32 (0.9)	1.81 (0.3)	0.05	1.69 (1.0)	1.80 (0.2)	0.71
	0.5x	1.53 (0.3)	1.34 (0.2)	0.11	1.52 (0.9)	1.39 (0.3)	0.62
	2x	1.92 (0.4)	0.93 (0.1)	<0.001	2.16 (0.7)	0.95 (0.1)	<0.001
	3x	5.09 (2.7)	1.06 (0.2)	<0.001	6.67 (3.7)	1.02 (0.3)	<0.001

Table 5.3: Mean (\pm ISD) expected and observed fold-change in contrast matching and the P-value of the corresponding paired T-tests for the 10% and 50% suprathreshold contrast in controls and cases.

5.4.4. Experiment 2- Suprathreshold contrast matching in bilaterally asymmetric

keratoconus

Significant disease asymmetry was noted in all five subjects in Experiment 2 (cases P4, P7, P9, P11 and P12 in Table 5.1). Their D-index values ranged from 1.25 to 6.9 units in the better eye and 9.1 to 33.3 units in the worse eye (Table 5.1). The contrast threshold function for the two representative participants of this experiment showed a relatively more attenuated contrast threshold function in the worse eye, relative to the better eye (Figure 5.4A and B). Interestingly, the binocular contrast threshold function always matched or was slightly superior to the better eye in all cases (Figure 5.4A and B). The AUCSF was lower for the worse eye (ranged from 0.4 to 0.8 units) compared to the better eye (ranged from 1.5 to 2.7 units) (Table 5.1). All other threshold parameters of contrast and spectacle corrected high contrast visual acuity in the worse eye were reduced compared to the better eye performances (Table 5.1).

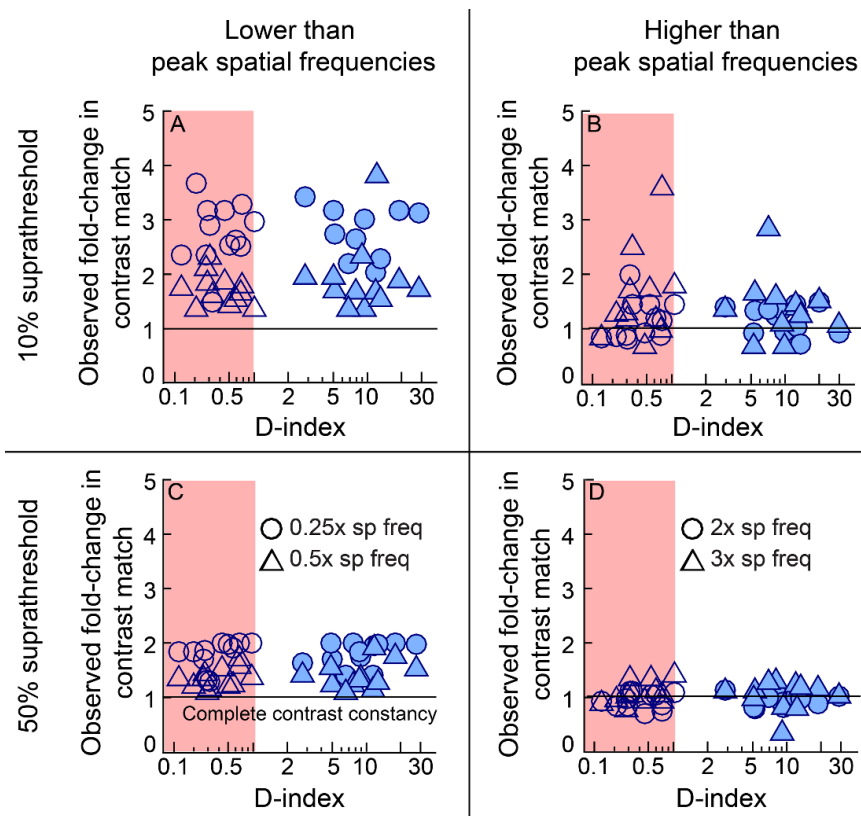


Figure 5.3: Scatter diagram of the fold-change in suprathreshold contrast match plotted as a function of the D-index for all controls (open symbols within the red band) and cases (filled symbols) that participated in the study. Panels A and B show data for 10% contrast while Panels C and D show data for 50% contrast.

Figure 5.4C and D show scatter plots of the fold-change in contrast required for achieving a match between the reference and test stimuli at the 10% and 50% suprathreshold levels while using the poorer eye, or under binocular viewing conditions, against the corresponding fold-change when using the better eye. The contrast matches obtained with the worse eye, (or under binocular viewing), were similar to those obtained with the better eye, independent of the test spatial frequency (Figure 5.4). The data points for spatial frequencies higher than the peak were closer to the unity fold-change, relative to those lower than the peak (Figure 5.4C and D). This effect was more pronounced for the 50% contrast than the 10% contrast (Figure 5.4C and D).

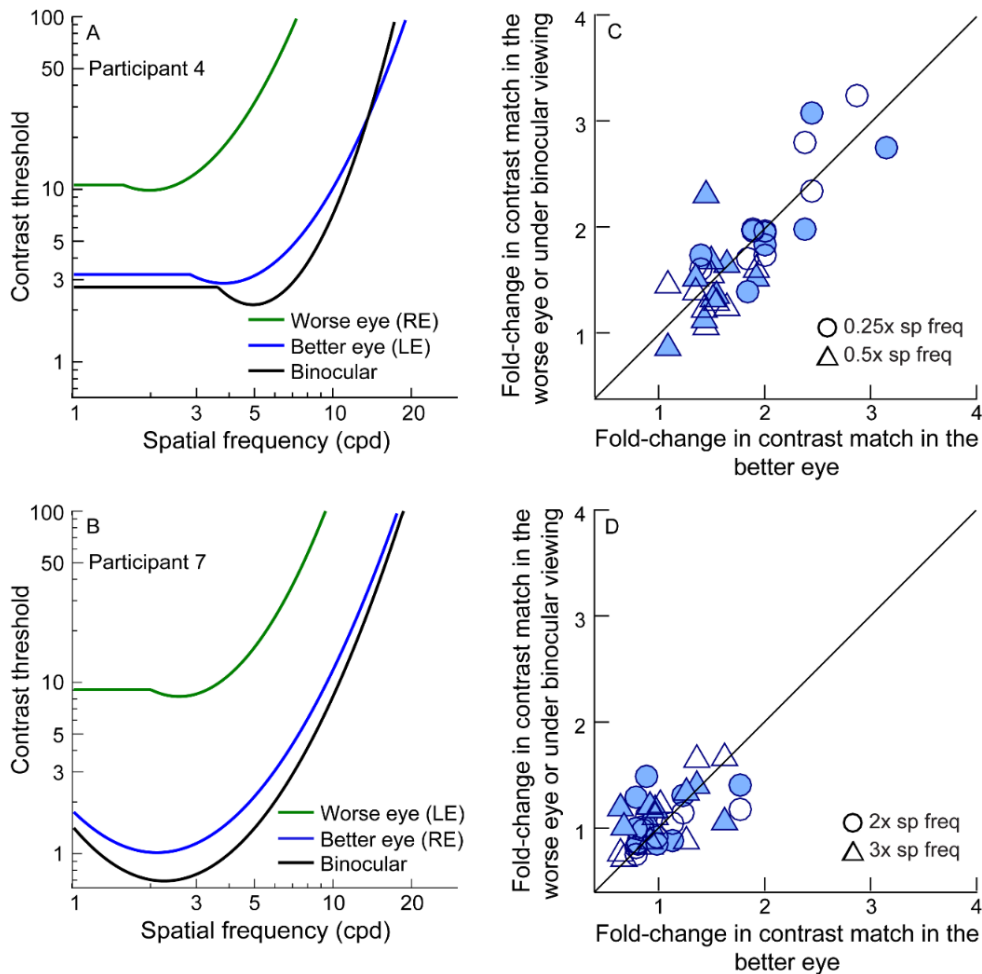


Figure 5.4: Panels A and B show contrast threshold functions of the worse eye, better eye and binocular viewing of two representative cases with keratoconus (out of 5 cases) that participated in Experiment 2. Both these participants had large interocular asymmetry in their disease severity [right eye was worse than left eye in Participant 4 and left eye was worse than right eye in Participant 7 (Table 5.1)]. Panels C and D show scatter diagram of the fold-change in suprathreshold contrast match observed for the worse eye viewing (filled symbols) or binocular viewing (open symbols) plotted against the corresponding fold-change obtained for the better eye viewing in five participants with bilateral asymmetry in keratoconus. Panels C and D represent data for spatial frequencies lower than the peak and higher than the peak, respectively. Given the similarity in data trends for the 10% and 50% suprathreshold contrast levels, both sets of data are plotted together, without identifying them separately, in these two panels. The diagonal 1:1 line indicates equal contrast matching performance in the test conditions in these two panels.

5.4.5. Experiment 3- Changes in suprathreshold contrast matching with short-term changes in the eye's optical quality

The changes in the contrast threshold function when wearing RGP contact lens correction as well as with spectacles during the different visits are shown in Figure 5.5A – C for the three keratoconic cases that participated in Experiment 3 (cases P3, P6 and P8 in Table 5.1). All the

three contrast sensitivity function parameters with the RGP contact lenses were significantly better compared to spectacles for all participants. Interestingly, an improvement in the threshold performance with the best corrected spectacles was noted during the last visit (second week after lens removal) and this trend was most prominent for Participant 8 in this study (Figure 5.5C), relative to participants 3 and 6. Notably, the severity of keratoconus was least in Participant 8, relative to the other two participants (Table 5.1). However, the performance did not reach the level of contact lens wear in any of the participants (Figure 5.5A – C).

Figure 5.5 plots the longitudinal data of each participant for all four spatial frequencies tested at the 10% and 50% suprathreshold contrast levels. As seen in previous results, the contrast matching data of all three subjects was close to the unity line for the 50% (Figure 5.5B, D and F) than for the 10% (Figure 5.5A, C and E) suprathreshold contrast level. The higher two spatial frequencies (2x and 3x) did not show any significant trends in the contrast matching fold-change values across the four visits for both suprathreshold stimuli (Figure 5.5). The lower two spatial frequencies (0.25x and 0.5x) did show a pattern with the fold-change in contrast match tending towards unity values in the second and third participants, but not in the first participant (Figure 5.5). These trends were more apparent for the 10% than for the 50% suprathreshold contrast stimuli (Figure 5.5F and G). However, the hypothesized pattern of an increase in the fold-change immediately after switching from contact lenses to spectacles was not observed in any participant, for any spatial frequency or contrast level (Figure 5.5).

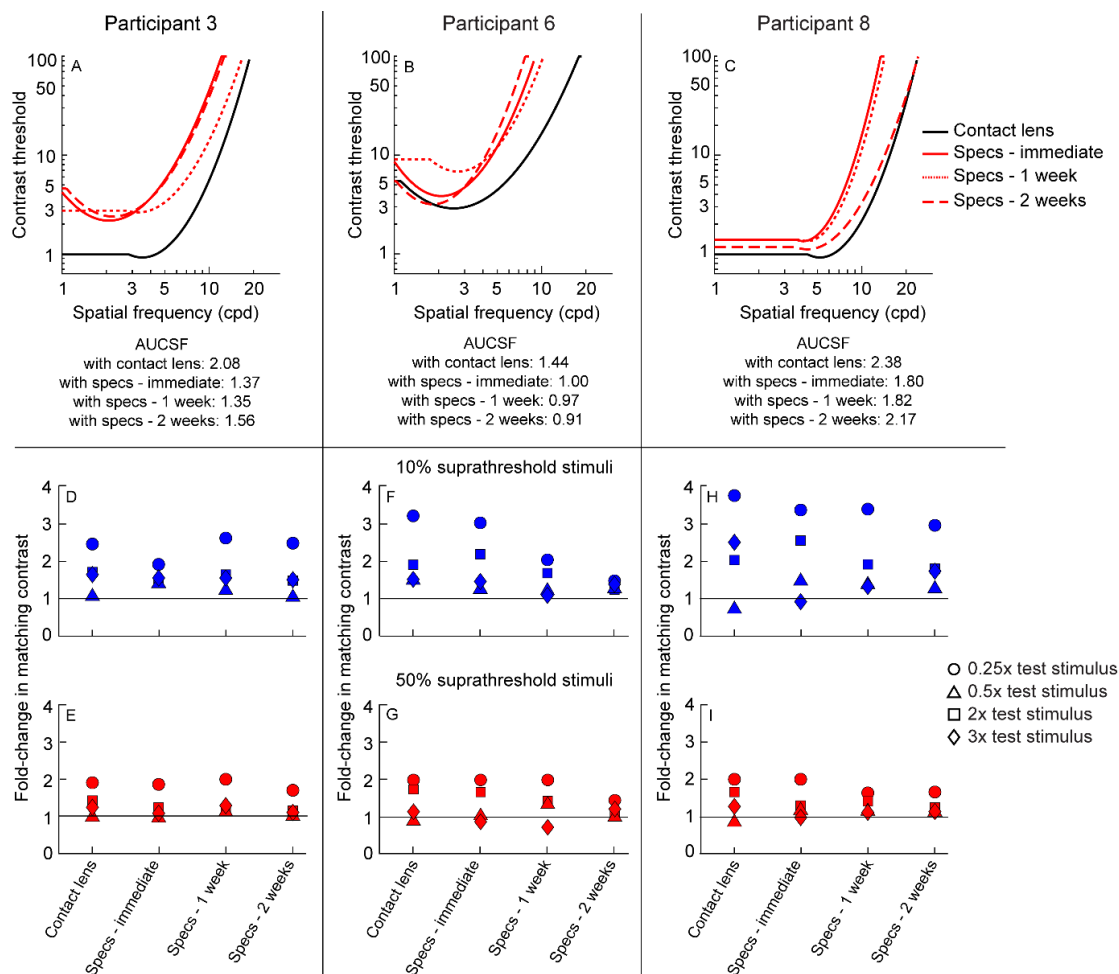


Figure 5.5: Panels A – C show the monocular contrast threshold functions of the three cases with keratoconus that participated in Experiment 3 (corresponding to Participants 3, 6 and 8 in Table 5.1). Contrast threshold curves are plotted for contact lens wear and with their best-corrected spectacle correction immediately after switching from contact lens wear (Specs - immediate), one week of spectacle wear (Specs - 1 week) and two weeks of spectacle wear (Specs - 2 weeks) for each participant. The area under the CSF obtained for each viewing condition and each participant is also noted in this figure. Panels D – I show fold-change in suprathreshold contrast match for three participants across the four viewing conditions tested in this experiment. Panels D, F and H show data for 10% suprathreshold contrast stimuli while Panels E, G and I show data for the 50% suprathreshold contrast stimuli.

5.5. Discussions

5.5.1. Summary of results

While losses in visual acuity and contrast sensitivity are well-known in keratoconus (Shneor et al., 2021, Xian et al., 2023), an assessment of suprathreshold performance in this disease condition has received little attention (Ng et al., 2022). The phenomenon of contrast constancy was used as a paradigm to address this issue in the present study. The results were consistent

across the three experiments conducted here and between keratoconic cases and controls: Stimuli at higher levels of suprathreshold contrast showed better contrast constancy than those at lower levels of suprathreshold contrast (Figure 5.2, Figure 5.3 and Table 5.3). Similarly, stimuli with spatial frequencies higher than the peak of the CSF showed better contrast constancy than those lower than the peak of the CSF (Figure 5.2, Figure 5.3 and Table 5.3). All these trends were independent of disease severity (Figure 5.3), its interocular symmetry (Figure 5.4) and short-term changes in the quality of threshold-level viewing experience (i.e., contact lens Vs. spectacles) (Figure 5.5). These results match well with the recent observation of intact contrast constancy for spatial frequencies that are habitually experienced by keratoconic eyes (Ng et al., 2022).

5.5.2. Implication of results for contrast perception in keratoconus

The study outcomes have three important implications for threshold and suprathreshold contrast perception in keratoconus. First, the optical degradation in keratoconus progressively constricts the “visible” region of spatial vision in keratoconus (Figure 5.1A) (Nilagiri et al., 2018, Shneor et al., 2021). The present results suggest that the perception of relative contrasts across different high spatial frequency stimuli may remain unchanged within this visible region (i.e., for spatial frequencies between the peak and cut-off value of the CSF) suggesting contrast constancy across a range of keratoconus disease severities (Figure 5.2, Figure 5.3). Patients with keratoconus may thus not experience any local contrast variation across high spatial frequency components of natural scenes in their suprathreshold viewing experience. Variations in contrast perception across spatial frequencies may start becoming apparent as the target approaches threshold levels of contrast, as suggested by the relatively weaker pattern of contrast constancy for 10% than for 50% suprathreshold contrast stimuli in this study (Figure 5.2 to Figure 5.4, Table 5.3). However, the observed fold-change in matching contrast for the 10% suprathreshold stimuli in keratoconus was still several orders of magnitude

smaller than the expected fold-change based on the contrast threshold function (Table 5.3). This suggests that any variations in contrast perception of high spatial frequencies may be minor for patients with keratoconus under low suprathreshold contrast viewing conditions. Second, the pattern of contrast constancy across high spatial frequencies was remarkably similar in the two eyes of patients with bilaterally asymmetric keratoconus (Figure 5.4). This observation suggests that the perceived contrast of high spatial frequencies at suprathreshold levels may be largely similar in the two eyes of these patients even while their optical quality and threshold-level performance may show significant interocular asymmetry. This observation leads to a prediction that keratoconic patients with bilaterally asymmetric disease severity may remain binocular for tasks involving suprathreshold judgments, while their threshold-level performance may be dictated by the performance of the better eye and a compromise in binocularity (Marella et al., 2021, Metlapally et al., 2019, Nilagiri et al., 2018). This prediction may be tested using appropriate paradigms in the future. Third, the pattern of contrast constancy for high spatial frequencies was similar for spectacles and contact lenses in this study (Figure 5.5), suggesting that correcting the optics of the keratoconic eye primarily serves to expand the region of visibility for spatial vision, as determined by the CSF, without having any significant impact on suprathreshold contrast perception. A natural scene with broad spatial frequency content may, however, appear sharper and crisper with these contact lenses owing to the overall expansion of the region of visibility to include higher spatial frequencies (Devi et al., 2022, Lim and Lim, 2020, Marta et al., 2021). Interestingly, Ng et al. (2022) recently observed that contrast constancy fails for spatial frequencies that are not within the habitual visual experience of the keratoconic visual system. This implies that keratoconic patients who are habitual spectacle wearers and potentially adapted to a low-pass filtered retinal image may experience variations in contrast perception for high spatial frequencies soon after they switch to contact lenses. Contrast processing in the visual system

eventually adjusts to the expanded range of spatial frequencies, as suggested from the lack of difference in results between spectacles and contact lenses in the seasoned contact lens wearers of the present study (Figure 5.5). The time course of such an adaptation needs further investigation. Describing other aspects of object appearance in the suprathreshold space (e.g., sharpness, clarity, etc) is beyond the scope of this study and also needs further investigation. In addition to the steep drop in the contrast sensitivity for higher spatial frequencies, the CSF of keratoconic cases also showed an overall loss of sensitivity, all relative to controls (Figure 5.1). This overall loss was greater for eyes with more severe keratoconus (Figure 5.1, Figure 5.4A and B) and for eyes with spectacles rather than contact lens correction (Figure 5.5A – C). The present study only assessed the relative perception of contrast across spatial frequencies for suprathreshold stimuli. The study did not address the impact of the absolute loss of contrast sensitivity at any given spatial frequency for suprathreshold stimuli. This issue is equally important in order to determine whether patients with keratoconus experience the suprathreshold visual scene with the same perceived contrast as healthy observers or if there are deficiencies in the perception of absolute contrast with this condition. Such an intactness or deficiency in absolute contrast perception will provide insight into any normalization of neural activity within a given spatial frequency channel to optimize suprathreshold visual experience, especially with disease progression in the two eyes or in the presence of asymmetric disease severities in the two eyes. The experimental paradigm needed to study this question is, however, not trivial and needs to be investigated further in a separate study.

5.5.3. Comparison of results with previous literature

The observation of near-complete contrast constancy for higher than peak spatial frequencies across the two different cohorts in the present study agrees with the results of previous studies on this topic, albeit for the normal subjects (Figure 5.6) (Brady and Field, 1995, Georgeson and Sullivan, 1975). In comparison, contrast constancy appears to breakdown for the two low

spatial frequency stimuli tested in this study, and more so with lower contrast stimuli (Figure 5.2 to Figure 5.5). The pattern of contrast matches observed in keratoconics for lower than peak spatial frequencies was very similar to those observed in healthy controls (Figure 5.2E and F). These results indicate that keratoconic patients as well as the control subjects may perceive suprathreshold low spatial frequency stimuli to have a lower contrast than their higher frequency counterparts. These results are partially at odds with the previous literature (Figure 5.6) (Georgeson and Sullivan, 1975, Brady and Field, 1995, Kulikowski, 1976). Like the present results, the data of Georgeson and Sullivan (1975) and, to a lesser extent, Brady and Field (1975) also showed poorer contrast constancy for lower than peak spatial frequencies, more so for lower than higher suprathreshold contrast stimuli (Figure 5.6A and C). The magnitude of the deviation was, however, not as much as was observed in the present study (Figure 5.6). These differences may arise from the differences in the methodologies employed to measure contrast constancy. First, the spatial frequencies of the reference pattern varied based on the threshold function of the subject in the present study while in previous studies it was held constant across subjects (Brady and Field, 1995, Georgeson and Sullivan, 1975, Kulikowski, 1976). Second, the perceptual matches in suprathreshold contrast were achieved using an adaptive staircase method in the present study whereas they were obtained using the method-of-adjustment in the previous studies. During the staircase method, the reference and test stimuli were presented sequentially for 500ms each in the present study while during the method-of-adjustment, they were presented simultaneously with a spatial separation between the two stimuli for as long as the subject required to complete the matching task in previous studies (Georgeson and Sullivan, 1975). Third, the stimulus size was fixed at 4° for all spatial frequencies in the present study while it was scaled to accommodate equal numbers of sine wave cycles in the previous studies (Georgeson and Sullivan, 1975, Brady and Field, 1995, Kulikowski, 1976). This posed a unique challenge to the subjects in the present study as some

of them reported difficulty in performing the matching task for lower spatial frequencies as only a limited number of cycles of the grating stimulus were present for them to judge the contrast. This was reflected in the increased number of trials during testing before obtaining the desired number of reversals in the staircase procedure and in the relatively larger inter-subject variability of the suprathreshold contrast match obtained for these spatial frequencies in controls and cases with keratoconus (Figure 5.2E and F). Fourth, in contrast to all the previous methodologies, the study by Smith (2015) used a rather unique experimental paradigm to test this phenomenon. Instead of the reference pattern having a fixed spatial frequency, suprathreshold contrast matches were tested for adjacent pairs of spatial frequencies spanning the entire region of visibility. This paradigm enabled the stimulation of the same spatial frequency channel for the reference and test stimuli. However, the perception of contrast at suprathreshold appears to be a robust system and therefore unlikely to be influenced by any methodological difference as shown by the alignment of the previous literature with the present study (Figure 5.6).

In summary, the present results may not necessarily reflect selective deficiencies of contrast processing in keratoconus but a uniqueness of the study methodology that may have led subjects to perceive suprathreshold low spatial frequency test patterns to have lower contrast than the reference pattern. The similarity of the findings of the present study to previous research does however indicate that, contrast constancy for high spatial frequencies is robust enough to withstand the methodological differences encountered across studies (Figure 5.6).

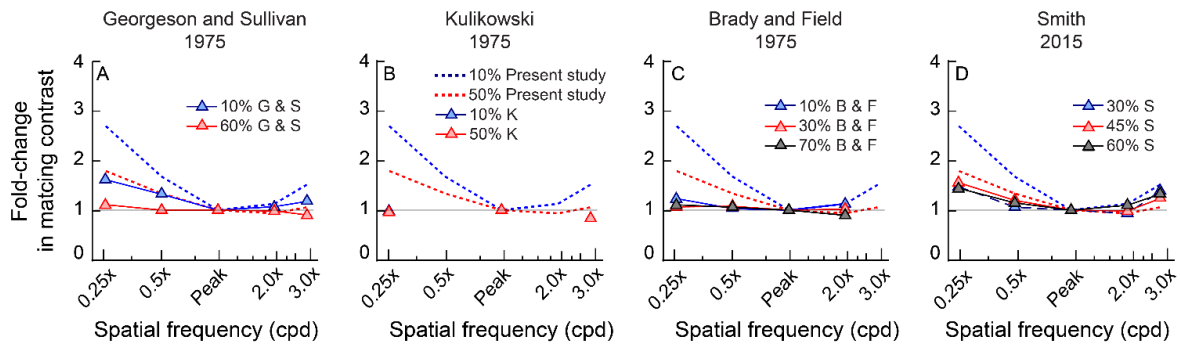


Figure 5.6: Comparative analysis of the present study results with those of previous studies investigating the contrast constancy phenomenon. The organization of this figure is similar to that of Figure 5.2E and F. The fold-change value from the previous literature (solid lines with symbols) was calculated from the physical contrast of the reference stimulus and the matched contrast of the test stimulus, in line with the methodology used in the present study. From the spectrum of spatial frequency and suprathreshold contrast level tested in these studies, only those closer to the ones used in the present study are plotted here. The results of the present study are shown as dashed coloured lines in all figure panels.

5.5.4. Interpretation of results in the context of the prevalent models of contrast constancy

The results obtained for the higher than peak spatial frequency may be interpreted in the context of two prominent models of contrast constancy reported in the literature. Georgeson and Sullivan (1975) postulated a normalization process involving active gain control of the different spatial frequency channels mediating contrast perception in the visual system. The extent of normalization required to achieve contrast constancy may be readily derived from the contrast threshold function, as performed in this study (Figure 5.1). In keratoconus, there would be a higher demand on the contrast gain control mechanism to achieve constancy for suprathreshold stimuli, relative to controls, as evident from the predictions shown in Figure 5.1B. The pattern of contrast constancy observed in our data was remarkably similar for cases and controls, despite the increased demand in the former cohort, and may indicate that the operating range for such a gain control mechanism is larger than has previously been observed in controls. This normalization process also appears to have a short time course of implementation (matter of several minutes) (Figure 5.5) and is mediated by monocular contrast processing channels (Figure 5.4), as suggested from the second and third experiments of this study. This gain control model inherently operates across different spatial frequency channels

and is unable to normalize contrast threshold differences occurring within a single channel (Georgeson and Sullivan, 1975). The methodological issues described in the previous section notwithstanding, this could be a plausible neurophysiological explanation for why contrast constancy was not observed for the lower than peak spatial frequencies in this study.

The visual system inherently possesses the ability to dynamically recalibrate the neural processing of blur to optimize spatial vision (Webster et al., 2002). For instance, the perceived sharpness of an image can be systematically biased within minutes of exposure to the same or related images that are synthetically blurred or over-sharpened by altering their amplitude spectrum (Webster et al., 2002). The perception of optimal focus of an image also seems to be inherently calibrated to the eye's own optical quality such that images corrected for all optical defects are adjudged not to be in best focus (Sawides et al., 2011, Artal et al., 2004). Such re-adjustments are also possible in the presence of interocular differences in blur, but with the binocular percept biased by the sharper of the two eyes' retinal images (Kompaniezy et al., 2013). The perceived focus of an image may also be optimized through a long-term form of adaptation with age-related losses in optical quality due to cataracts (Parkosadze et al., 2013). Such mechanisms of "blur adaptation" may also be at play in diseases like keratoconus and, perhaps, the maintenance of contrast constancy observed in this study and by Ng et al. (2022) are reflections of this underlying ability.

Brady and Field (1995) explain the contrast constancy phenomenon through a contrast-response gain function that remains constant across the spatial frequency channels. Suprathreshold contrast matching across spatial frequencies is determined only by the signal strength of the stimulus, independent of threshold level performance. Contrast threshold, on the other hand, is determined by the noise level in the visual system that scales with spatial frequency, resulting in a progressive reduction in the signal-to-noise ratio (Brady and Field, 1995). Threshold-level losses in keratoconus may be explained by increased noise in the visual

system arising from the degraded optical quality of the eye, even while the contrast-response gain function of the different spatial frequency channels remains unaltered in this disease condition. Thus, unlike the Georgeson and Sullivan model, there is no need for recalibration or re-normalization of neural inputs for suprathreshold contrast perception in keratoconus.

The present study assumed that the perceived contrast of the test and reference stimuli used for the matching experiment were linearly related to the physical contrasts of the stimuli presented on the computer monitor. That this assumption is too simplistic is suggested by Weber's law, which would require a compressive non-linear transducer present in the internal representation of the contrast (Shooner and Mullen, 2022). This will result in the expected fold-change in contrast matching shown in Figure 5.1B to vary non-linearly with the suprathreshold contrast level of the reference stimulus, in the absence of contrast constancy. The present study acknowledges this as a limitation of the present model and suggests that future studies of contrast constancy explore the impact of this non-linear transformation from physical stimulus to perception in greater detail. That the results of the cases and controls were identical in this study suggests that the pattern of this non-linearity remains unaltered in keratoconus (Figure 5.2E and F). The present results on keratoconus may thus not be differentially impacted by the simplistic model that was used here to calculate the expected fold-change in contrast matches.

5.6. Summary

The ability to retain the perceived invariance of suprathreshold contrast with spatial frequency in keratoconus is remarkably similar to controls and extends across a range of disease severity, interocular asymmetry and short-term changes in optical quality and threshold-level visual experience. Correction strategies aimed at improving the optical quality in keratoconus may therefore function primarily to expand the region of visibility and resolution acuity in this disease condition, with only a limited influence on the contrast perception of suprathreshold objects.

6. Chapter 6: Global summary and discussions

6.1. Summary of results

This thesis has largely focussed on understanding the structure-function relationship in keratoconus, where measures of visual function have been evaluated across various severities of structural loss. In spite of high contrast acuity being traditionally used as the marker for visual performance, the contrast sensitivity function better explains the intricacies of spatial vision, for example, the ability to detect the change in size and luminance of an object. Additionally, the presentation of this disease is usually asymmetric in nature, potentially resulting in a significant difference in retinal image quality between the eyes. Our day-to-day activities largely revolve around the binocular functioning of an individual, where combining the two eye's images are important to achieve optimum performance. Therefore, an assessment of depth perception (stereoacuity) is also important. This thesis focussed on three visual parameters: high contrast acuity, contrast sensitivity and stereoacuity. The structure-function relationship in other progressive eye conditions such as glaucoma has been extensively researched (Gardiner et al., 2005, Raza and Hood, 2015) but has not been evaluated in keratoconus before and is important due the similarly progressive nature of keratoconus. The following aims were addressed in this thesis: First, how does the threshold performance change over the natural course of the disease; Second, whether the contact lenses have a differential impact on improving the threshold performance in keratoconus; And third, whether the loss in threshold level contrast performance in keratoconus affects suprathreshold vision. The results of the three experiments are summarised below.

1. Chapter 3 specifically evaluated the first aim. The results showed that all visual functions, (high contrast acuity, contrast sensitivity function and stereoacuity), deteriorated with disease severity when subjects were best spectacle corrected. The structure-function relation was non-linear, indicating a varying rate of functional loss across the severity scale.

The pattern of loss was different for the different measures of visual function. There was a ceiling phase for high contrast acuity (Figure 3.6, Figure 3.7D and L, Figure 3.8) and it showed a steeper loss in function compared to the contrast sensitivity performance (Figure 3.8). In comparison, the contrast sensitivity function showed deterioration from an early stage of the disease. For stereoacuity, the performance was significantly poorer than age-similar controls even from an early stage of the condition. Subjects with an early form of the disease and low inter-ocular difference were the least vulnerable in terms of a drop in performance compared to age-matched controls (Figure 3.10).

2. Chapter 4 explored the second aim of the thesis. The results suggested that all the contact lenses tested, reduced the ocular higher order aberrations, and improved the threshold visual functions compared to the best-corrected spectacles, with the magnitude of improvement scaling with disease severity. The performance with the customized soft toric contact lenses was inferior to the other lens designs. The performances with a conventional RGP lens, the Rose K2 lens and scleral lenses were largely comparable (Figure 4.2 to Figure 4.7). Even with the best fit contact lens on the eye, the visual performance still did not reach the level of age-similar controls.

3. Chapter 5 investigated the third aim of the thesis. Results suggested that unlike the threshold performance, the contrast perception at suprathreshold appears comparable across a large range of spatial frequencies in keratoconic eyes. This constancy in contrast perception was more apparent for the 50% suprathreshold contrast level as well as for higher spatial frequencies. Moreover, the suprathreshold contrast performance of keratoconic eyes was similar to that of age-similar controls. The results remained similar across disease severity, inter-ocular asymmetry and short-term change in optical quality (Figure 5.2 to Figure 5.5).

6.2. Learnings from the thesis to implement in the clinical management of keratoconus

The studies conducted in this thesis have several important clinical implications.

6.2.1. Extrapolation of psychophysical testing to the clinical tests in the spatial and depth domain

High contrast visual acuity is routinely measured in the clinics using the logMAR visual acuity chart. Although high contrast acuity measurements have some limitations (see chapters 2 and 3), the letter-by-letter scoring (discussed in chapter 3) provides an obvious advantage compared to a line-by-line assessment in Snellen charts. Research has also demonstrated that measurements using COMPlog have been shown to be in good agreement with the ETDRS acuity charts. In addition, the time taken to conduct the test with a COMPlog method is only marginally longer (on average, 10 seconds longer) than ETDRS (Laidlaw et al., 2008). Given the importance of detecting change in visual function in the early stages of the disease, this technique is certainly advisable in the clinics and results have been shown to agree with other logMAR charts using Sloan letters.

The structure-function relationship showed a ceiling effect in the early stages of the disease for high contrast visual acuity with the use of a letter-by-letter assessment strategy (Figure 3.6 to Figure 3.8). This reemphasized the insensitive nature of high contrast acuity as a measure of visual function. In other words, this means that the high contrast acuity is not able to effectively capture the change in visual performance at early stages of the disease. While high contrast letter acuity could not elicit subtle difference in performance in early keratoconic eyes compared to the controls, the use of low contrast acuity charts could have possibly enhanced the detection ability in these cases. This assumption is in alignment with previous literature that has reported the usefulness of using standardized Bailey-Lovie format of acuity charts (Bailey and Lovie, 1976) with low contrast letters in detecting loss of performance in ocular

conditions that cause ocular aberrations rather than simple refractive blur (Regan and Neima, 1983, Ho and Bilton, 1986, Brown and Lovie-Kitchin, 1989). Ho and Bilton (1986) tested the distance and near acuity performance at different contrast levels and recommended that contrast levels as low as 10% would be sufficient to detect a loss in performance effectively.

In terms of assessing the contrast performance of an individual, the Pelli-Robson (PR) contrast sensitivity chart is the most widely used method in the clinics. In case of a PR sensitivity test, the assessment is usually carried out at a specific test distance. Therefore, the angular size of the letter remains constant. In the frequency domain, this translates to the spatial frequency component of the stimulus remains unchanged during the test. The contrast of the letters is systematically reduced and the minimum contrast a subject can perceive determines the contrast threshold. Technically, all the clinically available tests for measuring the high contrast visual acuity, low contrast visual acuity and the contrast sensitivity, probe different elements of an individual's contrast sensitivity function. For the acuity tests, the change is in the spatial frequency element as we move horizontally within contrast sensitivity space to find the threshold). In comparison, for the PR contrast sensitivity chart, the change is in contrast as we move vertically in contrast sensitivity space to find the threshold for a fixed spatial frequency. The quick CSF testing paradigm is quite unique in this aspect, specifically because both these aspects can be determined from this measurement that is used for the experiment in the thesis (Chapter 3; Figure 3.9). Panel B in this figure demonstrates the results for the cut-off spatial frequency (comparable to the visual acuity assessment) and the panel C demonstrates the results for the sensitivity at a given spatial frequency (comparable to the PR sensitivity chart). Although the slope of the structure-function relationship is different, the overall pattern remains similar. The quick CSF method used in this thesis provides a comprehensive measurement of contrast perception that considers both the elements of contrast vision- spatial frequency components and the contrast level of the spatial stimulus.

The literature on visual performance in keratoconus is largely focussed on assessing the threshold level performance, which helps in understanding the limits of vision. However, many of our day-to-day visual activities are significantly above threshold. For example, to process coarse detail in a natural scene on a bright sunny day, does not require contrast processing at threshold level. This motivated the study question in Chapter 5. A contrast matching paradigm was used to test the presence of the well-established (for normal observers) phenomena of contrast constancy. The absence of constancy in keratoconics would have indicated that the threshold contrast function loss (Figure 5.1) also applied to the suprathreshold space. Conversely, the presence of contrast constancy would indicate an active gain control mechanism across the different spatial frequency channels that could compensate for the increased loss in retinal image quality in keratoconus. The presence of contrast constancy indicated that the keratoconic eyes may not experience any local variation in contrast for suprathreshold viewing across a large range of spatial frequencies.

Stereoacuity was used as a measure of depth performance of the subjects. In this context, measuring binocular spatial vision performance could provide valuable insights into the habitual viewing experience of patients with different severities of keratoconus. This issue becomes pertinent in cases of bilaterally asymmetric keratoconus, where there is significantly different retinal image quality in the two eyes (Nilagiri et al., 2020). The visual system may optimize binocular spatial vision by weighting the binocular input in favour of the eye with better retinal image quality and suppressing the weaker eye. In an earlier study by Nilagiri et al. (2018), high contrast acuity was shown to be driven by the better of the two eyes during asymmetric disease presentation. However, it remains to be tested in patients with bilateral disease with different severities. It is therefore predicted that, binocular spatial vision may be determined by the better of the two eyes in bilaterally asymmetric disease presentations. For the stereoacuity measurements, the use of the random-dot stereogram and the Howard-Dolman

test provides assessment of the ability to detect disparity in finer steps compared to the available clinical tests such as the Titmus-fly test, Frisby test or the TNO test, which all use a significantly larger step-size. Results from Chapter 3 suggest a drop in stereoacuity performance from the very early stage of the disease condition. However, a differential pattern could be observed as the early keratoconus cases with low inter-ocular difference had better stereoacuity compared to the rest of the categories. While the loss in stereoacuity in keratoconus could still be detected with the clinical tests, it will be more difficult for these tests to differentiate between the different disease severity groups.

Although, the contrast threshold performance was carried out monocularly in our studies, suprathreshold contrast perception was measured both monocularly as well as binocularly. No difference in binocular suprathreshold performance was seen in cases, even with a significant disease asymmetry. This suggests that the patients may remain binocular at suprathreshold with no specific bias towards the better eye's contrast perception as is usually noted for threshold level performances (Marella et al., 2021). These results are in alignment with the literature, where actual depth performance was assessed using vernier stimuli, with the disparity level well above the threshold. In spite of a significant increase in vernier threshold through positional change or induced dioptric blur, the perception of suprathreshold depth remained unchanged (Patel et al., 2009, Bedell et al., 2012). These results possibly indicate that the inter-ocular differences may only contribute significantly to altering the stereoacuity threshold performance, but not to the perception of depth above the threshold level in these eyes.

6.2.2. Interpretation of temporal changes of keratoconic eyes in the clinic

In the clinical context of a progressive disease such as keratoconus, an understanding of the structure-function relationship is important for several reasons. First, the clinical protocol for evaluating the disease may differ across clinicians. These differences may arise for different reasons: the choice of index that is being used to define structure in keratoconus, the different

functions that are being tested to determine an individual's visual performance, or, the interval at which the follow up appointments are scheduled to monitor the progression of the disease. Secondly, there could be an inclination towards extrapolating a change in a specific function, to the other visual functions and overall visual performance. This assumption may not always be true and should be tested. The findings from Chapter 3 offer valuable insights into all these aspects. First, the varying patterns of functional loss among different structure-function relationships (Figure 3.6 to Figure 3.10) indicate that the extent of loss in one specific visual function may not be meaningfully extrapolated to the other functions and therefore, assessment for different visual outcomes is needed. Second, changing structural indices while interpreting these relationships is not straightforward. Although, the general pattern may suggest a loss in performance with disease severity, the difference in the pattern (Appendix 1B to 1G) indicates that replacement of a metric used to define structure may result in an underestimation or an overestimation of visual function during the natural course of the disease progression. This variability arises from the different sampling of corneal shape with these indices. The expectation would be that an index that provides a finer sampling of the cornea would allow a better understanding of the structure-function relationship. For example, for high contrast visual acuity, using the D-index revealed the initial ceiling zone (Figure 3.7D) whereas, using the maximum keratometry value did not reveal this early zone of insensitivity (Figure A1F). This can be interpreted as the D-index possibly revealing early forms of the disease, even before the functional impact becomes apparent. Clinicians should therefore be advised to keep to one particular structural index when it comes to detecting progression as well for comparing the visual performances of an individual with keratoconus during the course of the disease. Third, a clearly non-linear structure-function relationship (Figure 3.7) suggests that a given magnitude of structural change is not going to produce a fixed amount of functional loss. Therefore, the

functional evaluation must be captured over multiple time points before deriving any conclusion regarding the course of the disease.

With all these factors considered, increased awareness of these structure-function relationships may help eye care practitioners make more meaningful inferences about the nature of visual function loss experienced by patients at different severities of the disease. This will allow the eye care practitioner to better educate patients about their condition, better manage their expectations regarding activities of daily living and enable them to make informed decisions about various treatment options and lifestyle changes, if required. An understanding of the structure-function relationship will also allow eye care practitioners to develop targeted, evidence-based, interventions to preserve or enhance visual functions which are more vulnerable from the condition, while monitoring more resilient functions for potential changes over time.

6.2.3. Understanding the role of contact lenses in management of keratoconus

The continuous advancements in technology have led to the emergence of various new contact lens designs. The cost of procuring these lenses can vary significantly in different locations. This situation has two important implications. First, from the practitioner's standpoint, the wide array of lenses to choose from can often leave the practitioner unsure on which is the optimal lens to prescribe. Secondly, patient counselling becomes critical, so that the patients do not feel compelled into choosing a lens merely based on its higher price, which can become a significant burden to the ongoing treatment, especially in developing countries. Instead, patients should be presented with a valid and informed reason for their choice. The cross-over study design used in this thesis provided a unique and perfect platform compared to the existing literature, as it provided a comparative analysis between the lenses on a cohort, where the diverse nature of the disease (in terms of cone morphology and physiology of the visual system) has been taken into account.

The performance of the Kerasoft lenses was found to be inferior to the other lenses studied (Figure 4.1 to Figure 4.6). This difference was more apparent with increased disease severity. This would suggest that the Kerasoft lenses should be reserved for mild to moderate keratoconics. Fernandez-Velazquez (2012), in contrast, found a comparable visual performance of Kerasoft lenses with Rose K2 lenses. However, there are important differences that could explain the findings: First, the comparisons in the study by Fernandez-Velazquez (2012) were made with different lenses on two separate cohorts that were age-similar and matched for corneal curvature. However, the cone morphology (location and pattern), a prominent factor that influences visual performance, was not considered. Second, the comparison was made based on high contrast visual acuity alone and other measures of visual function were not assessed. Finally, the neural component of the patients, such as the extent to which the visual system was exposed to uncorrected blur were not accounted for between the cohorts.

The relative performance between the conventional RGP, Rose K2 and scleral lenses were similar in cases of mild to moderate keratoconus, suggesting that the most appropriate lens to issue would possibly not be based on improvement of visual function. Rather, it will depend on the other non-visual factors such as cost, the quality of lens fitting and subjective comfort with the lens. With increased disease severity, the differential impact of the lenses was more obvious, and the Rose K2 lens and the scleral lens performed relatively better compared to the conventional RGP lenses. Therefore, in patients with more advanced disease, the visual performance has a stronger role in determining the final prescription. The results suggest that the decision cannot be generalized across the disease population. The approach should be tailored to suit the individual and the practitioner has to be cognizant about the disease severity along with other nonvisual factors that have been discussed about earlier, to prescribe the right lens of choice.

In a clinical scenario, keratoconus is often considered as an ocular condition with structural and functional characteristics of the two eyes being independent of each other. As a consequence, this sometimes leads to each eye being treated separately depending on its stage of severity. A critical observation could be made in this context that the stereoacuity of keratoconic patients may be significantly reduced even at early stages of the disease, and that this loss is linked to interocular differences in disease severity (Figure 3.10 and Figure 3.11), possibly suggesting that clinical interventions in early to moderate keratoconus should incorporate approaches that will optimize binocularity by making the optical quality of both eyes similar, in addition to the conventional optimization of monocular visual acuities independently.

Another interesting finding of note is the contrast performance at suprathreshold space with the contact lenses, where the perception of contrast with the habitual contact lenses was found to be comparable to spectacle correction. This perhaps indicates that the contact lenses primarily serve to increase the visible space compared to the spectacles. As a result, objects may appear more sharp owing to inclusion of more high spatial frequency elements. However, within this visible range of spatial frequencies, variation in contrast is not expected. Practitioners should be aware of this while comparing the performance of these lenses during the day-to-day activities of an individual. Additionally, this result also shows the dynamic nature of the adaptive gain control mechanism of the visual system where the visual system readily recalibrates itself when exposed to a change in visual experience caused by a change in retinal image quality.

6.3. Future directions

The findings presented in this thesis warrant further investigation in different directions.

The structure-function relationship in Chapter 3 may be extended in three possible directions. First, the fundamental purpose of a structure-function analysis is to forecast changes in the dependent variable from the independent variable (Kanellopoulos and Asimellis, 2013). The same equation describing the cross-sectional data (Section 3.3) may therefore be utilised to predict longitudinal losses in spatial vision with keratoconus progression (Figure 3.7). Systematic departures in visual functions from these predictions may indicate limitations in the cross-sectional model adopted in Chapter 3 or signal the influence of factors that may not be easily accounted for in the cross-section analysis (e.g., changes in neural sensitivity following prolonged exposure to degraded retinal image quality (Sabesan and Yoon, 2009). However, following the natural progression of keratoconus through a longitudinal dataset would not be trivial because disease progression is usually aggressively managed through surgical interventions such as collagen crosslinking to restore the structure as well as to maintain visual quality in the patient (Caporossi et al., 2010). A retrospective analysis of patient records from large volume tertiary eye care centres before the advancement of surgical interventions may perhaps be one way to investigate the longitudinal structure-function relationship in keratoconus. Second, and related to the previous point, the regression analysis was determined using measures of structure that do not explicitly consider the morphology or the location of the cone in keratoconus. These parameters are known to influence the visual quality of the patient and, hence, these parameters also need to be incorporated into future regression models of the nature described in this study. Third, the measurement of the laboratory-based threshold performance explains components of vision independently, such as contrast, colour, motion etc. However, extrapolation of the results to an individual's day-to-day experience and quality of life might not be a straightforward task. Recent reports are incorporating several aspects of vision into creating task-based performances that measures the functional vision under a real world scenario with the help of new technologies such as virtual reality (Bennett et al., 2019).

Assessment of functional vision needs to be explored in greater detail to understand the holistic impact of the disease on an individual.

The contact lens study can be further expanded in three different ways: First, the assessment of visual functions was done after a brief period of adaptation. Given the existing literature on the symptomatic adaptation with the contact lenses (Carracedo et al., 2016), it would be ideal to assess the relative performance after a longer period of adaptation with each lens. Second, it would be interesting to assess if the adaptation also holds true from a neural perspective. Sabesan et al. (2017) demonstrated perceptual learning and an improvement in high contrast acuity measures after one week of training with an adaptive optics (AO) system that improves the retinal image quality significantly in keratoconic eyes. Given the contact lenses produce a significant improvement in retinal image quality compared to the habitual spectacles, it would be interesting to note the long-term improvement of lens wear and to perform a comparative analysis. Third, the optical performance of the eyes has been reported and compared between the lenses solely, in terms of the magnitude of the residual wavefront aberrations. However, the specific Zernike terms contributing to the overall wavefront aberration have not been compared. As the different contact lenses can have a differential impact on the pattern of aberration correction due to the shape of the back surface and lens fit, an independent analysis of the different orders of aberration post contact lens wear would provide a more detailed insight than the present study.

The work on suprathreshold vision can be expanded in two different ways: First, the sudden impact of optical correction and a significant change in visual experience (ability of the eye to perceive higher spatial frequencies) did not have any influence on the suprathreshold performance. The timeframe for this adaptation can be explored further. Second, an important question to be asked in understanding suprathreshold contrast perception in keratoconus comes from a recent report by Ng et al. (2022) who demonstrated the presence of contrast constancy

within the visible range of spatial frequencies for keratoconic eyes. However, suprathreshold assessment shows a loss in contrast perception when assessed for spatial frequencies that the subjects are not adapted to. It will be interesting to see how these eyes perform when they remain exposed to a superior image quality (thereby, getting exposed to higher spatial frequencies than usual) with the help of wavefront corrected contact lenses and training for the higher frequencies. The question needs to be asked whether there will be any form of adaptation and would that have an effect on the suprathreshold contrast perception. Third, the results suggest that the eye's contrast processing perhaps remains binocular even for a significantly asymmetric keratoconus. The extent this result affects depth perception is unknown. The results from the Chapter 3 indicate a significantly greater magnitude of loss in threshold stereoacuity compared to the controls. Therefore, it would be important to assess suprathreshold stereo performance as well.

6.4. Conclusions

The assessment of visual function needs to reach beyond the traditional measure of high contrast visual acuity. The contrast sensitivity function can identify early deterioration in spatial vision loss compared to high contrast acuity. The magnitude of loss in stereoacuity is greater than for high contrast acuity and contrast sensitivity and both the disease severity and the interocular difference play a significant role. Contact lenses significantly improve the optical and visual performance in keratoconus. However, the visual functions remain comparable between the lenses that were tested in this thesis for mild to moderate cohort of the lenses. Therefore, the effect of non-visual factors may be a critical element to consider when deciding the final lens prescription in these patients. The suprathreshold performance shows an active adaptive gain control mechanism in keratoconic eyes. In addition, the benefit of contact lens correction may remain limited to threshold visual function and does not benefit suprathreshold contrast performance.

Appendix 1

A1: Structure-function relationship with other indices of corneal structure

This analysis was undertaken as supplementary information to the experiment conducted in Chapter 3. The D-index used in the main experiment of this study is one of the many tomographic indices of corneal structure that may be used to detect keratoconus and its progression (Hashemi et al., 2016). Among the topometric indices proposed in the literature, index of surface variance (ISV), index of vertical asymmetry (IVA) and index of height decentration (IHD) have been shown to have good sensitivity and specificity in detecting keratoconus and its progression. In addition, the ISV and the IHD index have shown a relatively better ability to predict high contrast acuity (Kanellopoulos and Asimellis, 2013) and contrast sensitivity function (Xian et al., 2023). The ISV (a unitless entity) is a curvature-based index that represents the standard deviation of the sagittal radius of the particular cornea from its mean curvature. The IHD is an elevation-based index, that uses Fourier analysis to indicate the decentration of the elevation of the cornea in the vertical direction (Kanellopoulos and Asimellis, 2013). Supplementary analyses were therefore undertaken in this study to determine 1) the correlation between these indices across the severity of keratoconus, and 2) the pattern of the structure-function relationship for indices that are deemed sensitive/specific for keratoconus detection and progression. The former analysis was conducted by deriving the Spearman's rank correlation coefficient (rho-value) for all possible pairs of the nine prominent tomography indices described in the literature (Shetty et al., 2017, Hashemi et al., 2016). For the latter analysis, only three specific indices from this list – ISV, IHD and Max K – were chosen. The first two indices were chosen as alternatives to the D-index owing to their sensitivity/specificity in detecting keratoconus while the Max K was chosen as it still is commonly used clinically to ascertain the severity of keratoconus, even though it does not feature in the indices list according to the sensitivity/specificity criterion. These indices were

derived from the corneal tomography map of all study participants, in much the same way the D-index was derived in the main study. The latter analysis was also conducted only for high contrast visual acuity and the area under the contrast sensitivity function (AUCSF), given that stereoacuity was found to be grossly sub-normal across most severities of keratoconus in the main study (Figure 3.10).

Figure A1A plots a heatmap of the Spearman's rho-values for all possible combinations of the ten tomographic indices chosen for this analysis. A high correlation of these metrics with the D-index would suggest a comparable sampling of the corneal structure. The correlation analysis suggested that apart from the index of height asymmetry (IHA) (rho: 0.37; $p < 0.001$) and the index of vertical asymmetry (IVA) (rho: 0.63; $p < 0.001$), all the other metrics had a high correlation with the D-index (rho ≥ 0.75 ; $p < 0.001$). The index of height asymmetry is an elevation-based index that measures the difference in elevation between the superior and the inferior hemisphere of the cornea across the horizontal meridian and has units of microns. That the IVA showed the lowest correlation with the D-index perhaps indicates the inability of this index to adequately represent corneal structural change in keratoconus. This result is in agreement with the reports by Kanellopoulos and Asimellis (2013) who noted the complex nature of this index based on a significantly high inter and intra-observer variability (Kanellopoulos and Asimellis, 2013).

Figure A1B – G show scatter plots of the normalized high contrast visual acuity and AUCSF as a function of ISV, IHD and Max K, along with the best-fit logistic regression equation. The normalization of the data was identical to the main experiment. The results showed the same trend of the normalized visual acuity and AUCSF values deteriorating with an increase in the index values (Figure A1B – G, Table A1). The goodness of fit and the presence of distinct ceiling and flooring effects in visual acuity and AUCSF, however, differed across the three different indices. The R^2 values of the fit for ISV and Max K indices were comparable to the

D-index shown in the main study for both visual functions (Figure A1B, C, F and G). This is not surprising considering the excellent correlation between these indices ($\rho \geq 0.89$) (Figure A1A). The R^2 values for the IHD index were lower than that of the other three indices, with a large intersubject variability in the data (Figures A1D and E). Amongst the three indices, the ceiling effect in high contrast visual acuity was apparent for the ISV index, partly present for the IHD index and not present at all for the Max K index (Figures A1D and F). None of these indices showed a prominent floor effect for visual acuity (Figures A1B, D and F). The AUCSF trends for all three indices showed no prominent ceiling effect and their y-intercept values were all lower than that of visual acuity (Figures A1C, E and G, Table A1). The loss rate in AUCSF was also lower than that of visual acuity, with no prominent floor effect across all three indices tested (Figure A1B – G, Table A1).

Taken together, these results indicate that the structure-function relationship described in the main study is not unique to the D-index but may be generalized to a large extent across the different keratoconic indices described in the literature. While the overall trend of a loss in visual function with increasing disease severity is uniform across all indices, prominent variations in the trends are also apparent across indices. These variations may reflect either the granularity with which a given index signifies keratoconus severity (e.g., the Max K index may signify keratoconus severity with less granularity than the D-index) or the measurement precision of this index (as reflected in the intersubject variability of the data). A detailed analysis of the agreement between the different indices across different grades of keratoconus is required in the future to address these issues systematically. Whatever the reason, the results impose caution in using these indices interchangeably for the detection of keratoconus, determining its progression or while assessing its impact on different visual functions.

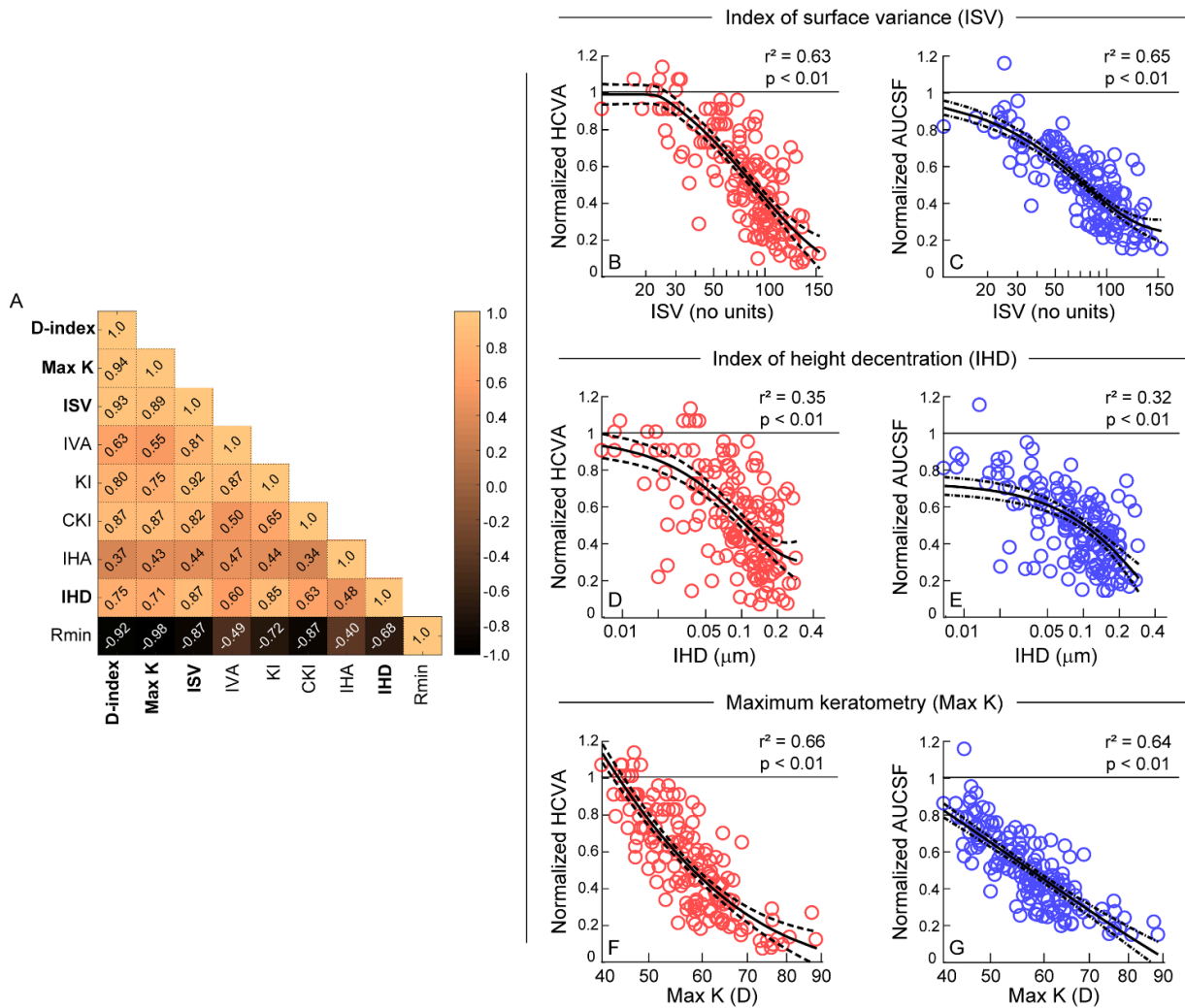


Figure A1: Panel A shows the structure-structure relationship between the different tomographic indices of the cornea described in the literature for the detection/progression of keratoconus (Kanellopoulos and Asimellis, 2013). The heatmap shows the Spearman's rank-correlation coefficient (ρ value) obtained while comparing any two structural indices of the keratoconic cohort that participated in this study. The upper diagonal of this heatmap indicates an autocorrelation and can be ignored. The Rmin metric depicts a worsening of keratoconus using negative values and hence is negatively correlated with all other indices. The indices chosen for the structure-function analysis in this study are identified using bold text in this heatmap. Panels B – G) Scatter diagram of the normalized high contrast visual acuity (HCVA) and area under the CSF (AUCSF) plotted as a function of the index of surface variance (ISV) (panels B and C), index of height decentration (IHD) (panels D and E) and the maximum keratometry (Max K) (panels F and G). The best-fit logistic regression equation (Eq. 4 in the main study) along with its $\pm 95\%$ confidence limits, R^2 , and p -values are shown along with the raw data in each panel. All other details are the same as Figure 3.7 in the main study.

Appendix 2

A2: Protocol approval by the Ethics committee

Ethics ETH2021-0434: Mr Preetam Kumar (External approval)

Date Created	19 Oct 2020
Date Submitted	16 Nov 2020
Date of last resubmission	18 Jul 2022
Academic Staff	Mr Preetam Kumar
Student ID	190020822
Category	Doctoral Researcher
Supervisor	Prof Chris Hull
Project	Assessment of visual function incases of keratoconus, with and / or without the procedure collagen cross linking
School	School of Health & Psychological Sciences
Department	Optometry & Visual Sciences
Current status	Registered

Ethics application

Project details

EP1) Project title

Assessment of visual function incases of keratoconus, with and / or without the procedure collagen cross linking

EP2) Principal Applicant

[Mr Preetam Kumar](#)

EP3) Co-Applicant(s) (City)

EP4) External Co-Applicant(s)

EP5) Supervisor(s)

[Prof Chris Hull](#)

[Dr Peter Campbell](#)

EP6) Project start date

01 Dec 2020

EP7) Estimated project end date

01 Feb 2022

EP8) Is City acting as the Sponsor, i.e. responsible for managing this project?

No

EP8.1) Name of the person signing off on behalf of City as the Sponsor.

Ethics

EE1) Please give a brief lay summary of the project (max 500 words).

Title: Assessment of visual function in keratoconus

Background: Keratoconus (KC) is a progressive disease that results in thinning and weakening of the cornea causing it to bulge outwards. This leads to poorer vision due to astigmatism, myopia and corneal scarring when more advanced. The condition is managed at its different stages with spectacles and contact lenses. If the corneal shape continues to deteriorate, it may be appropriate to stiffen the cornea using a procedure called corneal collagen cross-linking (CXL). Research investigating visual function in KC has largely focused on visual acuity and more recently contrast sensitivity and stereoacuity. The Collaborative Longitudinal Evaluation of Keratoconus study is the only study to report longitudinal assessment of several components of KC. All tests that have been reported are threshold measures. However, many daily activities involve supra-threshold visual tasks. Literature has suggested a systematic difference in suprathreshold level performance when compared to threshold level performance for normal individuals. The performance of keratoconus eyes for a suprathreshold task has not been explored in the literature.

The first aim of our study is to produce longitudinal data on the structural and functional measures in keratoconic eyes and thereby establish a structure-function relationship. The second aim is to investigate the structure-function relationship following CXL. The third aim of the study to compare suprathreshold contrast perception in keratoconus against age matched controls.

Study design: Due to the COVID pandemic the study is a hybrid study design collecting cross-sectional data to create pseudo-longitudinal design and a limited (12 month) longitudinal component.

Participants: Study participants will be recruited from the Bausch and Lomb contact lens Centre of the LV Prasad Eye Institute, Hyderabad. Power calculations demonstrate that 70 participants are required for the first two arms of the study: KC managed with spectacles or contact lenses and KC following CXL. Age-matched controls will be recruited from L V Prasad eye institute, India. Inclusion criteria are age over 15 years with a confirmed diagnosis of keratoconus, no other ocular co-morbidity and with no previous history of surgery or laser procedures.

Methods: Subjects with KC are required to visit the clinic for the assessment of ocular structure and visual function. All tests are non-invasive and their safety is well-established. Structural tests include: corneal topography (Allegro Oculyzer®); higher order aberrations (Tracey iTrace® wavefront aberrometer) measurement. Visual function measures include: high contrast visual acuity (COMPLOG® software); monocular and binocular contrast sensitivity (Quick CSF); stereoacuity (Random-dot stereogram). The suprathreshold task uses a psychophysical contrast matching paradigm. These tests will be carried out at baseline and at six-month intervals (± 2 months) for the longitudinal arm of the study. Participants will be asked not to wear their habitual contact lenses for 1 week prior to their appointment in line with clinic protocols.

IRB approval: This project was given IRB approval by the ethics committee of the LV Prasad Eye Institute on 27th July 2020, reference number LEC-BHR-P-07-20-467. An extension for the same study reference number was acquired on 24th August 2021. Contact details: mail: irb@lvpei.org; Tel: 040-68102511.

EE2) Please provide the name and contact details of the external research ethics committee.

Name

L V Prasad Eye Institute ethics committee

Contact details

mail: irb@lvpei.org

Tel: +91-40-68102511

Outcome

Outcome

OL1) Application reference number.

LEC-BHR-P-07-20-467

OL2) Was your application approved?

Yes

OL3) Please upload the outcome letter.

Attached files

Preetam Kumar IRB Approval letter_LVPEI.pdf

Hyderabad Eye Research Foundation
L V Prasad Eye Institute Ethics Committee
Kallam Anji Reddy Campus, Banjara Hills, Hyderabad
ECR/468/Inst./AP/2013/RR-19
NABH Registration No: EC-CT-2019-0126

To

Date: July 22, 2021

Mr Preetam Kumar
Principal Investigator,
L V Prasad Eye Institute,
KAR Campus, L V Prasad Marg,
Banjara Hills, Hyderabad – 500 034,

Subject: Ethics Committee Approval for Extension of the study

Protocol Title: “Assessment of visual function in cases of keratoconus, with and / or without the procedure collagen cross linking”

Ethics Ref No: LEC-BHR-P-07-20-467

Dear Dr Preetam Kumar:

This is with reference to your request regarding an extension of the above ongoing mentioned study. The members reviewed and discussed in detail the progress report submitted by you, after consideration, the committee has approved the study for one more year.

It is hereby confirmed that neither you nor any of the members of the study team participated in the decision making/voting procedures.

We here by confirm that the Institutional Review Board, L.V Prasad Eye Institute is organised and operates as per GCP and Applicable Indian regulations

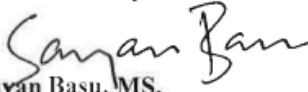
Ethics Committee
L.V. Prasad Eye Institute
Kallam Arji Reddy Campus,
Banjara Hills, Hyderabad-500 034.
Reg.No.ECR/468/Inst./AP/2013/RR-19

Hyderabad Eye Research Foundation
L V Prasad Eye Institute Ethics Committee
Kallam Anji Reddy Campus, Banjara Hills, Hyderabad
ECR/468/Inst./AP/2013/RR-19
NABH Registration No: EC-CT-2019-0126

The following members of the Ethics Committee were present at the meeting held on July 22, 2021 at 3:00pm, via zoom at L V Prasad Eye Institute, KAR Campus, Hyderabad 500 034

Name	Qualification	Designation/Title	Gender	Affiliations as to the Institution Yes/No
Justice T N C Rangarajan	M.A, B.L.	Chairperson and Legal Expert	Male	No
Dr Sayan Basu	MBBS, M.S	Member Secretary	Male	Yes
Mr Vijay Kumar Chejerla	M A.,LLB,FIIL,DPM	Social Scientist	Male	No
Dr Savitri Sharma	MBBS, MD, FAMS	Basic Medical Scientist	Female	Yes
Dr. B.R.Shamanna	MBBS,MD (SPM), DNB(SPM),MSC, London.	Clinician	Male	No
Dr Dilip Kumar Mishra	MBBS, MD	Basic Medical Scientist	Male	Yes
Dr Usha Raman	M.A, PhD	Lay person	Female	Yes
Dr. Subhabrata Chakrabarti	M SC, Ph D	Scientific Member	Male	Yes
Mr. Paul Balasundaram	B. Sc, M Div	Theology & National Coordinator	Male	No
Mrs Amita Desai	MA. M.Ed.	Social Scientist	Female	No

Yours sincerely


Sayan Basu, MS,

Member Secretary

L V Prasad Eye Institute Ethics Committee

L V Prasad Eye Institute, Hyderabad 500 034

Ethics Committee
L.V. Prasad Eye Institute
Kallam Arji Reddy Campus,
Banjara Hills, Hyderabad-500 034.
Reg.No.ECR/468/Inst./AP/2013/RR-19

Appendix 3

A3: Published work from the thesis

1. Kumar, P., Bandela, P.K. and Bharadwaj, S.R., 2020. Do visual performance and optical quality vary across different contact lens correction modalities in keratoconus? *Contact Lens and Anterior Eye*, 43(6), pp.568-576.
2. Kumar, P., Vaddavalli, P.K., Campbell, P., Hull, C.C. and Bharadwaj, S.R., 2023. Suprathreshold contrast perception of resolvable high spatial frequencies remain intact in keratoconus. *Vision Research*, 212, p.108310.
3. Kumar, P., Campbell, P., Vaddavalli, P.K., Hull, C.C. and Bharadwaj, S.R., 2023. Structure-Function Relationship in Keratoconus: Spatial and Depth Vision. *Translational Vision Science & Technology*, 12(12), pp.21-21.

References

- ALIO, J. L. & SHABAYEK, M. H. 2006. Corneal higher order aberrations: a method to grade keratoconus. *J Refract Surg*, 22, 539-45.
- ALIO, J. L., SHABAYEK, M. H. & ARTOLA, A. 2006. Intracorneal ring segments for keratoconus correction: long-term follow-up. *J Cataract Refract Surg*, 32, 978-85.
- AMBRÓSIO JR, R., FARIA-CORREIA, F., RAMOS, I., VALBON, B. F., LOPES, B., JARDIM, D. & LUZ, A. J. C. O. R. 2013. Enhanced screening for ectasia susceptibility among refractive candidates: the role of corneal tomography and biomechanics. 1, 28-38.
- AMBROSIO, R., JR., ALONSO, R. S., LUZ, A. & COCA VELARDE, L. G. 2006. Corneal-thickness spatial profile and corneal-volume distribution: tomographic indices to detect keratoconus. *J Cataract Refract Surg*, 32, 1851-9.
- AMBROSIO, R., JR., CAIADO, A. L., GUERRA, F. P., LOUZADA, R., SINHA, R. A., LUZ, A., DUPPS, W. J. & BELIN, M. W. 2011. Novel pachymetric parameters based on corneal tomography for diagnosing keratoconus. *J Refract Surg*, 27, 753-8.
- AMSLER, M. 1946. [Classic keratocene and crude keratocene; Unitary arguments]. *Ophthalmologica*, 111, 96-101.
- ANDREASSEN, T. T., SIMONSEN, A. H. & OXLUND, H. 1980. Biomechanical properties of keratoconus and normal corneas. *Exp Eye Res*, 31, 435-41.
- ARMSTRONG, B. K., SMITH, S. D., ROMAC COC, I., AGARWAL, P., MUSTAPHA, N. & NAVON, S. 2021. Screening for Keratoconus in a High-Risk Adolescent Population. *Ophthalmic Epidemiol*, 28, 191-197.
- ARTAL, P., CHEN, L., FERNANDEZ, E. J., SINGER, B., MANZANERA, S. & WILLIAMS, D. R. 2004. Neural compensation for the eye's optical aberrations. *J Vis*, 4, 281-7.
- ARTAL, P. & GUIRAO, A. 1998. Contributions of the cornea and the lens to the aberrations of the human eye. *Opt Lett*, 23, 1713-5.
- BAILEY, I. L. & LOVIE, J. E. 1976. New design principles for visual acuity letter charts. *Am J Optom Physiol Opt*, 53, 740-5.
- BAK-NIELSEN, S., RAMLAU-HANSEN, C. H., IVARSEN, A., PLANA-RIPOLL, O. & HJORTDAL, J. 2019. Incidence and prevalence of keratoconus in Denmark - an update. *Acta Ophthalmol*, 97, 752-755.
- BANDELA, P. K., SATGUNAM, P., GARG, P. & BHARADWAJ, S. R. 2016. Corneal Transplantation in Disease Affecting Only One Eye: Does It Make a Difference to Habitual Binocular Viewing? *PLoS One*, 11, e0150118.
- BARAN, I., BRADLEY, J. A., ALIPOUR, F., ROSENTHAL, P., LE, H. G. & JACOBS, D. S. 2012. PROSE treatment of corneal ectasia. *Cont Lens Anterior Eye*, 35, 222-7.
- BEDELL, H. E., GANTZ, L. & JACKSON, D. N. 2012. Perceived suprathreshold depth under conditions that elevate the stereothreshold. *Optom Vis Sci*, 89, 1768-73.
- BELIN, M. W. & DUNCAN, J. K. 2016. Keratoconus: The ABCD Grading System. *Klin Monbl Augenheilkd*, 233, 701-7.
- BELIN, M. W., JANG, H. S. & BORGSTROM, M. 2022. Keratoconus: Diagnosis and Staging. *Cornea*, 41, 1-11.
- BELIN, M. W. & KHACHIKIAN, S. S. 2007. Keratoconus: it is hard to define, but. *Am J Ophthalmol*, 143, 500-3.
- BENNETT, C. R., BEX, P. J., BAUER, C. M. & MERABET, L. B. 2019. The Assessment of Visual Function and Functional Vision. *Semin Pediatr Neurol*, 31, 30-40.
- BERGMANSON, J. P. G., BURNS, A. R. & NAROO, S. A. 2021. Central versus peripheral corneal thickness - A White spot on the corneal (anatomy) map. *Cont Lens Anterior Eye*, 44, 101473.
- BETTS, A. M., MITCHELL, G. L. & ZADNIK, K. 2002. Visual performance and comfort with the Rose K lens for keratoconus. *Optom Vis Sci*, 79, 493-501.

- BRADY, N. & FIELD, D. J. 1995. What's constant in contrast constancy? The effects of scaling on the perceived contrast of bandpass patterns. *Vision Res*, 35, 739-56.
- BRAINARD, D. H. 1997. The Psychophysics Toolbox. *Spat Vis*, 10, 433-6.
- BROWN, B. & LOVIE-KITCHIN, J. E. 1989. High and low contrast acuity and clinical contrast sensitivity tested in a normal population. *Optom Vis Sci*, 66, 467-73.
- BULLIMORE, M. A., BAILEY, I. L. & WACKER, R. T. 1991. Face recognition in age-related maculopathy. *Invest Ophthalmol Vis Sci*, 32, 2020-9.
- BYKHOVSKAYA, Y., LI, X., TAYLOR, K. D., HARITUNIAN, T., ROTTER, J. I. & RABINOWITZ, Y. S. 2016. Linkage Analysis of High-density SNPs Confirms Keratoconus Locus at 5q Chromosomal Region. *Ophthalmic Genet*, 37, 109-10.
- CAIRNS, G. & MCGHEE, C. N. 2005. Orbscan computerized topography: attributes, applications, and limitations. *J Cataract Refract Surg*, 31, 205-20.
- CAMPBELL, C. E. 2003. Matrix method to find a new set of Zernike coefficients from an original set when the aperture radius is changed. *J Opt Soc Am A Opt Image Sci Vis*, 20, 209-17.
- CAMPBELL, F. W. & GREEN, D. G. 1965. Optical and retinal factors affecting visual resolution. *J Physiol*, 181, 576-93.
- CAMPBELL, F. W. & ROBSON, J. G. 1968. Application of Fourier analysis to the visibility of gratings. *J Physiol*, 197, 551-66.
- CAPOROSI, A., MAZZOTTA, C., BAIOCCHI, S. & CAPOROSI, T. 2010. Long-term results of riboflavin ultraviolet a corneal collagen cross-linking for keratoconus in Italy: the Siena eye cross study. *Am J Ophthalmol*, 149, 585-93.
- CARNEY, L. G. 1982. Visual loss in keratoconus. *Arch Ophthalmol*, 100, 1282-5.
- CARNEY, L. G. & LEMBACH, R. G. 1991. Management of keratoconus: comparative visual assessments. *CLAO J*, 17, 52-8.
- CARRACEDO, G., MARTIN-GIL, A., PEIXOTO-DE-MATOS, S. C., ABEJON-GIL, P., MACEDO-DE-ARAUJO, R. & GONZALEZ-MEIJOME, J. M. 2016. Symptoms and Signs in Rigid Gas Permeable Lens Wearers During Adaptation Period. *Eye Contact Lens*, 42, 108-14.
- CHAN, E., CHONG, E. W., LINGHAM, G., STEVENSON, L. J., SANFILIPPO, P. G., HEWITT, A. W., MACKEY, D. A. & YAZAR, S. 2021. Prevalence of Keratoconus Based on Scheimpflug Imaging: The Raine Study. *Ophthalmology*, 128, 515-521.
- CHOI, J. A. & KIM, M. S. 2012. Progression of keratoconus by longitudinal assessment with corneal topography. *Invest Ophthalmol Vis Sci*, 53, 927-35.
- CHUNG, S. T. & LEGGE, G. E. 2016. Comparing the Shape of Contrast Sensitivity Functions for Normal and Low Vision. *Invest Ophthalmol Vis Sci*, 57, 198-207.
- COLIN, J., COCHENER, B., SAVARY, G. & MALET, F. 2000. Correcting keratoconus with intracorneal rings. *J Cataract Refract Surg*, 26, 1117-22.
- COLIN, J., COCHENER, B., SAVARY, G., MALET, F. & HOLMES-HIGGIN, D. 2001. INTACS inserts for treating keratoconus: one-year results. *Ophthalmology*, 108, 1409-14.
- COLIN, J. & MALET, F. J. 2007. Intacs for the correction of keratoconus: two-year follow-up. *J Cataract Refract Surg*, 33, 69-74.
- CORMACK, L. K., STEVENSON, S. B. & LANDERS, D. D. 1997. Interactions of spatial frequency and unequal monocular contrasts in stereopsis. *Perception*, 26, 1121-36.
- D'SOUZA, S., NAIR, A. P., SAHU, G. R., VAIDYA, T., SHETTY, R., KHAMAR, P., MULLICK, R., GUPTA, S., DICKMAN, M. M., NUIJTS, R., MOHAN, R. R., GHOSH, A. & SETHU, S. 2021. Keratoconus patients exhibit a distinct ocular surface immune cell and inflammatory profile. *Sci Rep*, 11, 20891.
- DAVIS, L. J., SCHECHTMAN, K. B., WILSON, B. S., ROSENSTIEL, C. E., RILEY, C. H., LIBASSI, D. P., GUNDEL, R. E., ROSENBERG, L., GORDON, M. O., ZADNIK, K. & COLLABORATIVE LONGITUDINAL EVALUATION OF KERATOCONUS STUDY, G. 2006. Longitudinal changes in visual acuity in keratoconus. *Invest Ophthalmol Vis Sci*, 47, 489-500.

- DE SANCTIS, U., LOIACONO, C., RICHIARDI, L., TURCO, D., MUTANI, B. & GRIGNOLO, F. M. 2008. Sensitivity and specificity of posterior corneal elevation measured by Pentacam in discriminating keratoconus/subclinical keratoconus. *Ophthalmology*, 115, 1534-9.
- DE STEFANO, V. S., FORD, M. R., SEVEN, I. & DUPPS, W. J., JR. 2020. Depth-Dependent Corneal Biomechanical Properties in Normal and Keratoconic Subjects by Optical Coherence Elastography. *Transl Vis Sci Technol*, 9, 4.
- DEVI, P., KUMAR, P., MARELLA, B. L. & BHARADWAJ, S. R. 2022. Impact of Degraded Optics on Monocular and Binocular Vision: Lessons from Recent Advances in Highly-Aberrated Eyes. *Semin Ophthalmol*, 37, 869-886.
- DONALDSON, D. D. 1972. A new instrument for keratography. *Arch Ophthalmol*, 88, 425-8.
- DUNCAN, J. K., BELIN, M. W. & BORGSTROM, M. 2016. Assessing progression of keratoconus: novel tomographic determinants. *Eye Vis (Lond)*, 3, 6.
- EDRINGTON, T. B., SZCZOTKA, L. B., BARR, J. T., ACHTENBERG, J. F., BURGER, D. S., JANOFF, A. M., OLAFSSON, H. E., CHUN, M. W., BOYLE, J. W., GORDON, M. O. & ZADNIK, K. 1999. Rigid contact lens fitting relationships in keratoconus. Collaborative Longitudinal Evaluation of Keratoconus (CLEK) Study Group. *Optom Vis Sci*, 76, 692-9.
- ELDER, M. J. 1994. Leber congenital amaurosis and its association with keratoconus and keratoglobus. *J Pediatr Ophthalmol Strabismus*, 31, 38-40.
- ELSAHN, A. F., RAPUANO, C. J., ANTUNES, V. A., ABDALLA, Y. F. & COHEN, E. J. 2009. Excimer laser phototherapeutic keratectomy for keratoconus nodules. *Cornea*, 28, 144-7.
- ERDINEST, N., WAJNSZTAJN, D., LONDON, N. & SOLOMON, A. 2023. Ocular surface inflammation and ectatic corneal disorders. *Curr Opin Allergy Clin Immunol*.
- ERDURMUS, M., YILDIZ, E. H., ABDALLA, Y. F., HAMMERSMITH, K. M., RAPUANO, C. J. & COHEN, E. J. 2009. Contact lens related quality of life in patients with keratoconus. *Eye Contact Lens*, 35, 123-7.
- FADEL, D. 2017. Modern scleral lenses: Mini versus large. *Cont Lens Anterior Eye*, 40, 200-207.
- FERDI, A. C., NGUYEN, V., GORE, D. M., ALLAN, B. D., ROZEMA, J. J. & WATSON, S. L. 2019. Keratoconus Natural Progression: A Systematic Review and Meta-analysis of 11 529 Eyes. *Ophthalmology*, 126, 935-945.
- FERNANDEZ-VELAZQUEZ, F. J. 2012. Kerasoft IC compared to Rose-K in the management of corneal ectasias. *Cont Lens Anterior Eye*, 35, 175-9.
- GARDINER, S. K., JOHNSON, C. A. & CIOFFI, G. A. 2005. Evaluation of the structure-function relationship in glaucoma. *Invest Ophthalmol Vis Sci*, 46, 3712-7.
- GEORGESON, M. A. & SULLIVAN, G. D. 1975. Contrast constancy: deblurring in human vision by spatial frequency channels. *J Physiol*, 252, 627-56.
- GEORGIU, T., FUNNELL, C. L., CASSELS-BROWN, A. & O'CONNOR, R. 2004. Influence of ethnic origin on the incidence of keratoconus and associated atopic disease in Asians and white patients. *Eye (Lond)*, 18, 379-83.
- GODEFROOIJ, D. A., DE WIT, G. A., UITERWAAL, C. S., IMHOF, S. M. & WISSE, R. P. 2017. Age-specific Incidence and Prevalence of Keratoconus: A Nationwide Registration Study. *Am J Ophthalmol*, 175, 169-172.
- GOMES, J. A., TAN, D., RAPUANO, C. J., BELIN, M. W., AMBROSIO, R., JR., GUELL, J. L., MALECAZE, F., NISHIDA, K., SANGWAN, V. S., GROUP OF PANELISTS FOR THE GLOBAL DELPHI PANEL OF, K. & ECTATIC, D. 2015. Global consensus on keratoconus and ectatic diseases. *Cornea*, 34, 359-69.
- GONZALEZ, V. & MCDONNELL, P. J. 1992. Computer-assisted corneal topography in parents of patients with keratoconus. *Arch Ophthalmol*, 110, 1413-4.
- GRAVES, B. 1925. "Keratoconus". *Br J Ophthalmol*, 9, 45.
- GREENE, P. B. 1945. Keratoconus posticus circumscriptus; report of a case. *Arch Ophthalmol*, 34, 432.
- GREENSTEIN, S. A., FRY, K. L. & HERSH, P. S. 2011. Corneal topography indices after corneal collagen crosslinking for keratoconus and corneal ectasia: one-year results. *J Cataract Refract Surg*, 37, 1282-90.

- GRIFFITHS, M., ZAHNER, K., COLLINS, M. & CARNEY, L. 1998. Masking of irregular corneal topography with contact lenses. *CLAO J*, 24, 76-81.
- GUIRAO, A. & WILLIAMS, D. R. 2003. A method to predict refractive errors from wave aberration data. *Optom Vis Sci*, 80, 36-42.
- GUMUS, K., GIRE, A. & PFLUGFELDER, S. C. 2011. The impact of the Boston ocular surface prosthesis on wavefront higher-order aberrations. *Am J Ophthalmol*, 151, 682-690 e2.
- HASHEMI, H., BEIRANVAND, A., YEKTA, A., MALEKI, A., YAZDANI, N. & KHABAZKHOOB, M. 2016. Pentacam top indices for diagnosing subclinical and definite keratoconus. *J Curr Ophthalmol*, 28, 21-6.
- HASHEMI, H., HEYDARIAN, S., HOOSHMAND, E., SAATCHI, M., YEKTA, A., AGHAMIRSALIM, M., VALADKHAN, M., MORTAZAVI, M., HASHEMI, A. & KHABAZKHOOB, M. 2020. The Prevalence and Risk Factors for Keratoconus: A Systematic Review and Meta-Analysis. *Cornea*, 39, 263-270.
- HASHEMI, H., KHABAZKHOOB, M. & FOTOUHI, A. 2013. Topographic Keratoconus is not Rare in an Iranian population: the Tehran Eye Study. *Ophthalmic Epidemiol*, 20, 385-91.
- HASHEMI, H., SHAYGAN, N., ASGARI, S., REZVAN, F. & ASGARI, S. 2014. ClearKone-Synergeyes or rigid gas-permeable contact lens in keratoconic patients: a clinical decision. *Eye Contact Lens*, 40, 95-8.
- HASTINGS, G. D., MARSACK, J. D., THIBOS, L. N. & APPLGATE, R. A. 2020. Combining optical and neural components in physiological visual image quality metrics as functions of luminance and age. *J Vis*, 20, 20.
- HAUN, A. M. & PELI, E. 2013. Perceived contrast in complex images. *J Vis*, 13, 3.
- HERSH, P. S., GREENSTEIN, S. A. & FRY, K. L. 2011. Corneal collagen crosslinking for keratoconus and corneal ectasia: One-year results. *J Cataract Refract Surg*, 37, 149-60.
- HO, A. & BILTON, S. M. 1986. Low contrast charts effectively differentiate between types of blur. *Am J Optom Physiol Opt*, 63, 202-8.
- HOLOPIGIAN, K. 1989. Clinical suppression and binocular rivalry suppression: the effects of stimulus strength on the depth of suppression. *Vision Res*, 29, 1325-33.
- HOWARD, H. J. 1919. A Test for the Judgment of Distance. *Trans Am Ophthalmol Soc*, 17, 195-235.
- HWANG, S., LIM, D. H. & CHUNG, T. Y. 2018. Prevalence and Incidence of Keratoconus in South Korea: A Nationwide Population-based Study. *Am J Ophthalmol*, 192, 56-64.
- IHALAINEN, A. 1986. Clinical and epidemiological features of keratoconus genetic and external factors in the pathogenesis of the disease. *Acta Ophthalmol Suppl (1985)*, 178, 1-64.
- JAIMES, M., XACUR-GARCIA, F., ALVAREZ-MELLONI, D., GRAUE-HERNANDEZ, E. O., RAMIREZ-LUQUIN, T. & NAVAS, A. 2011. Refractive lens exchange with toric intraocular lenses in keratoconus. *J Refract Surg*, 27, 658-64.
- JAIN, A. K. & SUKHIJA, J. 2007. Rose-K contact lens for keratoconus. *Indian J Ophthalmol*, 55, 121-5.
- JARVIS, J., TRIANTAPHILLIDOU, S. & GUPTA, G. 2022. Contrast discrimination in images of natural scenes. *J Opt Soc Am A Opt Image Sci Vis*, 39, B50-B64.
- JINABHAI, A., O'DONNELL, C. & RADHAKRISHNAN, H. 2012a. Changes in refraction, ocular aberrations, and corneal structure after suspending rigid gas-permeable contact lens wear in keratoconus. *Cornea*, 31, 500-8.
- JINABHAI, A., O'DONNELL, C., TROMANS, C. & RADHAKRISHNAN, H. 2014. Optical quality and visual performance with customised soft contact lenses for keratoconus. *Ophthalmic Physiol Opt*, 34, 528-39.
- JINABHAI, A., RADHAKRISHNAN, H., TROMANS, C. & O'DONNELL, C. 2012b. Visual performance and optical quality with soft lenses in keratoconus patients. *Ophthalmic Physiol Opt*, 32, 100-16.
- JONAS, J. B., NANGIA, V., MATIN, A., KULKARNI, M. & BHOJWANI, K. 2009. Prevalence and associations of keratoconus in rural maharashtra in central India: the central India eye and medical study. *Am J Ophthalmol*, 148, 760-5.

- KAMIYA, K., ISHII, R., SHIMIZU, K. & IGARASHI, A. 2014. Evaluation of corneal elevation, pachymetry and keratometry in keratoconic eyes with respect to the stage of Amsler-Krumeich classification. *Br J Ophthalmol*, 98, 459-63.
- KAMIYA, K., KONO, Y., TAKAHASHI, M. & SHOJI, N. 2018. Comparison of Simulated Keratometry and Total Refractive Power for Keratoconus According to the Stage of Amsler-Krumeich Classification. *Sci Rep*, 8, 12436.
- KAMIYA, K., SHIMIZU, K., ANDO, W., ASATO, Y. & FUJISAWA, T. 2008. Phakic toric Implantable Collamer Lens implantation for the correction of high myopic astigmatism in eyes with keratoconus. *J Refract Surg*, 24, 840-2.
- KANDEL, H., NGUYEN, V., PIERMAROCCHI, S., CEKIC, L., TEO, K., ARNALICH-MONTIEL, F., MIOTTO, S., DAIEN, V., GILLIES, M. C. & WATSON, S. L. 2022. Quality of life impact of eye diseases: a Save Sight Registries study. *Clin Exp Ophthalmol*, 50, 386-397.
- KANDEL, H., PESUDOVS, K. & WATSON, S. L. 2020. Measurement of Quality of Life in Keratoconus. *Cornea*, 39, 386-393.
- KANELLOPOULOS, A. J. & ASIMELLIS, G. 2013. Revisiting keratoconus diagnosis and progression classification based on evaluation of corneal asymmetry indices, derived from Scheimpflug imaging in keratoconic and suspect cases. *Clin Ophthalmol*, 7, 1539-48.
- KANSKI, J. J. & BOWLING, B. 2015. *Kanski's clinical ophthalmology e-book: a systematic approach*, Elsevier Health Sciences.
- KAWANA, K., MIYATA, K., TOKUNAGA, T., KIUCHI, T., HIRAOKA, T. & OSHIKA, T. 2005. Central corneal thickness measurements using Orbscan II scanning slit topography, noncontact specular microscopy, and ultrasonic pachymetry in eyes with keratoconus. *Cornea*, 24, 967-71.
- KHADKA, J., SCHONEVELD, P. G. & PESUDOVS, K. 2017. Development of a Keratoconus-Specific Questionnaire Using Rasch Analysis. *Optom Vis Sci*, 94, 395-403.
- KOC, M., TEKIN, K., KIZILTOPRAK, H., INANC, M., KOSEKAHYA, P., OZULKEN, K. & DURUKAN, I. 2020. Topometric and Tomographic Evaluation of Subclinical Keratoconus. *Ophthalmic Epidemiol*, 27, 289-297.
- KOMPANIEZ, E., SAWIDES, L., MARCOS, S. & WEBSTER, M. A. 2013. Adaptation to interocular differences in blur. *J Vis*, 13, 19.
- KRACHMER, J. H., FEDER, R. S. & BELIN, M. W. 1984. Keratoconus and related noninflammatory corneal thinning disorders. *Surv Ophthalmol*, 28, 293-322.
- KRUMEICH, J. H., DANIEL, J. & KNULLE, A. 1998. Live-epikeratophakia for keratoconus. *J Cataract Refract Surg*, 24, 456-63.
- KULIKOWSKI, J. J. 1976. Effective contrast constancy and linearity of contrast sensation. *Vision Res*, 16, 1419-31.
- KUMAR, P., ALI, M. H., REDDY, J. C. & VADDAVALLI, P. K. 2020. Short-term changes in topometric indices after discontinuation of rigid gas permeable lens wear in keratoconic eyes. *Indian J Ophthalmol*, 68, 2911-2917.
- KUMAR, P., MOHAMED, A., BHOMBAL, F., DUMPATI, S. & VADDAVALLI, P. K. 2019. Prosthetic replacement of the ocular surface ecosystem for corneal irregularity: Visual improvement and optical device characteristics. *Cont Lens Anterior Eye*, 42, 526-532.
- LAIDLAW, D. A., TAILOR, V., SHAH, N., ATAMIAN, S. & HARCOURT, C. 2008. Validation of a computerised logMAR visual acuity measurement system (COMPlog): comparison with ETDRS and the electronic ETDRS testing algorithm in adults and amblyopic children. *Br J Ophthalmol*, 92, 241-4.
- LAKENS, D. 2013. Calculating and reporting effect sizes to facilitate cumulative science: a practical primer for t-tests and ANOVAs. *Front Psychol*, 4, 863.
- LAWLESS, M., COSTER, D. J., PHILLIPS, A. J. & LOANE, M. 1989. Keratoconus: diagnosis and management. *Aust N Z J Ophthalmol*, 17, 33-60.
- LECCISOTTI, A. & FIELDS, S. V. 2003. Angle-supported phakic intraocular lenses in eyes with keratoconus and myopia. *J Cataract Refract Surg*, 29, 1530-6.

- LEE, J. C., CHIU, G. B., BACH, D., BABABEYGY, S. R., IRVINE, J. & HEUR, M. 2013. Functional and visual improvement with prosthetic replacement of the ocular surface ecosystem scleral lenses for irregular corneas. *Cornea*, 32, 1540-3.
- LESME, L. A., LU, Z. L., BAEK, J. & ALBRIGHT, T. D. 2010. Bayesian adaptive estimation of the contrast sensitivity function: the quick CSF method. *J Vis*, 10, 17 1-21.
- LEVINE, J. R. 1965. The true inventors of the keratoscope and photo-keratoscope. *Br J Hist Sci*, 2, 324-42.
- LIM, L. & LIM, E. W. L. 2020. Current perspectives in the management of keratoconus with contact lenses. *Eye (Lond)*, 34, 2175-2196.
- LIU, M., UDHE-STONE, C. & GOUDAR, C. T. 2011. Progress curve analysis of qRT-PCR reactions using the logistic growth equation. *Biotechnol Prog*, 27, 1407-14.
- MAEDA, N., KLYCE, S. D., SMOLEK, M. K. & THOMPSON, H. W. 1994. Automated keratoconus screening with corneal topography analysis. *Invest Ophthalmol Vis Sci*, 35, 2749-57.
- MAHMOUD, A. M., ROBERTS, C. J., LEMBACH, R. G., TWA, M. D., HERDERICK, E. E., MCMAHON, T. T. & GROUP, C. S. 2008. CLMI: the cone location and magnitude index. *Cornea*, 27, 480-7.
- MANDATHARA, P. S., STAPLETON, F. J. & WILLCOX, M. D. P. 2017. Outcome of Keratoconus Management: Review of the Past 20 Years' Contemporary Treatment Modalities. *Eye Contact Lens*, 43, 141-154.
- MANDATHARA SUDHARMAN, P., RATHI, V. & DUMAPATI, S. 2010. Rose K lenses for keratoconus--an Indian experience. *Eye Contact Lens*, 36, 220-2.
- MARCOS, S. 2003. Image quality of the human eye. *Int Ophthalmol Clin*, 43, 43-62.
- MARELLA, B. L., CONWAY, M. L., SUTTLE, C. & BHARADWAJ, S. R. 2021. Contrast Rivalry Paradigm Reveals Suppression of Monocular Input in Keratoconus. *Invest Ophthalmol Vis Sci*, 62, 15.
- MARSACK, J. D., PARKER, K. E., PESUDOV, K., DONNELLY, W. J., 3RD & APPLGATE, R. A. 2007. Uncorrected wavefront error and visual performance during RGP wear in keratoconus. *Optom Vis Sci*, 84, 463-70.
- MARSACK, J. D., RAVIKUMAR, A., NGUYEN, C., TICAK, A., KOENIG, D. E., ELSWICK, J. D. & APPLGATE, R. A. 2014. Wavefront-guided scleral lens correction in keratoconus. *Optom Vis Sci*, 91, 1221-30.
- MARSACK, J. D., THIBOS, L. N. & APPLGATE, R. A. 2004. Metrics of optical quality derived from wave aberrations predict visual performance. *J Vis*, 4, 322-8.
- MARTA, A., MARQUES, J. H., ALMEIDA, D., JOSE, D. & BARBOSA, I. 2021. Keratoconus and Visual Performance with Different Contact Lenses. *Clin Ophthalmol*, 15, 4697-4705.
- MARTINEZ-ABAD, A. & PINERO, D. P. 2017. New perspectives on the detection and progression of keratoconus. *J Cataract Refract Surg*, 43, 1213-1227.
- MAS TUR, V., MACGREGOR, C., JAYASWAL, R., O'BRART, D. & MAYCOCK, N. 2017. A review of keratoconus: Diagnosis, pathophysiology, and genetics. *Surv Ophthalmol*, 62, 770-783.
- MATHAN, J. J., GOKUL, A., SIMKIN, S. K., MEYER, J. J., PATEL, D. V. & MCGHEE, C. N. J. 2020. Topographic screening reveals keratoconus to be extremely common in Down syndrome. *Clin Exp Ophthalmol*, 48, 1160-1167.
- MAZZOTTA, C., CAPOROSI, T., DENARO, R., BOVONE, C., SPARANO, C., PARADISO, A., BAIOCCHI, S. & CAPOROSI, A. 2012. Morphological and functional correlations in riboflavin UV A corneal collagen cross-linking for keratoconus. *Acta Ophthalmol*, 90, 259-65.
- MCMAHON, T. T., SZCZOTKA-FLYNN, L., BARR, J. T., ANDERSON, R. J., SLAUGHTER, M. E., LASS, J. H., IYENGAR, S. K. & GROUP, C. S. 2006. A new method for grading the severity of keratoconus: the Keratoconus Severity Score (KSS). *Cornea*, 25, 794-800.
- MEDEIROS, F. A., ZANGWILL, L. M., BOWD, C., MANSOURI, K. & WEINREB, R. N. 2012. The structure and function relationship in glaucoma: implications for detection of progression and measurement of rates of change. *Invest Ophthalmol Vis Sci*, 53, 6939-46.

- METLAPALLY, S., BHARADWAJ, S. R., ROORDA, A., NILAGIRI, V. K., YU, T. T. & SCHOR, C. M. 2019. Binocular cross-correlation analyses of the effects of high-order aberrations on the stereoacuity of eyes with keratoconus. *J Vis*, 19, 12.
- MEYER, J. J., GOKUL, A., VELLARA, H. R., PRIME, Z. & MCGHEE, C. N. 2017. Repeatability and Agreement of Orbscan II, Pentacam HR, and Galilei Tomography Systems in Corneas With Keratoconus. *Am J Ophthalmol*, 175, 122-128.
- MON-WILLIAMS, M., TRESILIAN, J. R., STRANG, N. C., KOCHHAR, P. & WANN, J. P. 1998. Improving vision: neural compensation for optical defocus. *Proc Biol Sci*, 265, 71-7.
- MONTALT, J. C., PORCAR, E., ESPANA-GREGORI, E. & PERIS-MARTINEZ, C. 2018. Visual quality with corneo-scleral contact lenses for keratoconus management. *Cont Lens Anterior Eye*, 41, 351-356.
- MOSHIRFAR, M., GREGOIRE, F. J., MIRZAIAN, G., WHITEHEAD, G. F. & KANG, P. C. 2006. Use of Verisyse iris-supported phakic intraocular lens for myopia in keratoconic patients. *J Cataract Refract Surg*, 32, 1227-32.
- MUFTUOGLU, O., AYAR, O., HURMERIC, V., ORUCOGLU, F. & KILIC, I. 2015. Comparison of multimetric D index with keratometric, pachymetric, and posterior elevation parameters in diagnosing subclinical keratoconus in fellow eyes of asymmetric keratoconus patients. *J Cataract Refract Surg*, 41, 557-65.
- NAM, S. M., IM, C. Y., LEE, H. K., KIM, E. K., KIM, T. I. & SEO, K. Y. 2010. Accuracy of RTVue optical coherence tomography, Pentacam, and ultrasonic pachymetry for the measurement of central corneal thickness. *Ophthalmology*, 117, 2096-103.
- NAROO, S. A., GHATAORE, P., CARDALL, M. & ILLAHI, W. 2022. Contact lens prescribing trends in the UK hospital eye service. *Cont Lens Anterior Eye*, 45, 101594.
- NAU, A. C. 2008. A comparison of synergeyes versus traditional rigid gas permeable lens designs for patients with irregular corneas. *Eye Contact Lens*, 34, 198-200.
- NEGISHI, K., KUMANOMIDO, T., UTSUMI, Y. & TSUBOTA, K. 2007. Effect of higher-order aberrations on visual function in keratoconic eyes with a rigid gas permeable contact lens. *Am J Ophthalmol*, 144, 924-929.
- NG, C. J., SABESAN, R., BARBOT, A., BANKS, M. S. & YOON, G. 2022. Suprathreshold Contrast Perception Is Altered by Long-term Adaptation to Habitual Optical Blur. *Invest Ophthalmol Vis Sci*, 63, 6.
- NG, J. S. & WONG, A. 2022. Line-by-line visual acuity scoring equivalence with letter-by-letter visual acuity scoring. *Clin Exp Optom*, 105, 414-419.
- NILAGIRI, V. K., METLAPALLY, S., KALAISELVAN, P., SCHOR, C. M. & BHARADWAJ, S. R. 2018. LogMAR and Stereoacuity in Keratoconus Corrected with Spectacles and Rigid Gas-permeable Contact Lenses. *Optom Vis Sci*, 95, 391-398.
- NILAGIRI, V. K., METLAPALLY, S., SCHOR, C. M. & BHARADWAJ, S. R. 2020. A computational analysis of retinal image quality in eyes with keratoconus. *Sci Rep*, 10, 1321.
- NOTTINGHAM, J. 1854. Practical observations on conical cornea, and on the short sight, and other defects of vision connected with it.
- O'DONNELL, C. & MALDONADO-CODINA, C. 2005. Agreement and repeatability of central thickness measurement in normal corneas using ultrasound pachymetry and the OCULUS Pentacam. *Cornea*, 24, 920-4.
- OCHAB, M. & PUSZYNSKI, K. 2020. Piece-wise linear models of biological systems-Application, analysis, and comparison with nonlinear models using the example of the p53 regulatory module. *PLoS One*, 15, e0243823.
- ORTIZ-TOQUERO, S., FERNANDEZ, I. & MARTIN, R. 2020. Classification of Keratoconus Based on Anterior Corneal High-order Aberrations: A Cross-validation Study. *Optom Vis Sci*, 97, 169-177.

- PANTHIER, C., MORAN, S. & BOURGES, J. L. 2020. Evaluation of vision-related quality of life in keratoconus patients, and associated impact of keratoconus severity indicators. *Graefes Arch Clin Exp Ophthalmol*, 258, 1459-1468.
- PARKOSADZE, K., KALMAKHELIDZE, T., TOLMACHEVA, M., CHICHUA, G., KEZELI, A., WEBSTER, M. A. & WERNER, J. S. 2013. Persistent biases in subjective image focus following cataract surgery. *Vision Res*, 89, 10-7.
- PATEL, S. S., BEDELL, H. E., TSANG, D. K. & UKWADE, M. T. 2009. Relationship between threshold and suprathreshold perception of position and stereoscopic depth. *J Opt Soc Am A Opt Image Sci Vis*, 26, 847-61.
- PEARSON, A. R., SONEJI, B., SARVANANTHAN, N. & SANDFORD-SMITH, J. H. 2000. Does ethnic origin influence the incidence or severity of keratoconus? *Eye (Lond)*, 14 (Pt 4), 625-8.
- PELLI, D. G. 1997. The VideoToolbox software for visual psychophysics: transforming numbers into movies. *Spat Vis*, 10, 437-42.
- PERIN, J., PREISSER, J. S., PHILLIPS, C. & QAQISH, B. 2014. Regression analysis of correlated ordinal data using orthogonalized residuals. *Biometrics*, 70, 902-9.
- PINERO, D. P., ALIO, J. L., ALESON, A., ESCAF VERGARA, M. & MIRANDA, M. 2010. Corneal volume, pachymetry, and correlation of anterior and posterior corneal shape in subclinical and different stages of clinical keratoconus. *J Cataract Refract Surg*, 36, 814-25.
- PINERO, D. P., NIETO, J. C. & LOPEZ-MIGUEL, A. 2012. Characterization of corneal structure in keratoconus. *J Cataract Refract Surg*, 38, 2167-83.
- QUISLING, S., SJOBERG, S., ZIMMERMAN, B., GOINS, K. & SUTPHIN, J. 2006. Comparison of Pentacam and Orbscan II on posterior curvature topography measurements in keratoconus eyes. *Ophthalmology*, 113, 1629-32.
- RABINOWITZ, Y. S. 1995. Videokeratographic indices to aid in screening for keratoconus. *J Refract Surg*, 11, 371-9.
- RABINOWITZ, Y. S. & RASHEED, K. 1999. KISA% index: a quantitative videokeratography algorithm embodying minimal topographic criteria for diagnosing keratoconus. *J Cataract Refract Surg*, 25, 1327-35.
- RANDLEMAN, J. B., WOODWARD, M., LYNN, M. J. & STULTING, R. D. 2008. Risk assessment for ectasia after corneal refractive surgery. *Ophthalmology*, 115, 37-50.
- RAO, S. N., RAVIV, T., MAJMUDAR, P. A. & EPSTEIN, R. J. 2002. Role of Orbscan II in screening keratoconus suspects before refractive corneal surgery. *Ophthalmology*, 109, 1642-6.
- RAVIKUMAR, A., MARSACK, J. D., BEDELL, H. E., SHI, Y. & APPLGATE, R. A. 2013. Change in visual acuity is well correlated with change in image-quality metrics for both normal and keratoconic wavefront errors. *J Vis*, 13, 28.
- RAZA, A. S. & HOOD, D. C. 2015. Evaluation of the Structure-Function Relationship in Glaucoma Using a Novel Method for Estimating the Number of Retinal Ganglion Cells in the Human Retina. *Invest Ophthalmol Vis Sci*, 56, 5548-56.
- REGAN, D. & NEIMA, D. 1983. Low-contrast letter charts as a test of visual function. *Ophthalmology*, 90, 1192-200.
- REINSTEIN, D. Z., ARCHER, T. J. & GOBBE, M. 2009. Corneal epithelial thickness profile in the diagnosis of keratoconus. *J Refract Surg*, 25, 604-10.
- RIDLEY, F. 1956. Contact lenses in treatment of keratoconus. *Br J Ophthalmol*, 40, 295-304.
- RIZZUTI, A. B. 1970. Diagnostic illumination test for keratoconus. *Am J Ophthalmol*, 70, 141-3.
- ROMANO, V., VINCIGUERRA, R., ARBABI, E. M., HICKS, N., ROSETTA, P., VINCIGUERRA, P. & KAYE, S. B. 2018. Progression of Keratoconus in Patients While Awaiting Corneal Cross-linking: A Prospective Clinical Study. *J Refract Surg*, 34, 177-180.
- ROSEN, R., LUNDSTROM, L., VENKATARAMAN, A. P., WINTER, S. & UNSBO, P. 2014. Quick contrast sensitivity measurements in the periphery. *J Vis*, 14, 3.
- ROWSEY, J. J., REYNOLDS, A. E. & BROWN, R. 1981. Corneal topography. Corneoscope. *Arch Ophthalmol*, 99, 1093-1100.

- SAAD, A., DEBELLEMANIERE, G., ZEBOULON, P., RIZK, M., ROUGER, H., MAZHARIAN, A., GRISE-DULAC, A., PANTHIER, C. & GATINEL, D. 2023. Discrimination between keratoconus, forme fruste keratoconus, and normal eyes using a novel OCT-based tomographer. *J Cataract Refract Surg*, 49, 1092-1097.
- SAAD, A. & GATINEL, D. 2010. Topographic and tomographic properties of forme fruste keratoconus corneas. *Invest Ophthalmol Vis Sci*, 51, 5546-55.
- SABESAN, R., BARBOT, A. & YOON, G. 2017. Enhanced neural function in highly aberrated eyes following perceptual learning with adaptive optics. *Vision Res*, 132, 78-84.
- SABESAN, R., JOHNS, L., TOMASHEVSKAYA, O., JACOBS, D. S., ROSENTHAL, P. & YOON, G. 2013. Wavefront-guided scleral lens prosthetic device for keratoconus. *Optom Vis Sci*, 90, 314-23.
- SABESAN, R. & YOON, G. 2009. Visual performance after correcting higher order aberrations in keratoconic eyes. *J Vis*, 9, 6 1-10.
- SABESAN, R. & YOON, G. 2010. Neural compensation for long-term asymmetric optical blur to improve visual performance in keratoconic eyes. *Invest Ophthalmol Vis Sci*, 51, 3835-9.
- SANTODOMINGO-RUBIDO, J., CARRACEDO, G., SUZAKI, A., VILLA-COLLAR, C., VINCENT, S. J. & WOLFFSOHN, J. S. 2022. Keratoconus: An updated review. *Cont Lens Anterior Eye*, 45, 101559.
- SAWIDES, L., DE GRACIA, P., DORRONSORO, C., WEBSTER, M. A. & MARCOS, S. 2011. Vision is adapted to the natural level of blur present in the retinal image. *PLoS One*, 6, e27031.
- SCHMIDT, P. P. 1994. Sensitivity of random dot stereoacuity and Snellen acuity to optical blur. *Optom Vis Sci*, 71, 466-71.
- SCHONEVELD, P., PESUDOVS, K. & COSTER, D. J. 2009. Predicting visual performance from optical quality metrics in keratoconus. *Clin Exp Optom*, 92, 289-96.
- SCHOR, C. M. & WOOD, I. 1983. Disparity range for local stereopsis as a function of luminance spatial frequency. *Vision Res*, 23, 1649-54.
- SCHORNACK, M. M. 2015. Scleral lenses: a literature review. *Eye Contact Lens*, 41, 3-11.
- SCHORNACK, M. M. & PATEL, S. V. 2010. Scleral lenses in the management of keratoconus. *Eye Contact Lens*, 36, 39-44.
- SEVERINSKY, B., WAJNSZTAJN, D. & FRUCHT-PERY, J. 2013. Silicone hydrogel mini-scleral contact lenses in early stage after corneal collagen cross-linking for keratoconus: a retrospective case series. *Clin Exp Optom*, 96, 542-6.
- SHAJARI, M., STEINWENDER, G., HERRMANN, K., KUBIAK, K. B., PAVLOVIC, I., PLAWETZKI, E., SCHMACK, I. & KOHNEN, T. 2019. Evaluation of keratoconus progression. *Br J Ophthalmol*, 103, 551-557.
- SHEHADEH, M. M., DIAKONIS, V. F., JALIL, S. A., YOUNIS, R., QADOUMI, J. & AL-LABADI, L. 2015. Prevalence of Keratoconus Among a Palestinian Tertiary Student Population. *Open Ophthalmol J*, 9, 172-6.
- SHERAFAT, H., WHITE, J. E., PULLUM, K. W., ADAMS, G. G. & SLOPER, J. J. 2001. Anomalies of binocular function in patients with longstanding asymmetric keratoconus. *Br J Ophthalmol*, 85, 1057-60.
- SHETTY, R., ARORA, V., JAYADEV, C., NUIJTS, R. M., KUMAR, M., PUTTAIAH, N. K. & KUMMELIL, M. K. 2014. Repeatability and agreement of three Scheimpflug-based imaging systems for measuring anterior segment parameters in keratoconus. *Invest Ophthalmol Vis Sci*, 55, 5263-8.
- SHETTY, R., RAO, H., KHAMAR, P., SAINANI, K., VUNNAVA, K., JAYADEV, C. & KAWERI, L. 2017. Keratoconus Screening Indices and Their Diagnostic Ability to Distinguish Normal From Ectatic Corneas. *Am J Ophthalmol*, 181, 140-148.
- SHNEOR, E., FRUCHT-PERY, J., GRANIT, E. & GORDON-SHAAG, A. 2020. The prevalence of corneal abnormalities in first-degree relatives of patients with keratoconus: a prospective case-control study. *Ophthalmic Physiol Opt*, 40, 442-451.

- SHNEOR, E., PINERO, D. P. & DORON, R. 2021. Contrast sensitivity and higher-order aberrations in Keratoconus subjects. *Sci Rep*, 11, 12971.
- SHOONER, C. & MULLEN, K. T. 2022. Linking perceived to physical contrast: Comparing results from discrimination and difference-scaling experiments. *J Vis*, 22, 13.
- SHORTER, E., HARTHAN, J., NAU, C. B., NAU, A., BARR, J. T., HODGE, D. O. & SCHORNACK, M. M. 2018. Scleral Lenses in the Management of Corneal Irregularity and Ocular Surface Disease. *Eye Contact Lens*, 44, 372-378.
- SMIDDY, W. E., HAMBURG, T. R., KRACHER, G. P. & STARK, W. J. 1988. Keratoconus. Contact lens or keratoplasty? *Ophthalmology*, 95, 487-92.
- SMITH, W. S. 2015. Contrast constancy revisited: the perceived contrast of sinusoidal gratings above threshold. *Q J Exp Psychol (Hove)*, 68, 363-80.
- SMOLEK, M. K. & KLYCE, S. D. 1997. Current keratoconus detection methods compared with a neural network approach. *Invest Ophthalmol Vis Sci*, 38, 2290-9.
- SPOERL, E. & SEILER, T. 1999. Techniques for stiffening the cornea. *J Refract Surg*, 15, 711-3.
- SPOERL, E., WOLLENSAK, G., DITTERT, D. D. & SEILER, T. 2004. Thermomechanical behavior of collagen-cross-linked porcine cornea. *Ophthalmologica*, 218, 136-40.
- SWANN, P. G. & WALDRON, H. E. 1986. Keratoconus: the clinical spectrum. *J Am Optom Assoc*, 57, 204-9.
- TANABE, U., FUJIKI, K., OGAWA, A., UEDA, S. & KANAI, A. 1985. [Prevalence of keratoconus patients in Japan]. *Nippon Ganka Gakkai Zasshi*, 89, 407-11.
- TEMSTET, C., SANDALI, O., BOUHERAOUA, N., HAMICHE, T., GALAN, A., EL SANHARAWI, M., BASLI, E., LAROCHE, L. & BORDERIE, V. 2015. Corneal epithelial thickness mapping using Fourier-domain optical coherence tomography for detection of forme fruste keratoconus. *J Cataract Refract Surg*, 41, 812-20.
- THIBOS, L. N., HONG, X., BRADLEY, A. & APPLGATE, R. A. 2004. Accuracy and precision of objective refraction from wavefront aberrations. *J Vis*, 4, 329-51.
- THIBOS, L. N., WHEELER, W. & HORNER, D. 1997. Power vectors: an application of Fourier analysis to the description and statistical analysis of refractive error. *Optom Vis Sci*, 74, 367-75.
- TO, M. P., GILCHRIST, I. D., TROSCIANKO, T. & TOLHURST, D. J. 2011. Discrimination of natural scenes in central and peripheral vision. *Vision Res*, 51, 1686-98.
- TOMIDOKORO, A., OSHIKA, T., AMANO, S., HIGAKI, S., MAEDA, N. & MIYATA, K. 2000. Changes in anterior and posterior corneal curvatures in keratoconus. *Ophthalmology*, 107, 1328-32.
- TONG, F., MENG, M. & BLAKE, R. 2006. Neural bases of binocular rivalry. *Trends Cogn Sci*, 10, 502-11.
- TOPRAK, I., VEGA, A., ALIO DEL BARRIO, J. L., ESPLA, E., CAVAS, F. & ALIO, J. L. 2021. Diagnostic Value of Corneal Epithelial and Stromal Thickness Distribution Profiles in Forme Fruste Keratoconus and Subclinical Keratoconus. *Cornea*, 40, 61-72.
- TORRES NETTO, E. A., AL-OTAIBI, W. M., HAFEZI, N. L., KLING, S., AL-FARHAN, H. M., RANDLEMAN, J. B. & HAFEZI, F. 2018. Prevalence of keratoconus in paediatric patients in Riyadh, Saudi Arabia. *Br J Ophthalmol*, 102, 1436-1441.
- TOWNSLEY, M. J. C. 1967. New equipment and methods for determining the contour of the human cornea. 11, 72-81.
- TUFT, S. J., MOODALEY, L. C., GREGORY, W. M., DAVISON, C. R. & BUCKLEY, R. J. 1994. Prognostic factors for the progression of keratoconus. *Ophthalmology*, 101, 439-47.
- UCAKHAN, O. O., CETINKOR, V., OZKAN, M. & KANPOLAT, A. 2011. Evaluation of Scheimpflug imaging parameters in subclinical keratoconus, keratoconus, and normal eyes. *J Cataract Refract Surg*, 37, 1116-24.
- VAZIRANI, J. & BASU, S. 2013. Keratoconus: current perspectives. *Clin Ophthalmol*, 7, 2019-30.
- VELLARA, H. R. & PATEL, D. V. 2015. Biomechanical properties of the keratoconic cornea: a review. *Clin Exp Optom*, 98, 31-8.

- VINCENT, S. J., ALONSO-CANEIRO, D. & COLLINS, M. J. 2018. The temporal dynamics of miniscleral contact lenses: Central corneal clearance and centration. *Cont Lens Anterior Eye*, 41, 162-168.
- VINCIGUERRA, P., ALBE, E., TRAZZA, S., ROSETTA, P., VINCIGUERRA, R., SEILER, T. & EPSTEIN, D. 2009. Refractive, topographic, tomographic, and aberrometric analysis of keratoconic eyes undergoing corneal cross-linking. *Ophthalmology*, 116, 369-78.
- VISSER, N., BERENDSCHOT, T. T., VERBAKEL, F., TAN, A. N., DE BRABANDER, J. & NUIJTS, R. M. 2011. Evaluation of the comparability and repeatability of four wavefront aberrometers. *Invest Ophthalmol Vis Sci*, 52, 1302-11.
- WAGNER, H., BARR, J. T. & ZADNIK, K. 2007. Collaborative Longitudinal Evaluation of Keratoconus (CLEK) Study: methods and findings to date. *Cont Lens Anterior Eye*, 30, 223-32.
- WANDELL, B. A. 1995. *Foundations of vision*, sinauer Associates.
- WEBSTER, M. A., GEORGESON, M. A. & WEBSTER, S. M. 2002. Neural adjustments to image blur. *Nat Neurosci*, 5, 839-40.
- WEED, K. H., MACEWEN, C. J. & MCGHEE, C. N. 2007. The Dundee University Scottish Keratoconus Study II: a prospective study of optical and surgical correction. *Ophthalmic Physiol Opt*, 27, 561-7.
- WEI, R. H., KHOR, W. B., LIM, L. & TAN, D. T. 2011. Contact lens characteristics and contrast sensitivity of patients with keratoconus. *Eye Contact Lens*, 37, 307-11.
- WESLEY, N. J. C. 1969. Practical application and new concepts with the photo-electronic keratoscope. 13, 32.
- WESTHEIMER, G. & MCKEE, S. P. J. J. 1980. Stereoscopic acuity with defocused and spatially filtered retinal images. 70, 772-778.
- WILSON, S. E. & KLYCE, S. D. 1991. Advances in the analysis of corneal topography. *Surv Ophthalmol*, 35, 269-77.
- WILSON, S. E., LIN, D. T. & KLYCE, S. D. 1991. Corneal topography of keratoconus. *Cornea*, 10, 2-8.
- WOLLENSAK, G. 2010. Histological changes in human cornea after cross-linking with riboflavin and ultraviolet A. *Acta Ophthalmol*, 88, e17-8.
- WOLLENSAK, G., SPOERL, E. & SEILER, T. 2003. Riboflavin/ultraviolet-a-induced collagen crosslinking for the treatment of keratoconus. *Am J Ophthalmol*, 135, 620-7.
- XIAN, Y., SUN, L., YE, Y., ZHANG, X., ZHAO, W., SHEN, Y., LU, Z. L., ZHOU, X. & ZHAO, J. 2023. The Characteristics of Quick Contrast Sensitivity Function in Keratoconus and Its Correlation with Corneal Topography. *Ophthalmol Ther*, 12, 293-305.
- ZADNIK, K., BARR, J. T., EDRINGTON, T. B., EVERETT, D. F., JAMESON, M., MCMAHON, T. T., SHIN, J. A., STERLING, J. L., WAGNER, H. & GORDON, M. O. 1998. Baseline findings in the Collaborative Longitudinal Evaluation of Keratoconus (CLEK) Study. *Invest Ophthalmol Vis Sci*, 39, 2537-46.
- ZADNIK, K., BARR, J. T., GORDON, M. O. & EDRINGTON, T. B. 1996. Biomicroscopic signs and disease severity in keratoconus. Collaborative Longitudinal Evaluation of Keratoconus (CLEK) Study Group. *Cornea*, 15, 139-46.